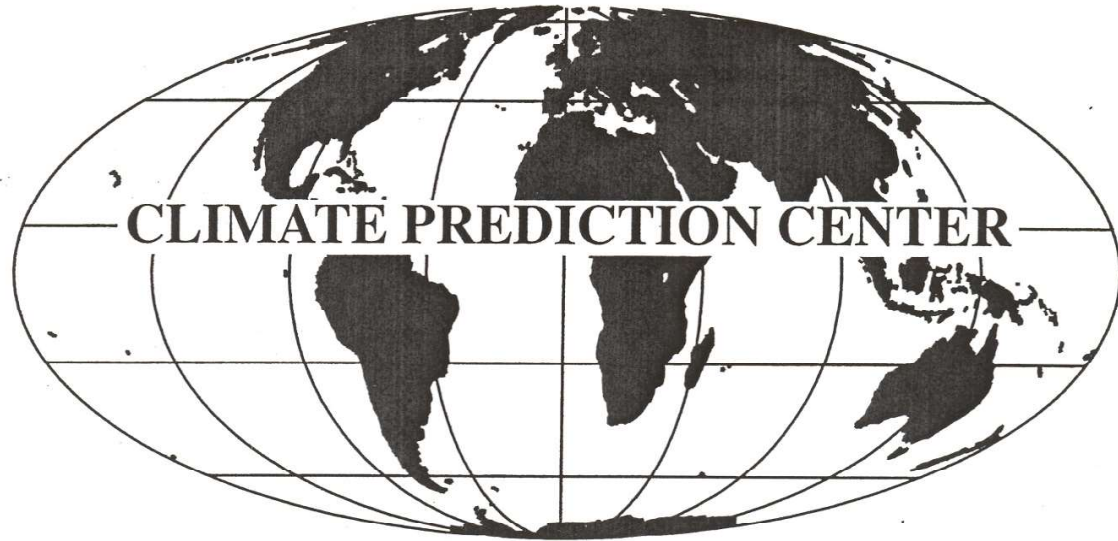


CLIMATE DIAGNOSTICS BULLETIN



JANUARY 2024

NEAR REAL-TIME OCEAN / ATMOSPHERE

Monitoring, Assessments, and Prediction

U.S. DEPARTMENT OF COMMERCE
National Oceanic and Atmospheric Administration
National Weather Service
National Centers for Environmental Prediction

CLIMATE DIAGNOSTICS BULLETIN



**CLIMATE PREDICTION CENTER
Attn: Climate Diagnostics Bulletin
Room 3116, NCWCP
5830 University Research Court
College Park, MD 20740**

Chief Editor: Wei Shi

Editors: Michelle L'Heureux and Emerson LaJoie

Bulletin Production: Wei Shi

External Collaborators:

Center for Ocean-Atmospheric Prediction Studies (COAPS)

Cooperative Institute for Research in the Atmosphere (CIRA)

Earth & Space Research

International Research Institute for Climate and Society (IRI)

Joint Institute for the Study of the Atmosphere and Ocean (JISAO)

Lamont-Doherty Earth Observatory (LDEO)

NOAA-CIRES, Climate Diagnostics Center

NOAA-AOML, Atlantic Oceanographic and Meteorological Laboratory

NOAA-NESDIS-STAR, Center for Satellite Applications and Research

NOAA-NDBC, National Data Buoy Center

Scripps Institution of Oceanography

Software: Most of the bulletin figures generated at CPC are created using the Grid Analysis and Display System (GrADS).

- Climate Diagnostics Bulletin available on the World Wide Web

The CDB is available on the World Wide Web. The address of the online version of the CDB is:

<http://www.cpc.ncep.noaa.gov/products/CDB>

If you have any problems accessing the bulletin, contact Dr. Wei Shi by E-mail:

Wei.Shi@noaa.gov

Table of Contents

TROPICS

- Highlights page 6
Table of Atmospheric Indices page 7
Table of Oceanic Indices page 8

FIGURE

| | |
|--|-----------|
| Time Series | |
| Southern Oscillation Index (SOI) | T1 |
| Tahiti and Darwin SLP Anomalies | T1 |
| OLR Anomalies | T1 |
| CDAS/Reanalysis SOI & Equatorial SOI | T2 |
| 200-hPa Zonal Wind Anomalies | T3 |
| 500-hPa Temperature Anomalies | T3 |
| 30-hPa and 50-hPa Zonal Wind Anomalies | T3 |
| 850-hPa Zonal Wind Anomalies | T4 |
| Equatorial Pacific SST Anomalies | T5 |
| Time-Longitude Sections | |
| Mean and Anomalous Sea Level Pressure | T6 |
| Mean and Anomalous 850-hPa Zonal Wind | T7 |
| Mean and Anomalous OLR | T8 |
| Mean and Anomalous SST | T9 |
| Pentad SLP Anomalies | T10 |
| Pentad OLR Anomalies | T11 |
| Pentad 200-hPa Velocity Potential Anomalies | T12 |
| Pentad 850-hPa Zonal Wind Anomalies | T13 |
| Anomalous Equatorial Zonal Wind | T14 |
| Mean and Anomalous Depth of the 20°C Isotherm | T15 |
| Mean & Anomaly Fields | |
| Depth of the 20°C Isotherm | T16 |
| Subsurface Equatorial Pacific Temperatures | T17 |
| SST | T18 |
| SLP | T19 |
| 850-hPa Vector Wind | T20 |
| 200-hPa Vector Wind | T21 |
| 200-hPa Streamfunction | T22 |
| 200-hPa Divergence | T23 |
| 200-hPa Velocity Potential and Divergent Wind | T24 |
| OLR | T25 |
| SSM/I Tropical Precipitation Estimates | T26 |
| Cloud Liquid Water | T27 |
| Precipitable Water | T28 |
| Divergence & E-W Divergent Circulation | T29 - T30 |
| Pacific Zonal Wind & N-S Divergent Circulation | T31 - T32 |

Appendix 1: Outside Contributions

- Tropical Drifting Buoys

A1.1

FIGURE

| | |
|------------------------------------|-------------|
| Pacific Wind Stress and Anomalies | A1.2 |
| Satellite-Derived Surface Currents | A1.3 - A1.4 |

FORECAST FORUM

Discussion page 45

| | |
|--|---------|
| Canonical Correlation Analysis Forecasts | F1 - F2 |
| NCEP Coupled Model Forecasts | F3 - F4 |
| NCEP Markov Model Forecasts | F5 - F6 |
| LDEO Model Forecasts | F7 - F8 |
| ENSO-CLIPER Model Forecast | F9 |
| Model Forecasts of Niño 3.4 | F10 |

EXTRATROPICS

Highlights page 57

Table of Teleconnection Indices page 59

| | |
|-----------------------------------|---------|
| Global Surface Temperature | E1 |
| Temperature Anomalies (Land Only) | E2 |
| Global Precipitation | E3 |
| Regional Precipitation Estimates | E4 - E5 |
| U. S. Precipitation | E6 |

Northern Hemisphere

| | |
|--|-----|
| Teleconnection Indices | E7 |
| Mean and Anomalous SLP | E8 |
| Mean and Anomalous 500-hPa heights | E9 |
| Mean and Anomalous 300-hPa Wind Vectors | E10 |
| 500-hPa Persistence | E11 |
| Time-Latitude Sections of 500-hPa Height Anomalies | E12 |
| 700-hPa Storm Track | E13 |

Southern Hemisphere

| | |
|--|-----|
| Mean and Anomalous SLP | E14 |
| Mean and Anomalous 500-hPa heights | E15 |
| Mean and Anomalous 300-hPa Wind Vectors | E16 |
| 500-hPa Persistence | E17 |
| Time-Latitude Sections of 500-hPa Height Anomalies | E18 |

Stratosphere

| | |
|-------------------------------|---------|
| Height Anomalies | S1 - S2 |
| Temperatures | S3 - S4 |
| Ozone | S5 - S6 |
| Vertical Component of EP Flux | S7 |
| Ozone Hole | S8 |

Appendix 2: Additional Figures

| | |
|--|------|
| Arctic Oscillation and 500-hPa Anomalies | A2.1 |
| Snow Cover | A2.2 |

Tropical Highlights - January 2024

During January 2024, sea surface temperatures (SSTs) remained well above-average across the equatorial Pacific (Fig. T18). The latest monthly Niño indices were +0.8°C for the Niño 1+2 region, +1.8°C for the Niño 3.4 region and +1.9°C for the Niño 3 region (Table T2). The depth of the oceanic thermocline (measured by the depth of the 20°C isotherm) was above-average in the eastern equatorial Pacific (Figs. T15, T16). The corresponding sub-surface temperatures were 1-5°C above-average in the far eastern equatorial Pacific (Fig. T17).

Also during January, the lower-level wind were near average over much of the equatorial Pacific, while the upper-level wind anomalies were easterly over the eastern equatorial Pacific (Table T1, Figs. T20, T21). Meanwhile, tropical convection was slightly enhanced around the Date Line and near average over Indonesia (Fig. T25). Collectively, these oceanic and atmospheric anomalies were consistent with weakening El Niño conditions.

For the latest status of the ENSO cycle see the ENSO Diagnostic Discussion at:
http://www.cpc.ncep.noaa.gov/products/analysis_monitoring/enso_advisory/index.html

| Month | SLP Anomalies | | Tahiti minus Darwin SOI | 850-hPa Zonal Wind Index | | | 200-hPa Wind Index | OLR Index |
|--------|---------------|--------|-------------------------|--------------------------|--------------------|--------------------|--------------------|-----------|
| | Tahiti | Darwin | | 5N-5S 135E-180 | 5N-5S 175W-140W | 5N-5S 135W-120W | | |
| JAN 24 | 0.4 | -0.5 | 0.5 | 0.6 | 0.0 | -0.6 | -1.3 | -0.0 |
| DEC 23 | 0.2 | 0.6 | -0.2 | 0.1 | -0.9 | -1.5 | -1.6 | -1.3 |
| NOV 23 | -0.1 | 1.3 | -0.8 | -0.5 | -1.2 | -1.1 | -1.7 | -1.2 |
| OCT 23 | 1.2 | 2.1 | -0.5 | -0.6 | -0.8 | -1.2 | -0.9 | -0.6 |
| SEP 23 | -0.9 | 1.4 | -1.3 | 0.1 | -0.3 | 0.5 | 0.5 | -0.8 |
| AUG 23 | 0.2 | 1.7 | -0.8 | -0.3 | -0.6 | -0.1 | -0.6 | -0.3 |
| JUL 23 | 0.2 | 0.7 | -0.3 | 0.1 | 0.3 | 1.3 | 0.6 | -0.7 |
| JUN 23 | 0.3 | -0.1 | 0.3 | 0.4 | 0.1 | 0.4 | -0.4 | -0.3 |
| MAY 23 | -0.3 | 1.6 | -1.0 | -0.4 | 0.4 | 0.6 | 1.3 | -0.2 |
| APR 23 | -0.3 | -0.8 | 0.2 | 0.3 | 0.5 | 0.2 | 1.1 | 0.6 |
| MAR 23 | 0.4 | 0.1 | 0.2 | 0.2 | 0.7 | 0.2 | 1.0 | 1.4 |
| FEB 23 | 1.0 | -1.5 | 1.4 | 0.7 | 1.5 | 1.1 | 2.9 | 1.4 |
| JAN 23 | 1.9 | -0.7 | 1.4 | 1.4 | 1.3 | 1.1 | 0.9 | 1.8 |

TABLE T1 - Atmospheric index values for the most recent 12 months. Indices are standardized by the mean annual standard deviation, except for the Tahiti and Darwin SLP anomalies which are in units of hPa. Positive (negative) values of 200-hPa zonal wind index imply westerly (easterly) anomalies. Positive (negative) values of 850-hPa zonal wind indices imply easterly (westerly) anomalies. Anomalies are departures from the 1991-2020 base period means.

| Month | PACIFIC SST | | | | | | ATLANTIC SST | | | GLOBAL | | | | |
|--------|------------------------------|-----------------------------|--------------------------------|------------------------------|-----------------------------|----------------------------|--------------|------|------|-----------------------------|-----|------|-----|------|
| | Niño 1+2 0-10S 90W-80W | Niño 3 5N-5S 150W-90W | Niño 3.4 5N-5S 170W-120W | Niño 4 5N-5S 160E-150W | N. ATL 5N-20N 60W-30W | S. ATL 0-20S 30W-10E | | | | TROPICS 10N-10S 0-360 | | | | |
| JAN 24 | 0.8 | 25.4 | 1.9 | 27.6 | 1.8 | 28.3 | 1.5 | 29.7 | 1.1 | 27.1 | 1.2 | 26.8 | 1.1 | 28.7 |
| DEC 23 | 1.4 | 24.3 | 2.1 | 27.3 | 2.0 | 28.6 | 1.4 | 29.8 | 1.0 | 27.8 | 1.2 | 25.9 | 1.0 | 28.6 |
| NOV 23 | 2.2 | 23.9 | 2.1 | 27.3 | 1.9 | 28.7 | 1.4 | 30.1 | 0.9 | 28.5 | 0.7 | 24.6 | 1.0 | 28.6 |
| OCT 23 | 2.5 | 23.3 | 2.0 | 27.1 | 1.6 | 28.4 | 1.2 | 29.9 | 1.1 | 29.1 | 0.1 | 23.4 | 0.8 | 28.3 |
| SEP 23 | 2.8 | 23.4 | 2.1 | 27.1 | 1.5 | 28.3 | 1.1 | 29.8 | 1.3 | 29.5 | 0.3 | 23.2 | 0.9 | 28.1 |
| AUG 23 | 3.3 | 24.2 | 2.0 | 27.2 | 1.3 | 28.2 | 1.0 | 29.7 | 1.3 | 29.0 | 0.4 | 23.4 | 0.8 | 28.0 |
| JUL 23 | 3.2 | 25.1 | 1.6 | 27.5 | 1.1 | 28.4 | 0.7 | 29.5 | 1.3 | 28.5 | 0.3 | 24.0 | 0.7 | 28.1 |
| JUN 23 | 2.6 | 25.8 | 1.2 | 27.9 | 0.9 | 28.6 | 0.6 | 29.5 | 1.3 | 28.0 | 0.3 | 25.2 | 0.6 | 28.5 |
| MAY 23 | 2.0 | 26.6 | 0.9 | 28.1 | 0.5 | 28.4 | 0.3 | 29.1 | 0.8 | 27.2 | 0.6 | 26.8 | 0.6 | 29.0 |
| APR 23 | 2.5 | 28.2 | 0.4 | 28.0 | 0.2 | 28.0 | 0.3 | 28.8 | 0.5 | 26.4 | 0.3 | 27.2 | 0.5 | 29.0 |
| MAR 23 | 1.5 | 28.1 | 0.4 | 27.5 | -0.0 | 27.2 | -0.1 | 28.1 | 0.4 | 26.0 | 0.2 | 27.3 | 0.2 | 28.4 |
| FEB 23 | 0.7 | 26.8 | -0.1 | 26.3 | -0.4 | 26.3 | -0.5 | 27.6 | 0.1 | 25.7 | 0.4 | 26.9 | 0.0 | 27.8 |
| JAN 23 | -0.2 | 24.3 | -0.5 | 25.2 | -0.7 | 25.9 | -0.6 | 27.6 | -0.1 | 25.9 | 0.7 | 26.3 | 0.0 | 27.6 |

TABLE T2..Mean and anomalous sea surface temperature (°C) for the most recent 12 months. Anomalies are departures from the 1991-2020 adjusted OI climatology (Smith and Reynolds 1998, *J. Climate*, **11**, 3320-3323).

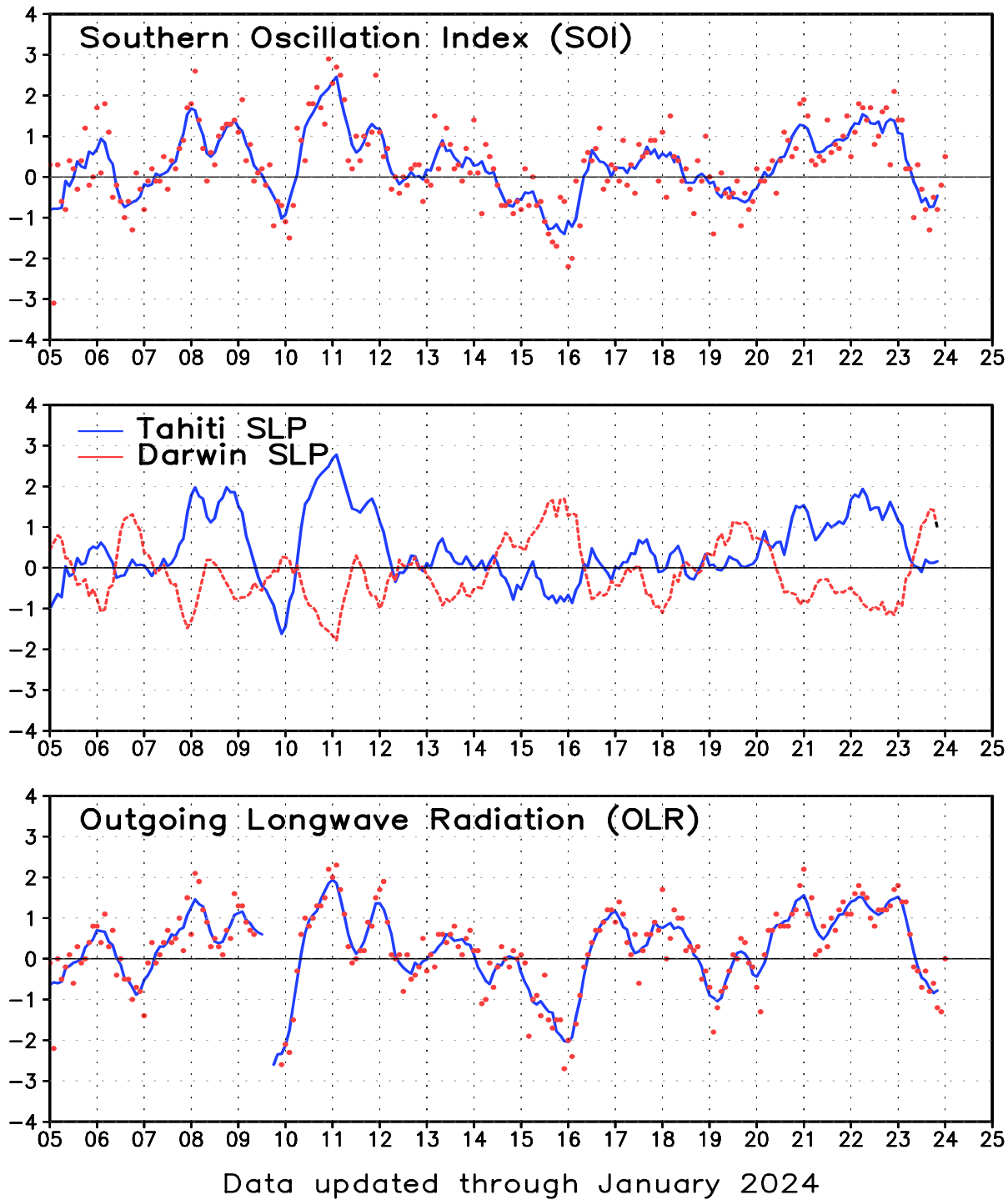


FIGURE T1. Five-month running mean of the Southern Oscillation Index (SOI) (top), sea-level pressure anomaly (hPa) at Darwin and Tahiti (middle), and outgoing longwave radiation anomaly (OLR) averaged over the area 5N-5S, 160E-160W (bottom). Anomalies in the top and middle panels are departures from the 1991-2020 base period means and are normalized by the mean annual standard deviation. Anomalies in the bottom panel are departures from the 1991-2020 base period means. Individual monthly values are indicated by “x”s in the top and bottom panels. The x-axis labels are centered on July.

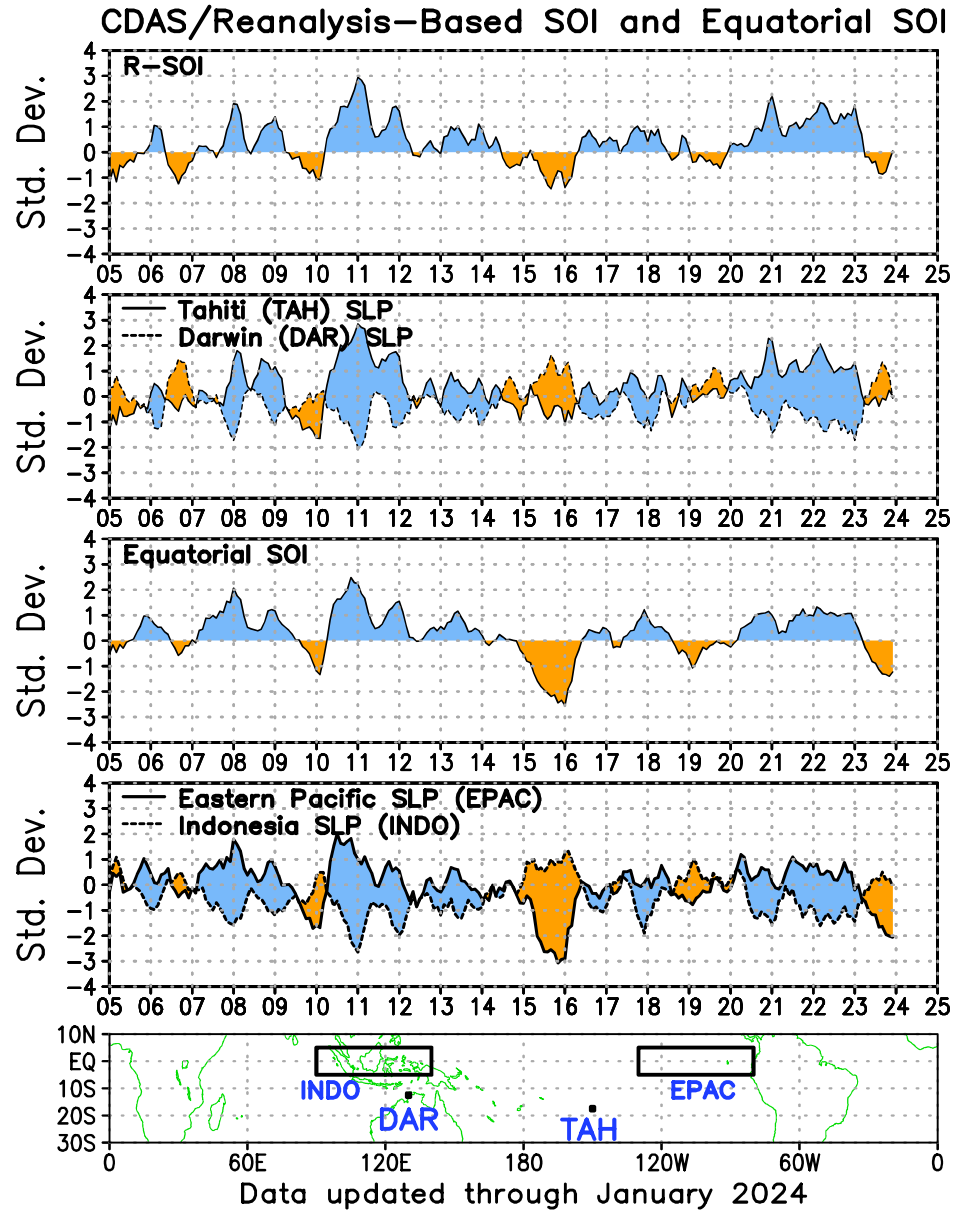


FIGURE T2. Three-month running mean of a CDAS/Reanalysis-derived (a) Southern Oscillation Index (RSOI), (b) standardized pressure anomalies near Tahiti (solid) and Darwin (dashed), (c) an equatorial SOI ([EPAC] - [INDO]), and (d) standardized equatorial pressure anomalies for (EPAC) (solid) and (INDO) (dashed). Anomalies are departures from the 1991-2020 base period means and are normalized by the mean annual standard deviation. The equatorial SOI is calculated as the normalized difference between the standardized anomalies averaged between 5°N - 5°S , 80°W - 130°W (EPAC) and 5°N - 5°S , 90°E - 140°E (INDO).

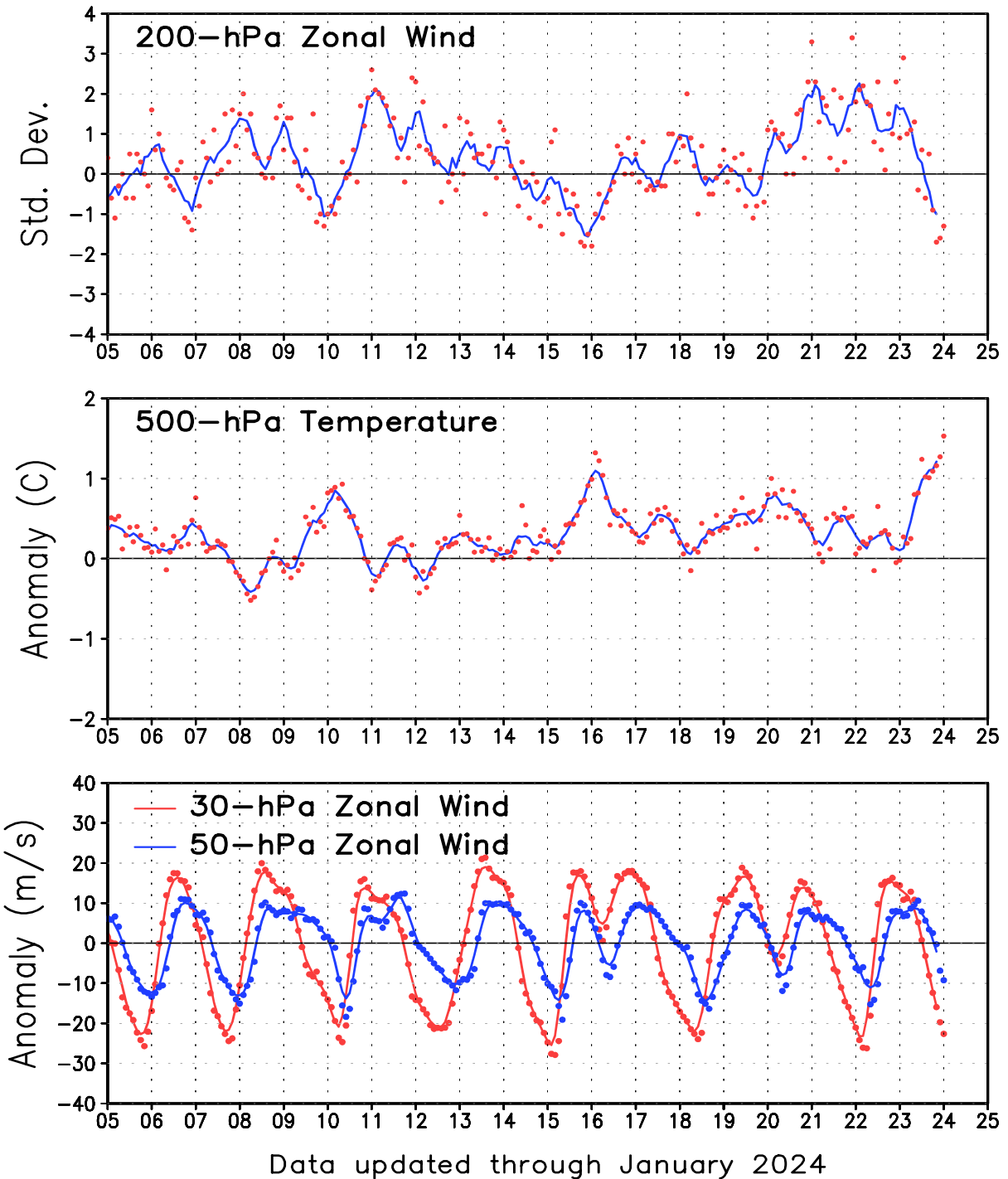


FIGURE T3. Five-month running mean (solid lines) and individual monthly mean (dots) of the 200-hPa zonal wind anomalies averaged over the area 5N-5S, 165W-110W (top), the 500-hPa virtual temperature anomalies averaged over the latitude band 20N-20S (middle), and the equatorial zonally-averaged zonal wind anomalies at 30-hPa (red) and 50-hPa (blue) (bottom). In the top panel, anomalies are normalized by the mean annual standard deviation. Anomalies are departures from the 1991-2020 base period means. The x-axis labels are centered on January.

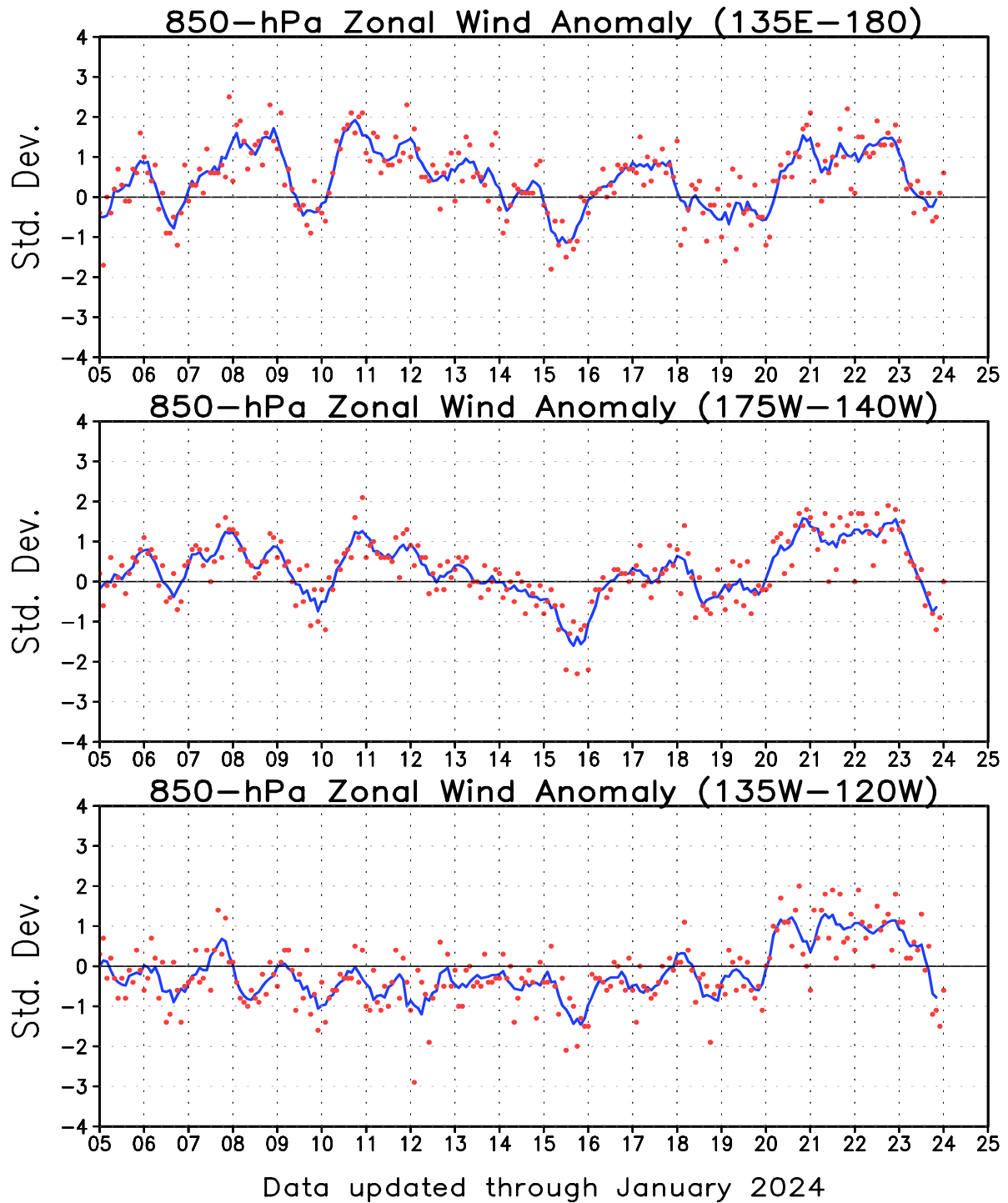


FIGURE T4. Five-month running mean (solid line) and individual monthly mean (dots) of the standardized 850-hPa zonal wind anomaly index in the latitude belt 5N-5S for 135E-180 (top), 175W-140W (middle) and 135W-120W (bottom). Anomalies are departures from the 1991-2020 base period means and are normalized by the mean annual standard deviation. The x-axis labels are centered on January. Positive (negative) values indicate easterly (westerly) anomalies.

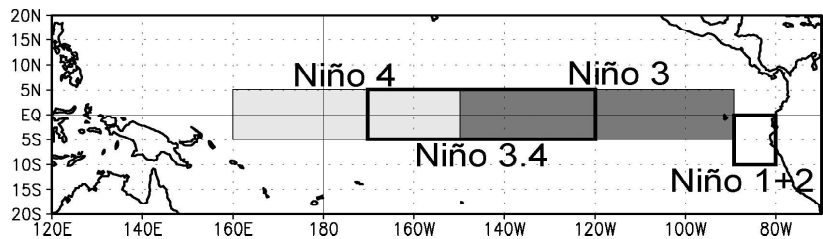
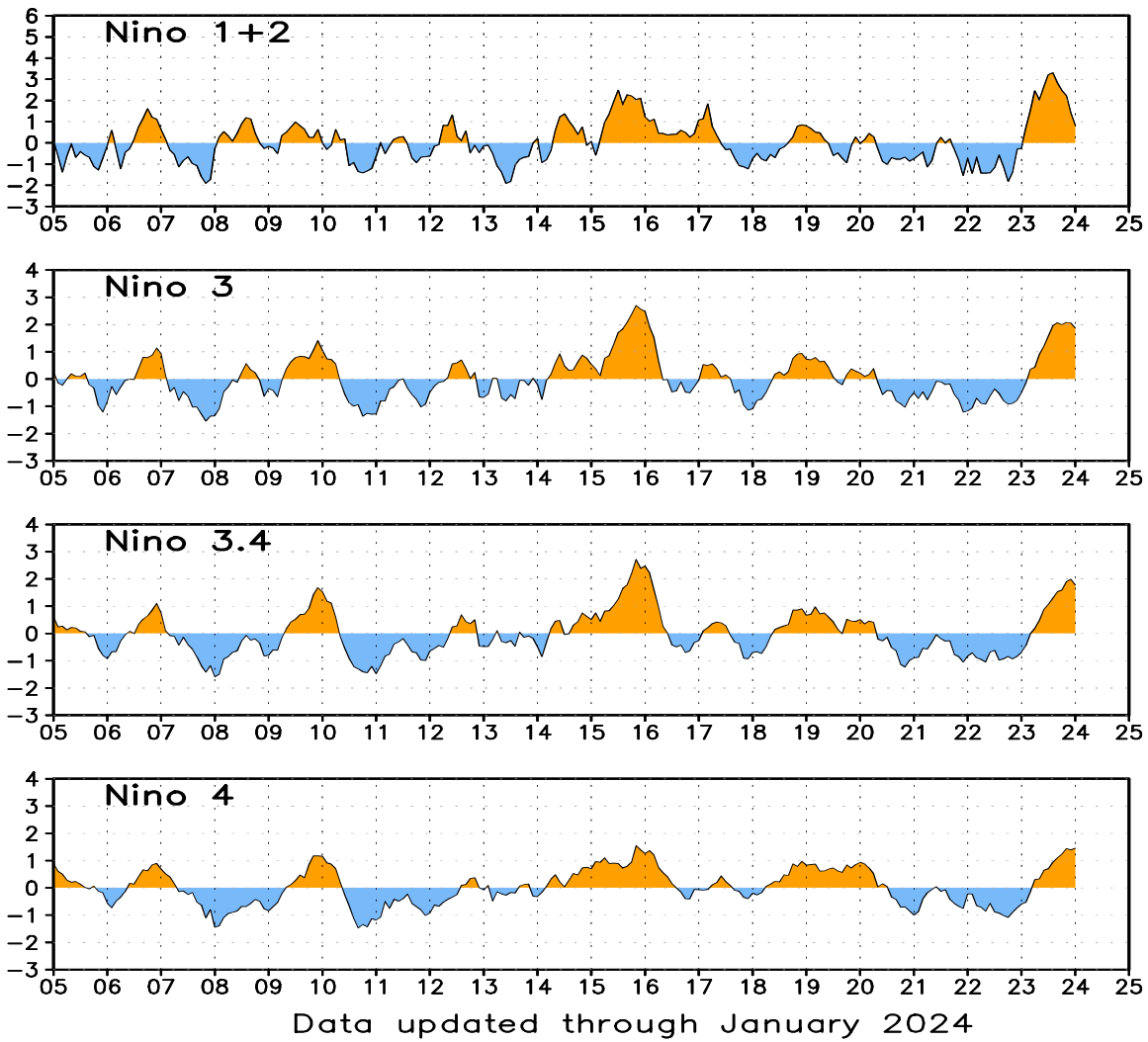


FIGURE T5. Niño region indices, calculated as the area-averaged sea surface temperature anomalies (C) for the specified region. The Niño 1+2 region (top) covers the extreme eastern equatorial Pacific between 0-10S, 90W-80W. The Niño-3 region (2nd from top) spans the eastern equatorial Pacific between 5N-5S, 150W-90W. The Niño 3.4 region 3rd from top) spans the east-central equatorial Pacific between 5N-5S, 170W-120W. The Niño 4 region (bottom) spans the date line and covers the area 5N-5S, 160E-150W. Anomalies are departures from the 1991-2020 base period monthly means (*Smith and Reynolds 1998, J. Climate, 11, 3320-3323*). Monthly values of each index are also displayed in [Table 2](#).

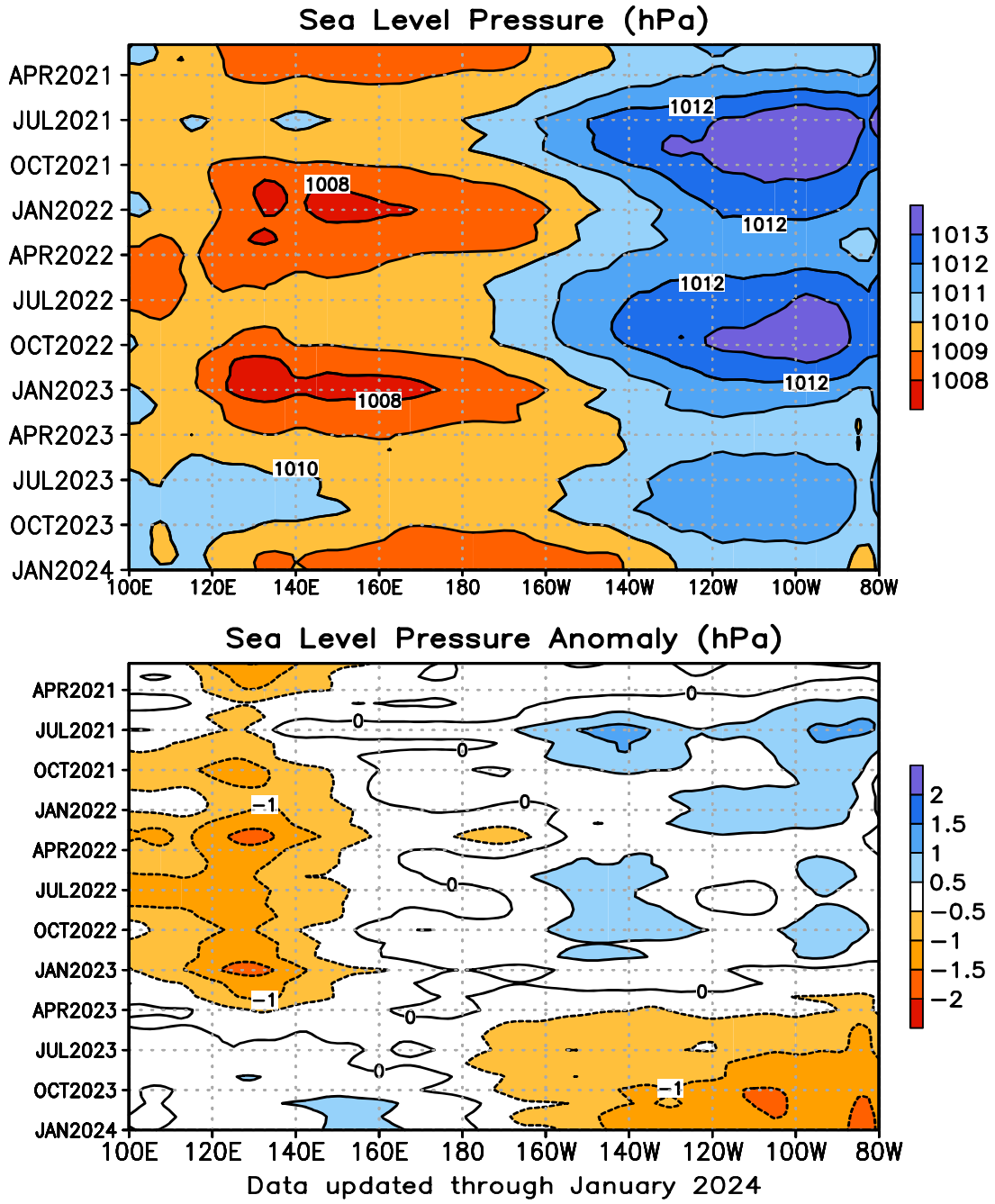


FIGURE T6. Time-longitude section of mean (top) and anomalous (bottom) sea level pressure (SLP) averaged between 5N-5S (CDAS/Reanalysis). Contour interval is 1.0 hPa (top) and 0.5 hPa (bottom). Dashed contours in bottom panel indicate negative anomalies. Anomalies are departures from the 1991-2020 base period monthly means. The data are smoothed temporally using a 3-month running average.

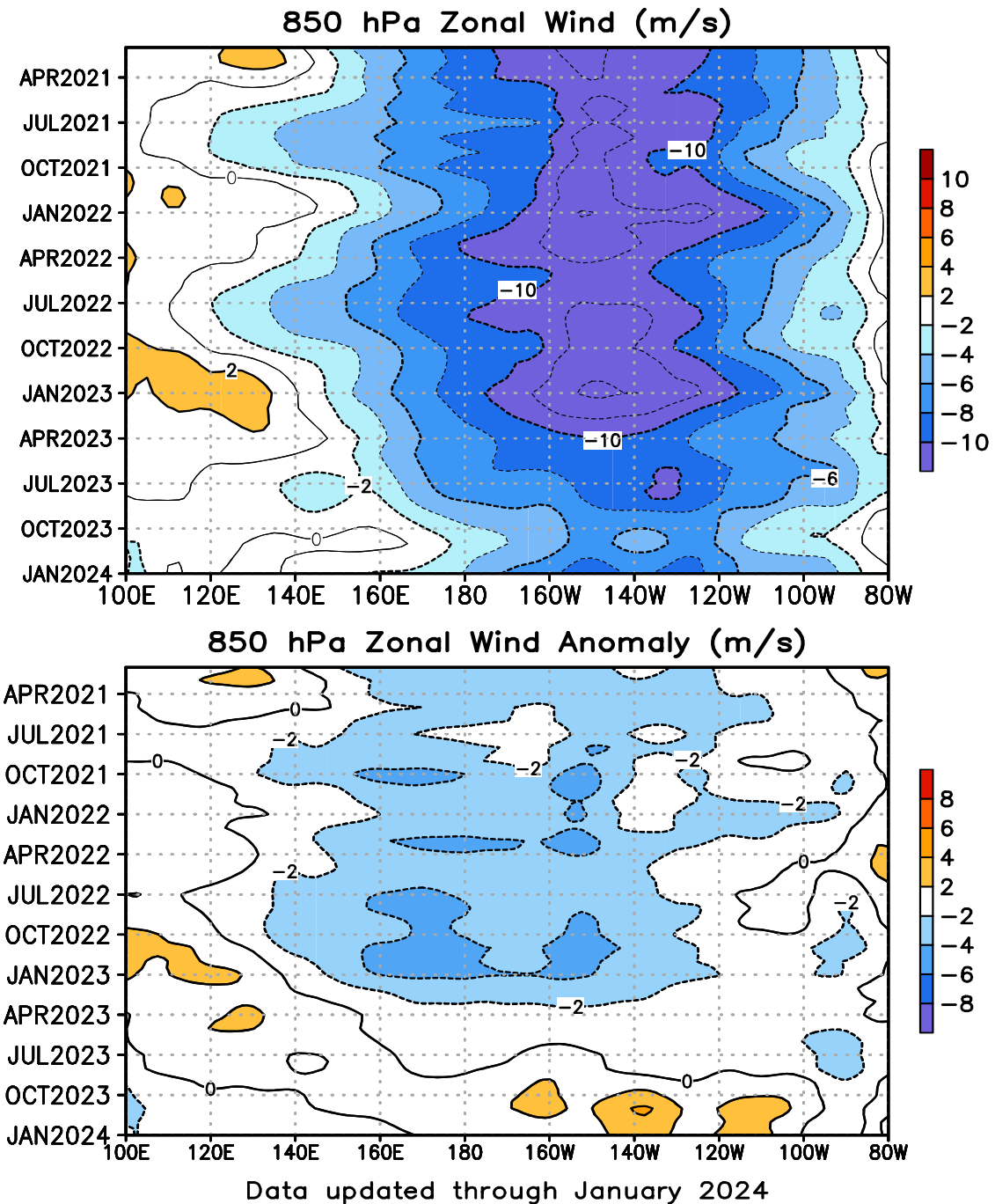


FIGURE T7. Time-longitude section of mean (top) and anomalous (bottom) 850-hPa zonal wind averaged between 5N-5S (CDAS/Reanalysis). Contour interval is 2 ms^{-1} . Blue shading and dashed contours indicate easterlies (top) and easterly anomalies (bottom). Anomalies are departures from the 1991-2020 base period monthly means. The data are smoothed temporally using a 3-month running average.

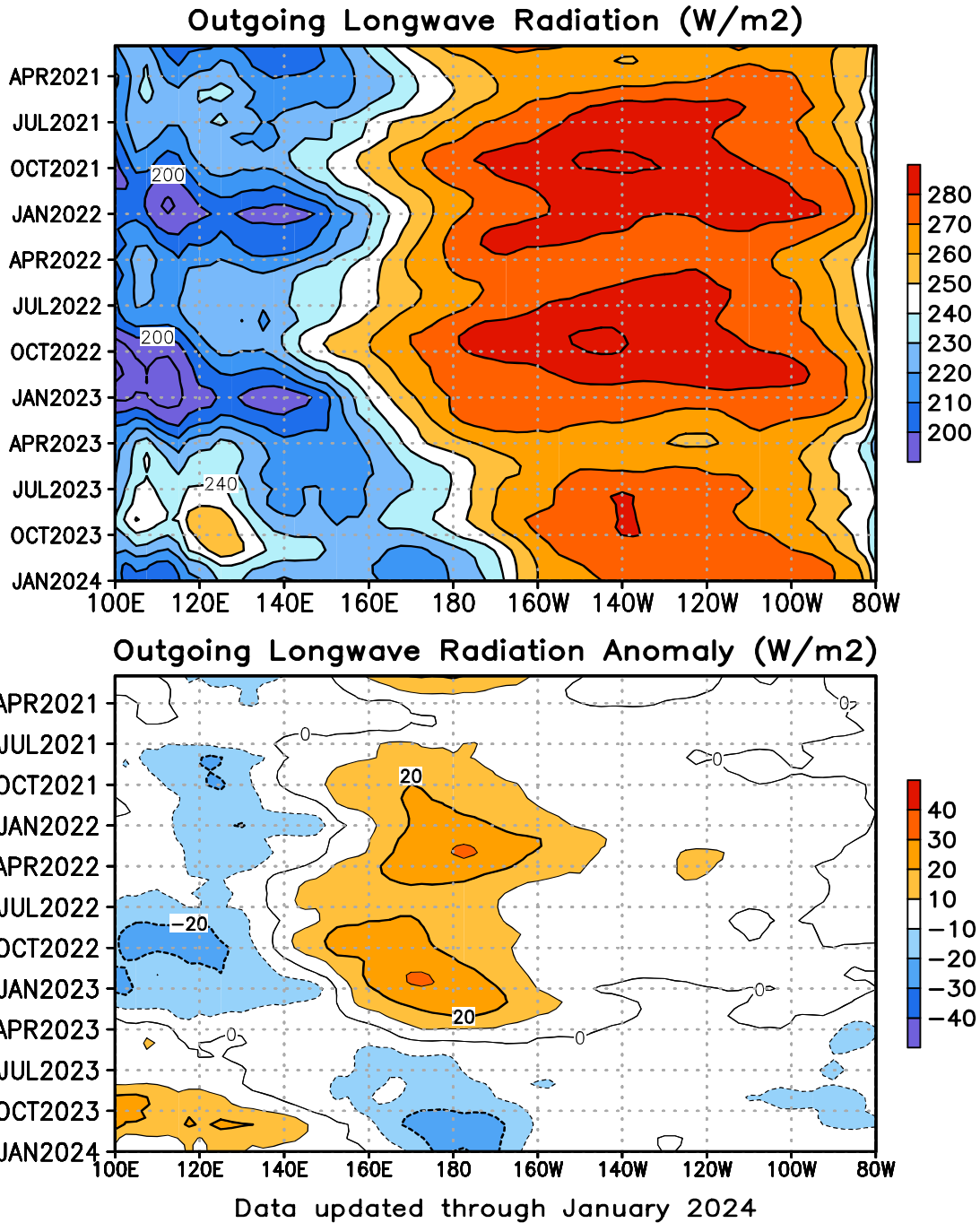


FIGURE T8. Time-longitude section of mean (top) and anomalous (bottom) outgoing longwave radiation (OLR) averaged between 5N-5S. Contour interval is 10 Wm⁻². Dashed contours in bottom panel indicate negative OLR anomalies. Anomalies are departures from the 1991-2020 base period monthly means. The data are smoothed temporally using a 3-month running average.

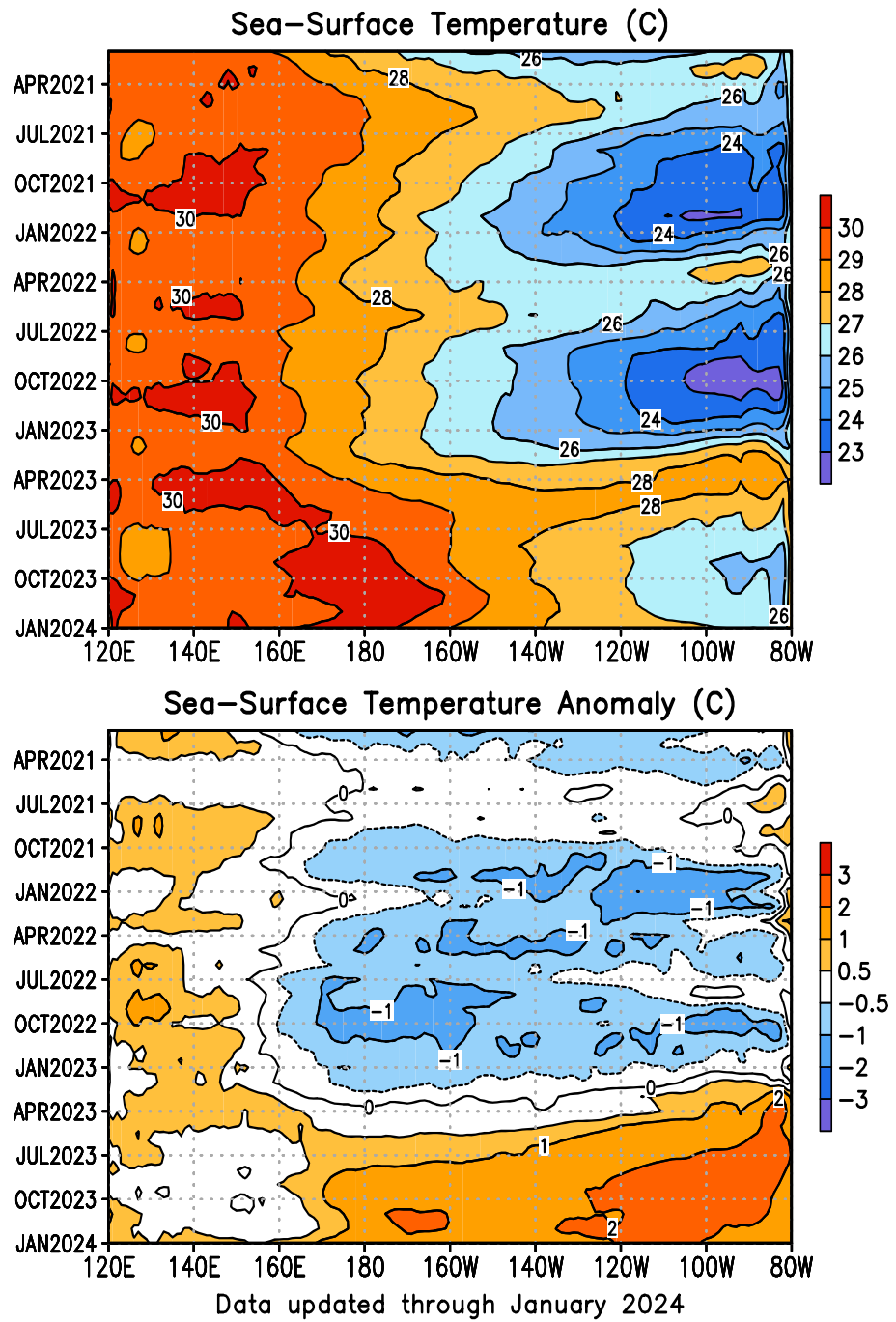


FIGURE T9. Time-longitude section of monthly mean (top) and anomalous (bottom) sea surface temperature (SST) averaged between 5N-5S. Contour interval is 1C (top) and 0.5C (bottom). Dashed contours in bottom panel indicate negative anomalies. Anomalies are departures from the 1991-2020 base period means (Smith and Reynolds 1998, *J. Climate*, **11**, 3320-3323).

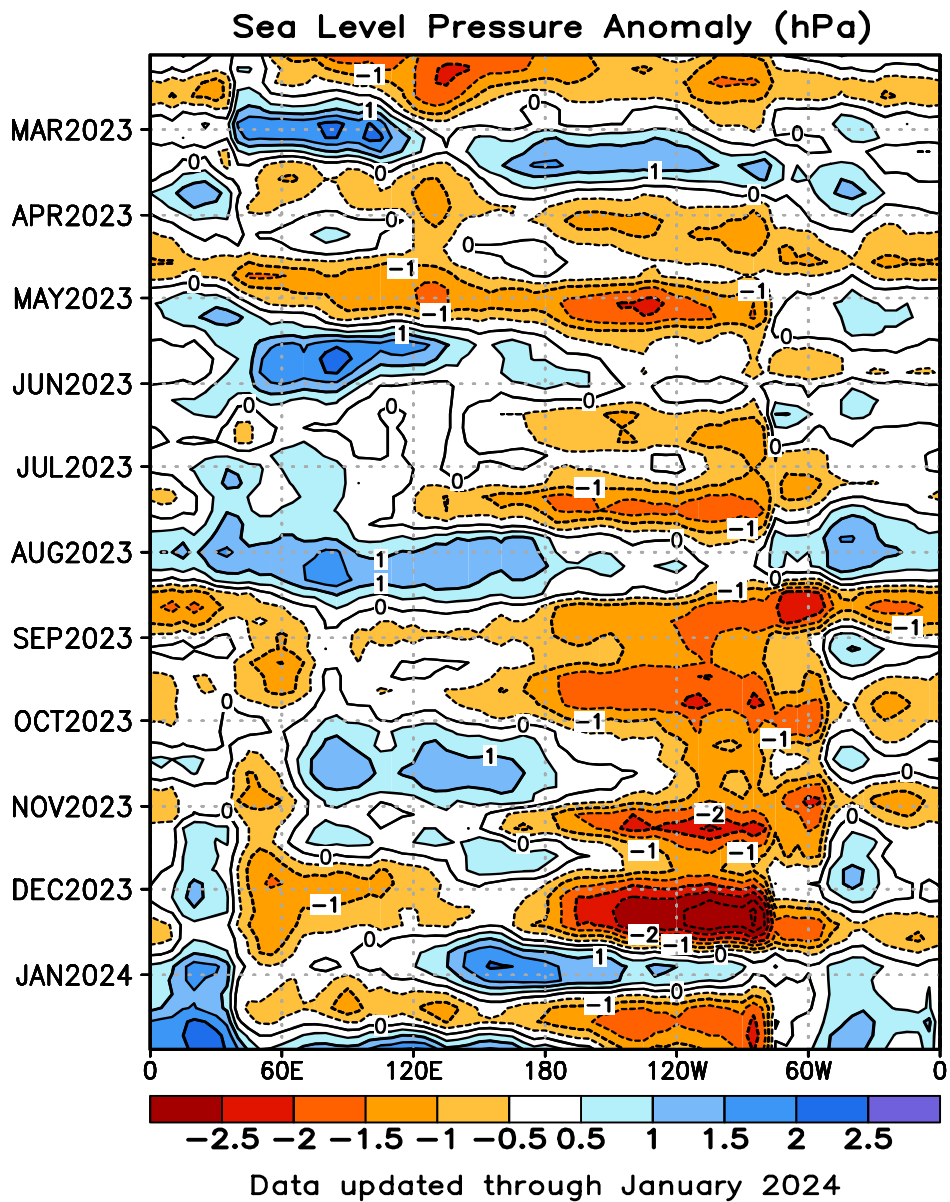


FIGURE T10. Time-longitude section of anomalous sea level pressure (hPa) averaged between 5N-5S (CDAS/Reanalysis). Contour interval is 1 hPa. Dashed contours indicate negative anomalies. Anomalies are departures from the 1991-2020 base period pentad means. The data are smoothed temporally using a 3-point running average.

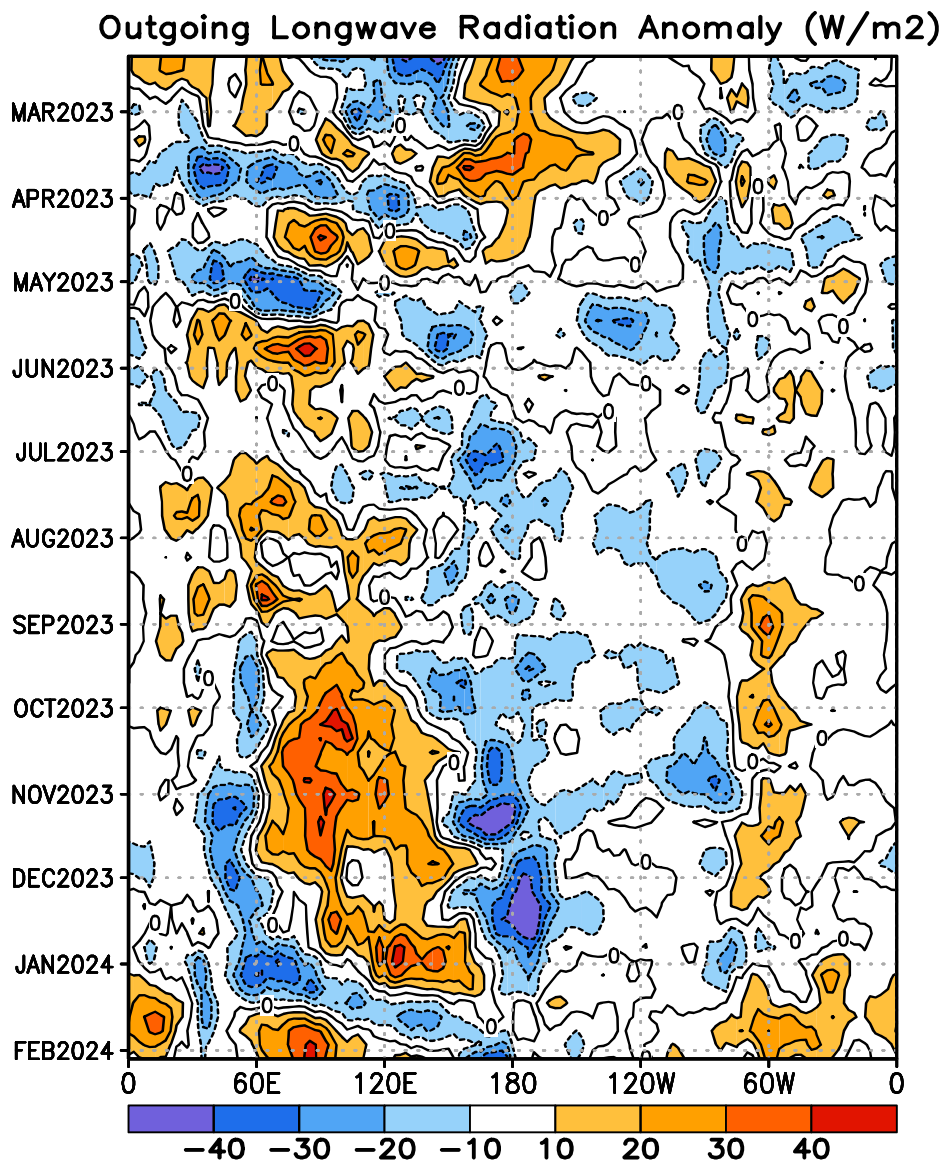


FIGURE T11. Time-longitude section of anomalous outgoing longwave radiation averaged between 5N-5S. Contour interval is 15 Wm⁻². Dashed contours indicate negative anomalies. Anomalies are departures from the 1991-2020 base period pentad means. The data are smoothed temporally using a 3-point running average.

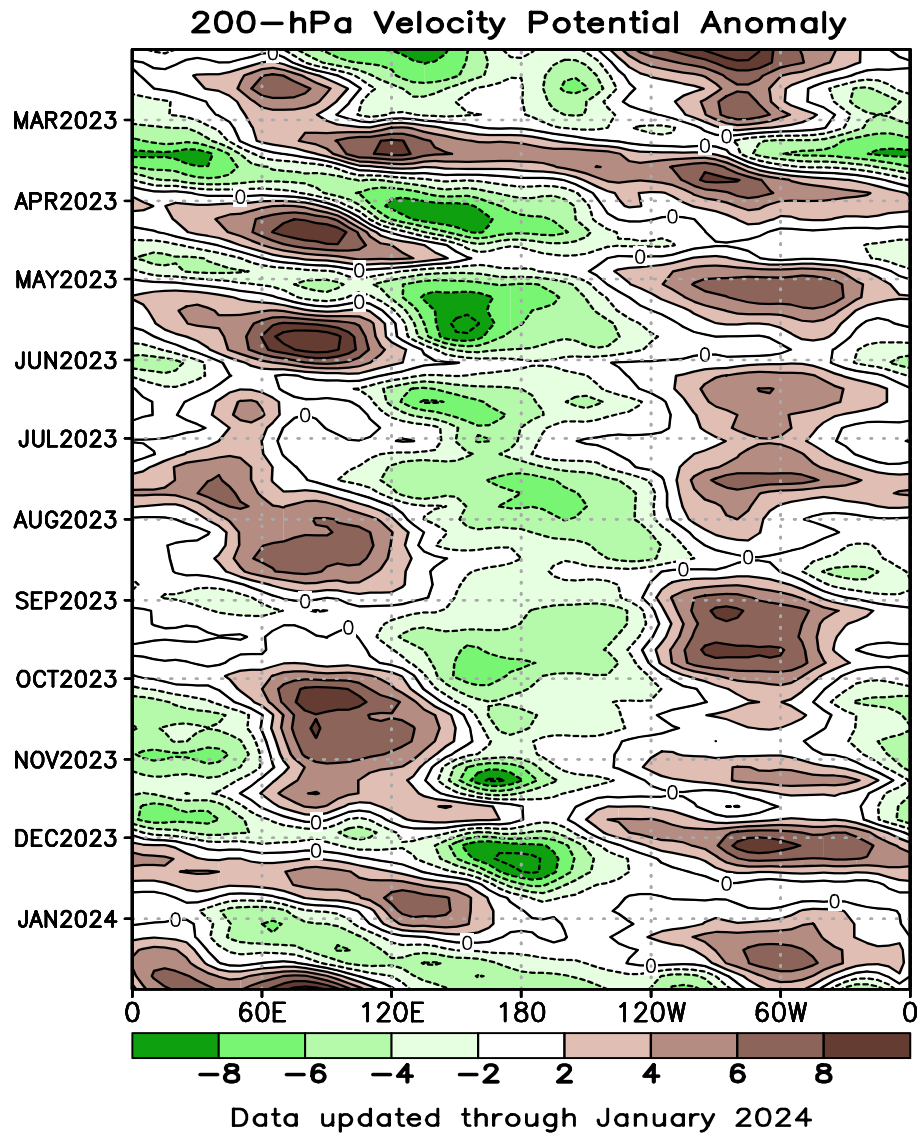


FIGURE T12. Time-longitude section of anomalous 200-hPa velocity potential averaged between 5N-5S (CDAS/Reanalysis). Contour interval is $3 \times 10^6 \text{ m}^2\text{s}^{-1}$. Dashed contours indicate negative anomalies. Anomalies are departures from the 1991-2020 base period pentad means. The data are smoothed temporally using a 3-point running average.

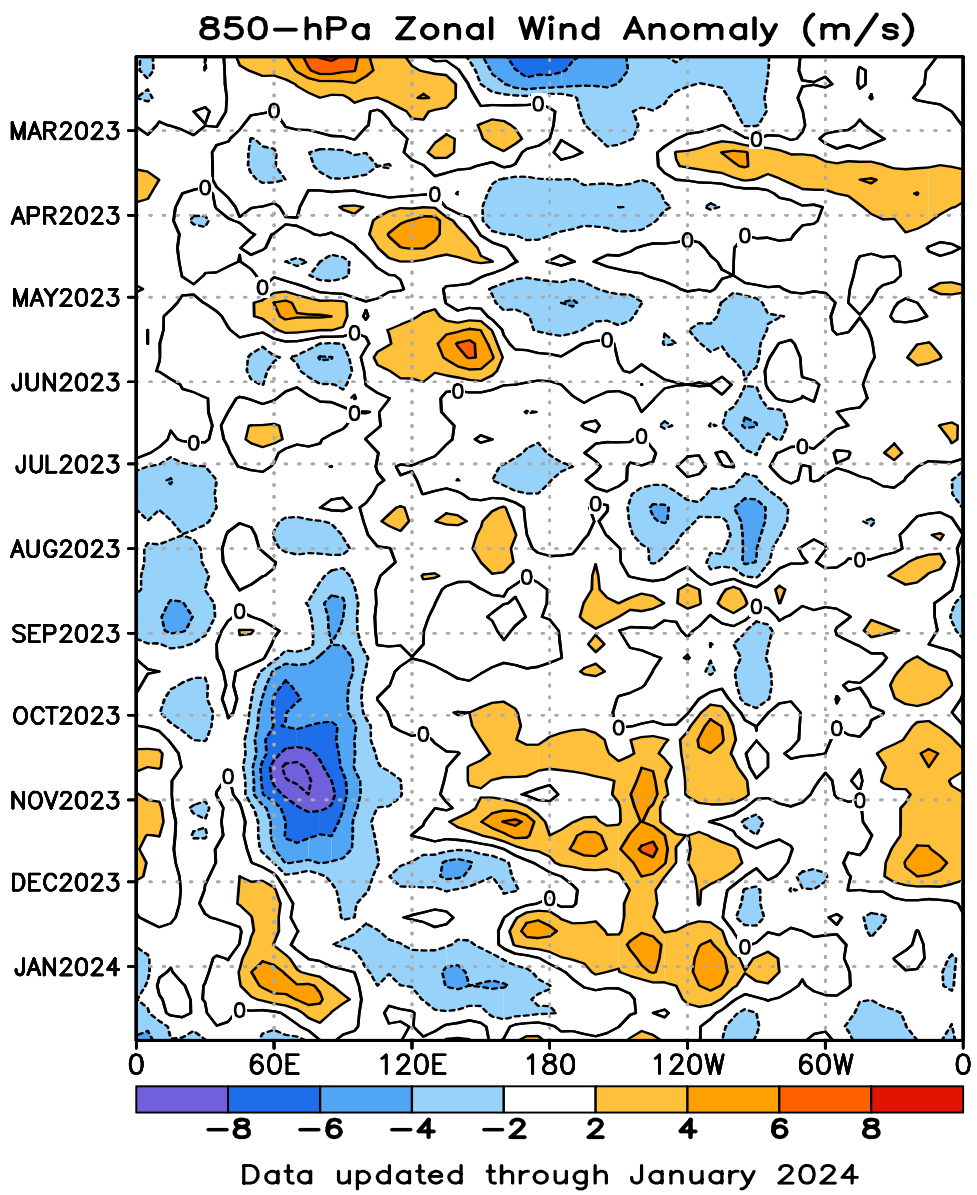


FIGURE T13. Time-longitude section of anomalous 850-hPa zonal wind averaged between 5N-5S (CDAS/Reanalysis). Contour interval is 2 ms^{-1} . Dashed contours indicate negative anomalies. Anomalies are departures from the 1991-2020 base period pentad means. The data are smoothed temporally by using a 3-point running average.

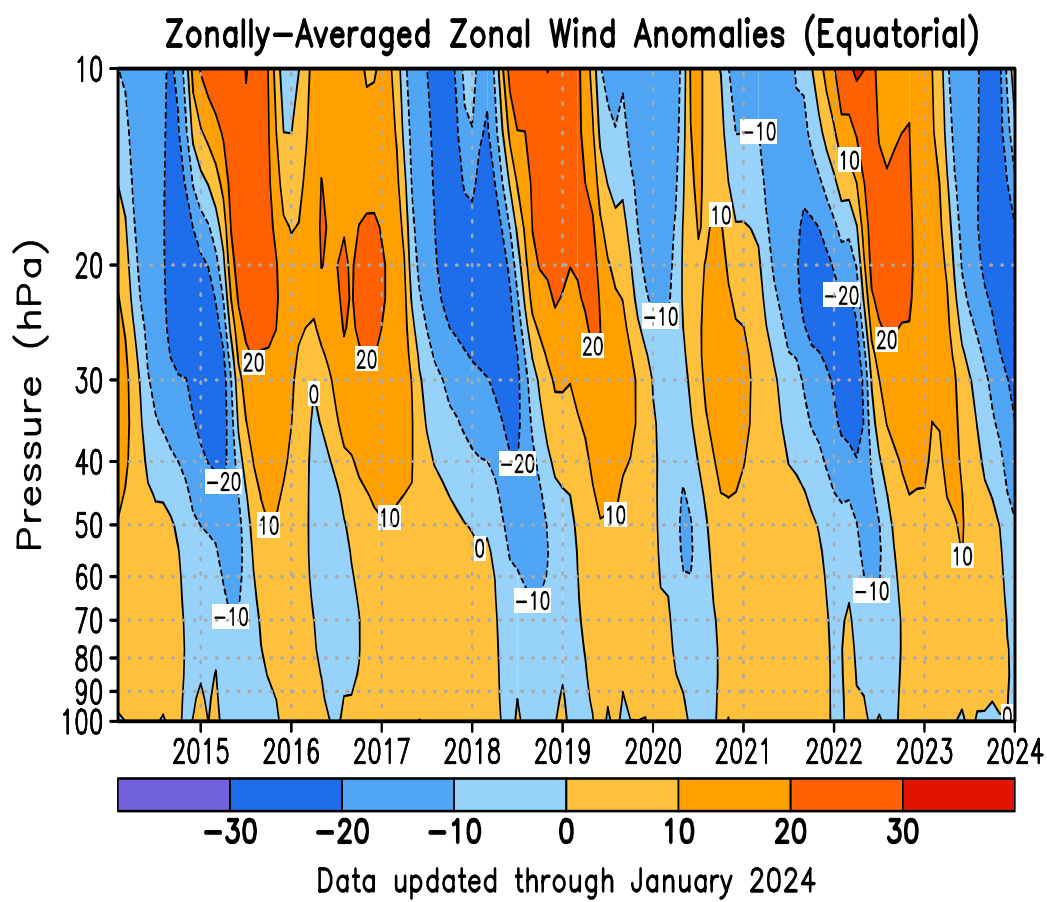


FIGURE T14. Equatorial time-height section of anomalous zonally-averaged zonal wind (m s^{-1}) (CDAS/Reanalysis). Contour interval is 10 ms^{-1} . Anomalies are departures from the 1991-2020 base period monthly means.

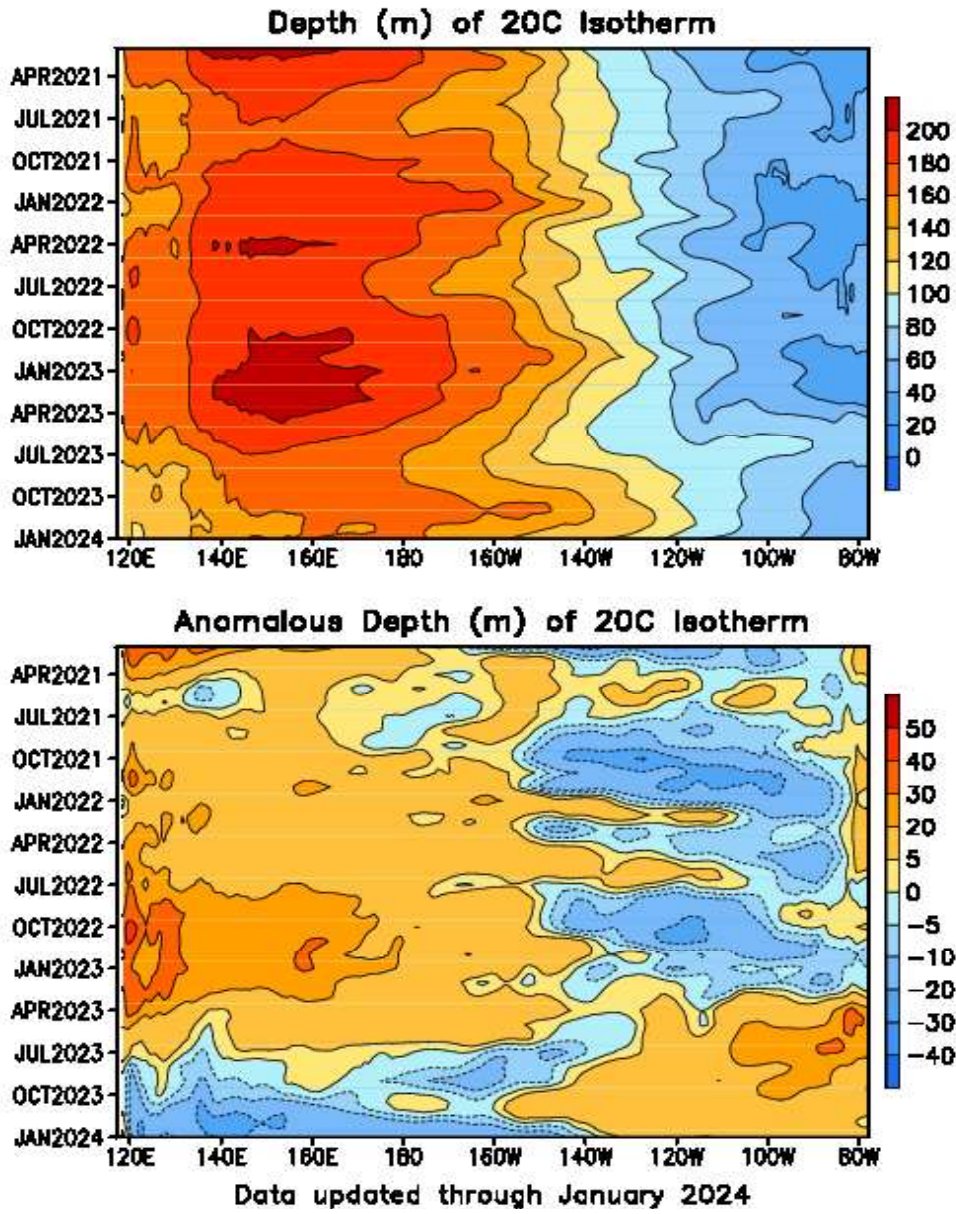


FIGURE T15. Mean (top) and anomalous (bottom) depth of the 20C isotherm averaged between 5N-5S in the Pacific Ocean. Data are derived from the NCEP's global ocean data assimilation system which assimilates oceanic observations into an oceanic GCM (Behringer, D. W., and Y. Xue, 2004: Evaluation of the global ocean data assimilation system at NCEP: The Pacific Ocean. AMS 84th Annual Meeting, Seattle, Washington, 11-15). The contour interval is 10 m. Dashed contours in bottom panel indicate negative anomalies. Anomalies are departures from the 1991-2020 base period means.

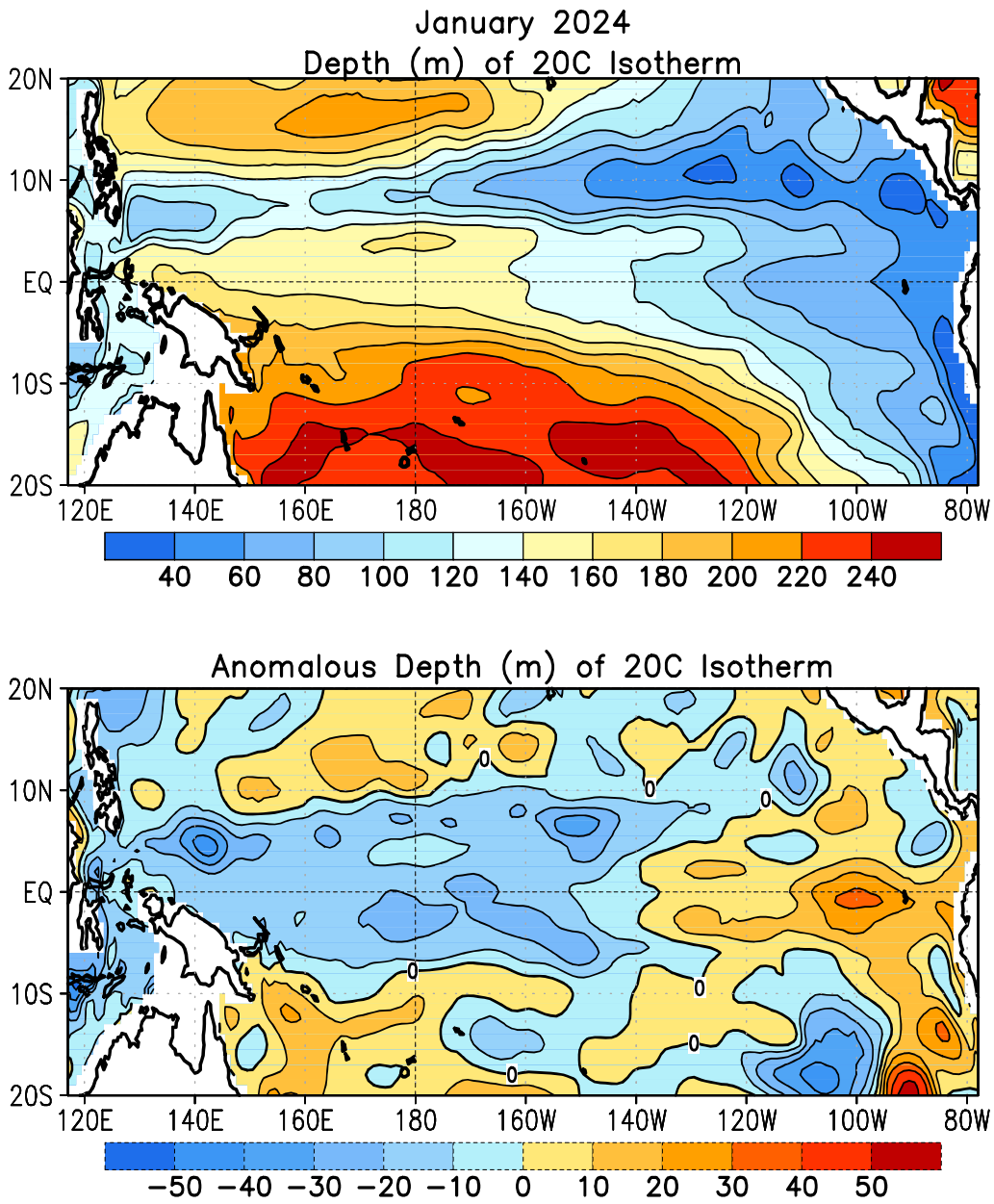


FIGURE T16. Mean (top) and anomalous (bottom) depth of the 20°C isotherm for JAN 2024. Contour interval is 40 m (top) and 10 m (bottom). Dashed contours in bottom panel indicate negative anomalies. Data are derived from the NCEP's global ocean data assimilation system version 2 which assimilates oceanic observations into an oceanic GCM (Xue, Y. and Behringer, D.W., 2006: Operational global ocean data assimilation system at NCEP, to be submitted to BAMS). Anomalies are departures from the 1991-2020 base period means.

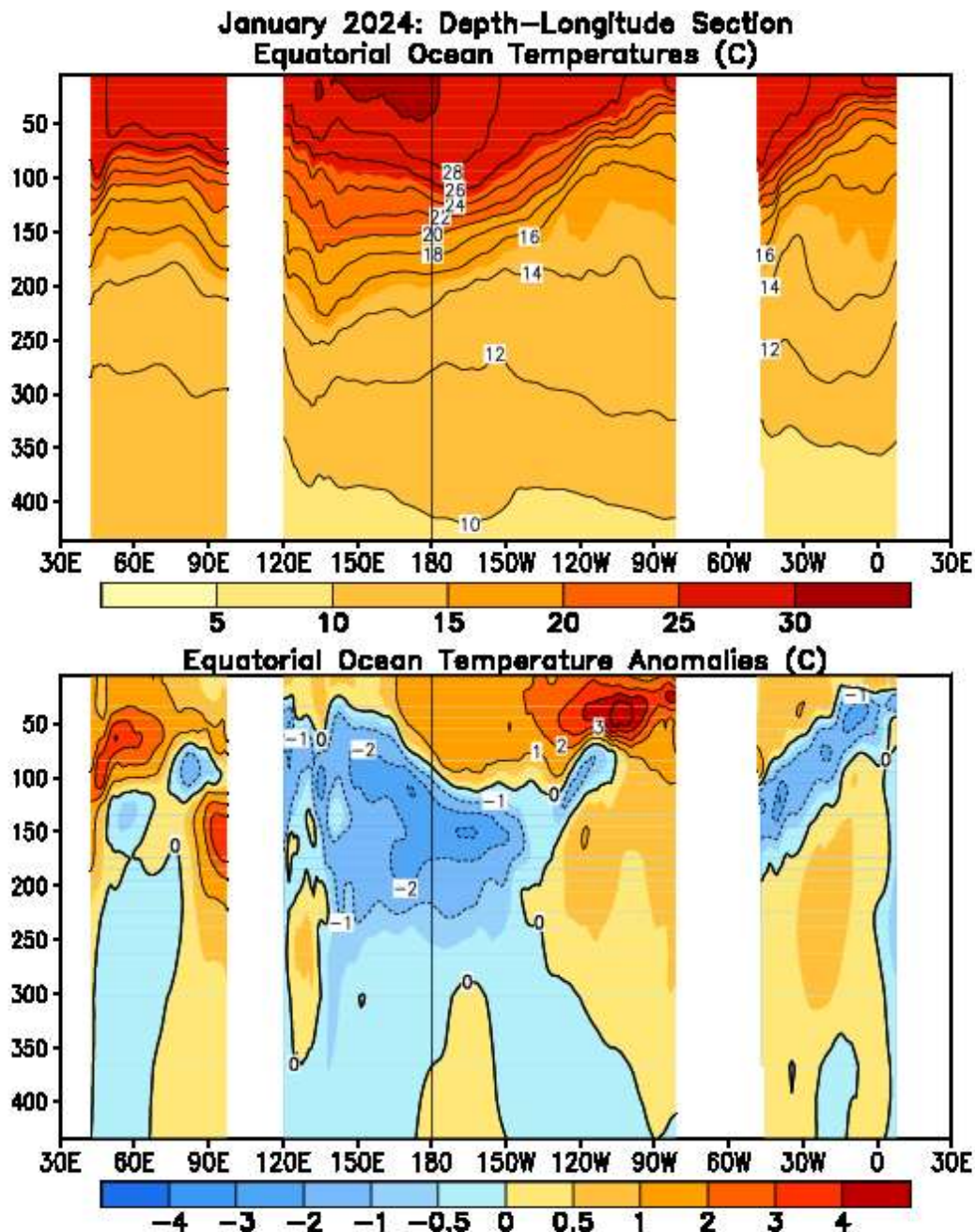


FIGURE T17. Equatorial depth-longitude section of ocean temperature (top) and ocean temperature anomalies (bottom) for JAN 2024. Contour interval is 1°C. Dashed contours in bottom panel indicate negative anomalies. Data are derived from the NCEP's global ocean data assimilation system version 2 which assimilates oceanic observations into an oceanic GCM (Xue, Y. and Behringer, D.W., 2006: Operational global ocean data assimilation system at NCEP, to be submitted to BAMS). Anomalies are departures from the 1991-2020 base period means.

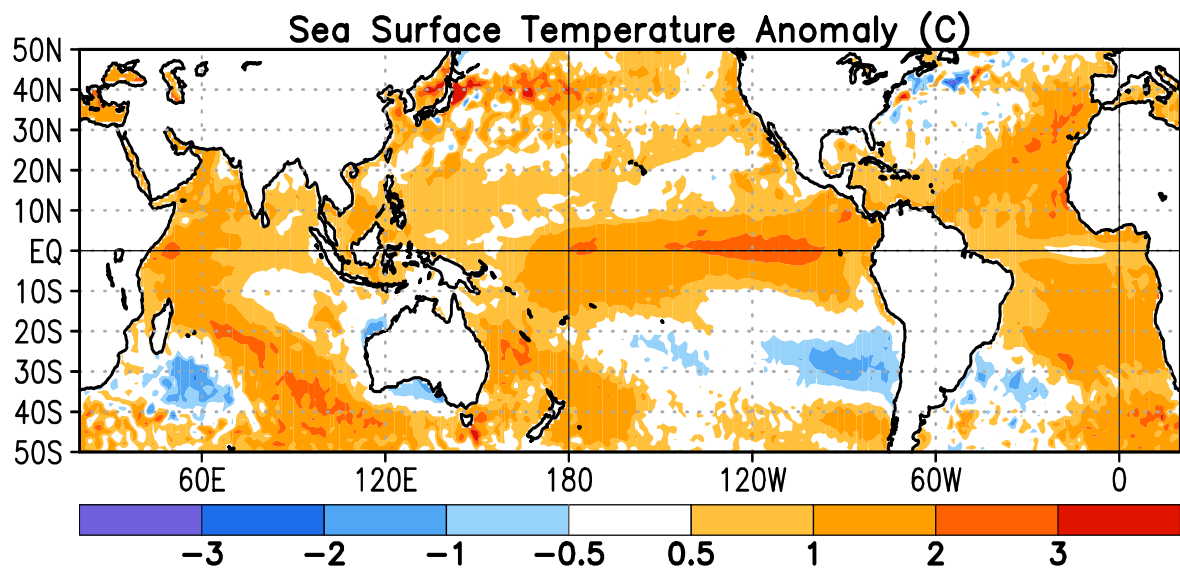
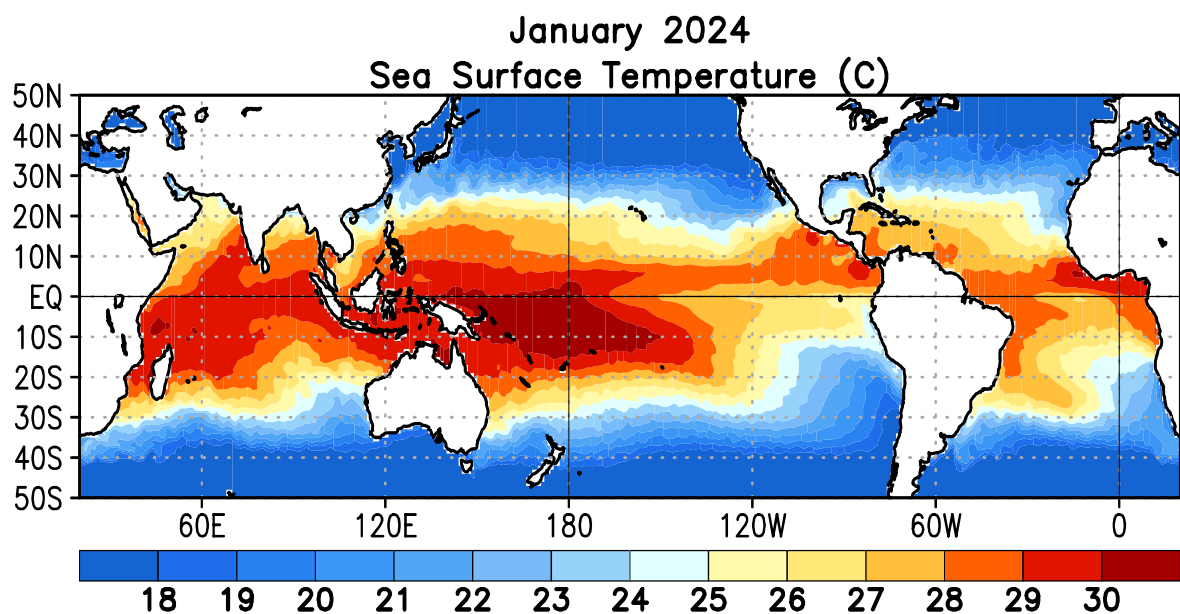


FIGURE T18. Mean (top) and anomalous (bottom) sea surface temperature (SST). Anomalies are departures from the 1991-2020 base period monthly means (Smith and Reynolds 1998, *J. Climate*, **11**, 3320-3323).

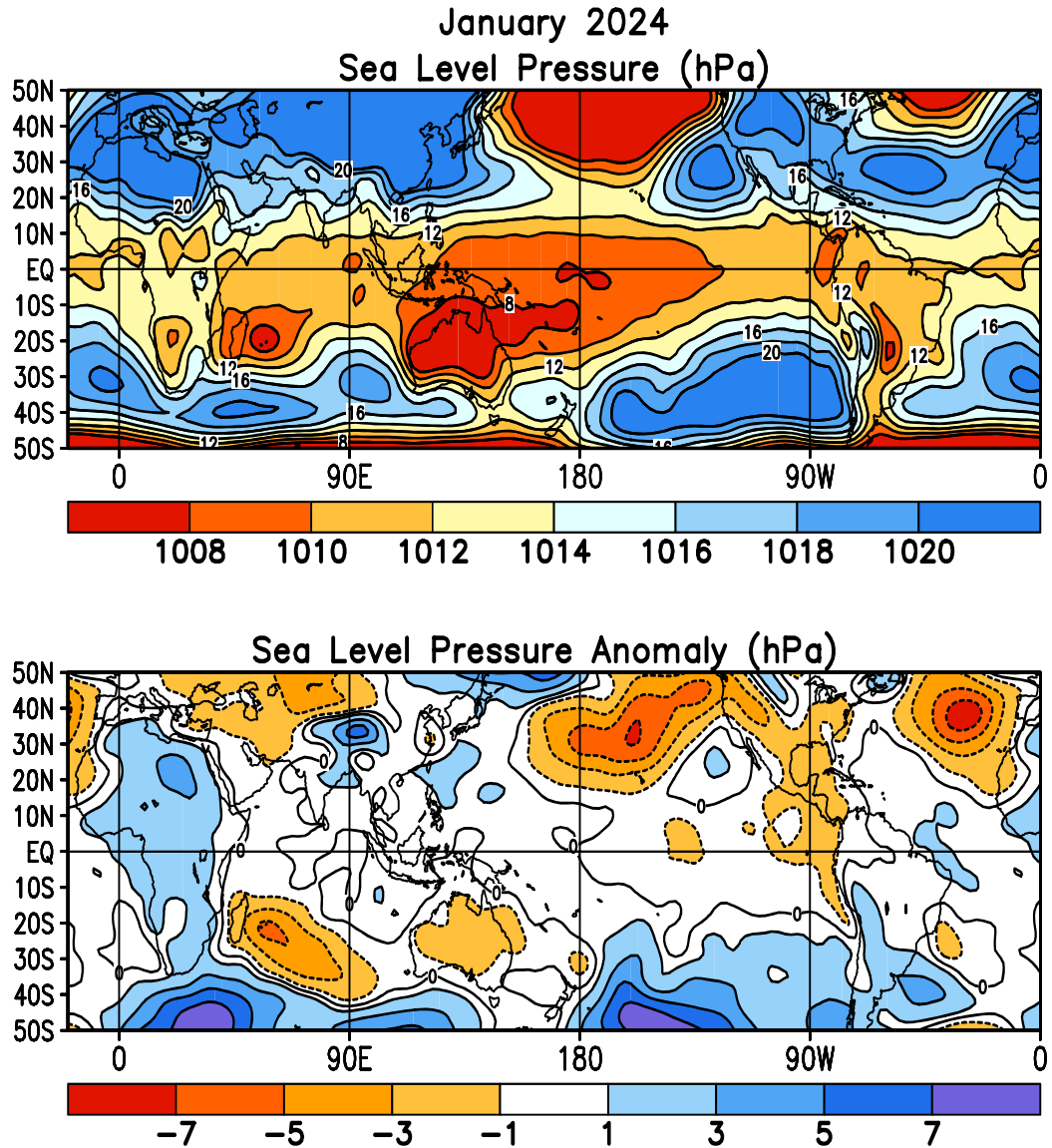


FIGURE T19. Mean (top) and anomalous (bottom) sea level pressure (SLP) (CDAS/Reanalysis). In top panel, 1000 hPa has been subtracted from contour labels, contour interval is 2 hPa, and values below 1000 hPa are indicated by dashed contours. In bottom panel, anomaly contour interval is 1 hPa and negative anomalies are indicated by dashed contours. Anomalies are departures from the 1991-2020 base period monthly means.

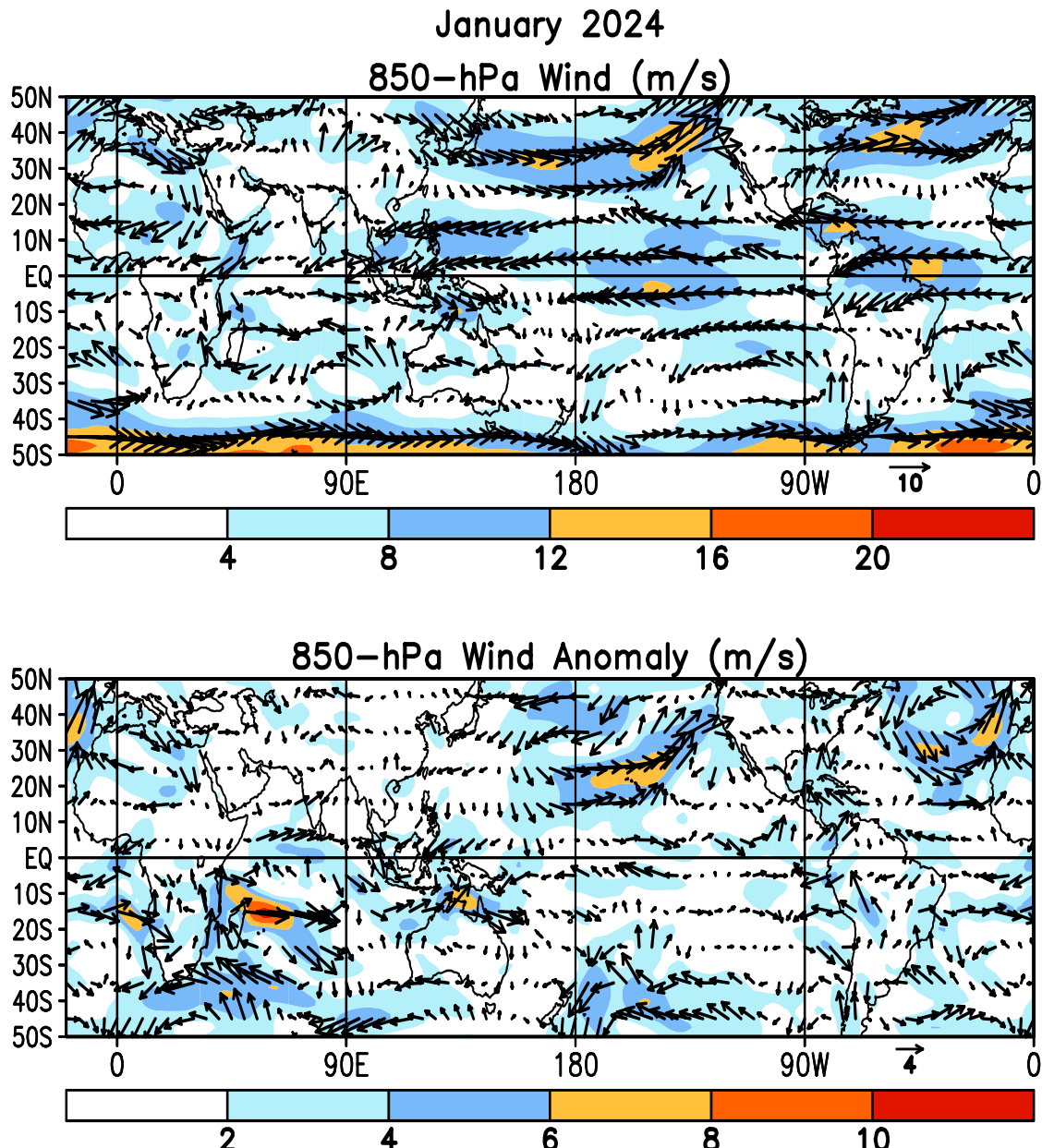


FIGURE T20. Mean (top) and anomalous (bottom) 850-hPa vector wind (CDAS/Reranysis) for JAN 2024. Contour interval for isotachs is 4 ms^{-1} (top) and 2 ms^{-1} (bottom). Anomalies are departures from the 1991-2020 base period monthly means.

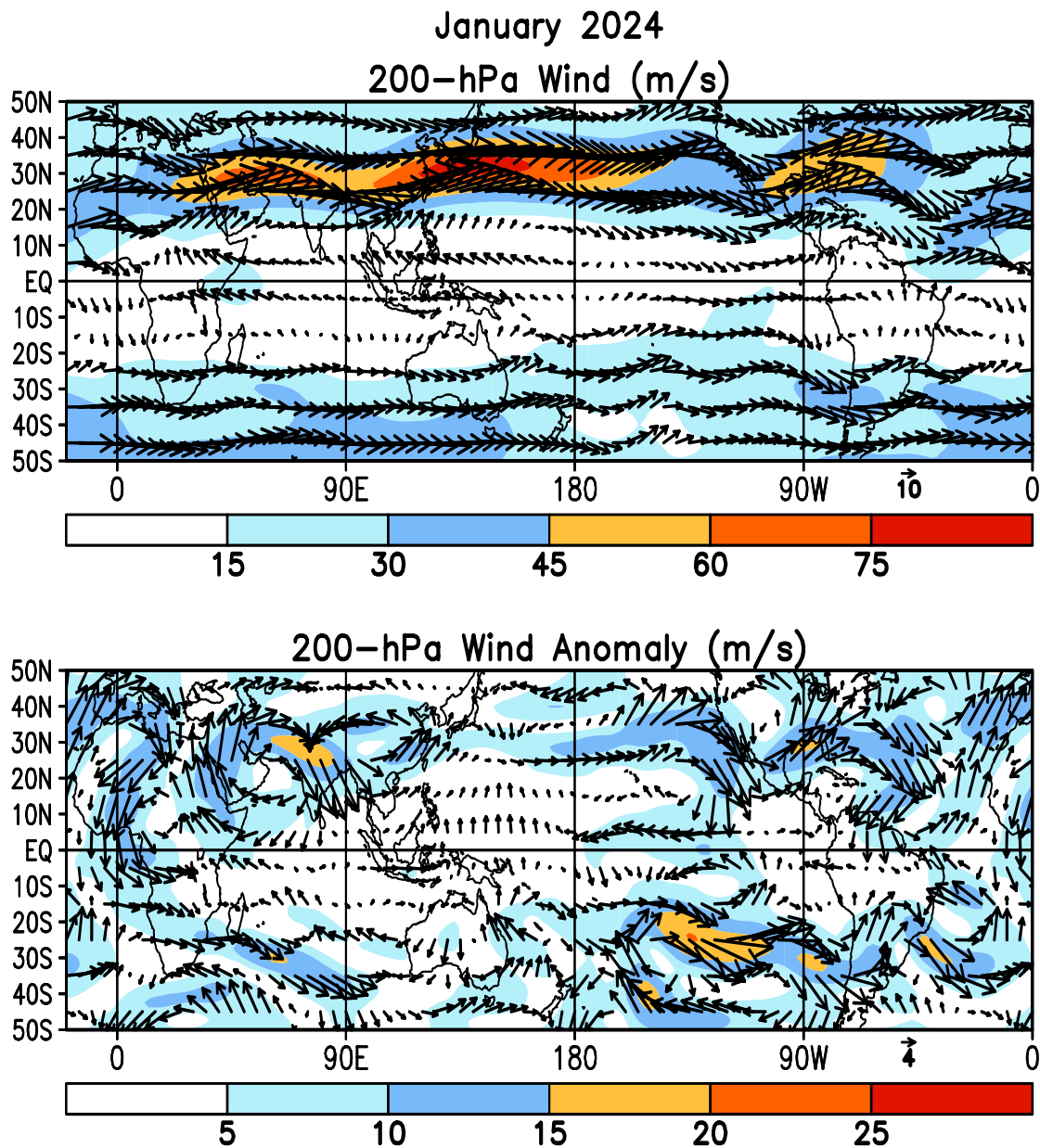


FIGURE T21. Mean (top) and anomalous (bottom) 200-hPa vector wind (CDAS/Reanalysis) for JAN 2024. Contour interval for isotachs is 15 ms^{-1} (top) and 5 ms^{-1} (bottom). Anomalies are departures from 1991-2020 base period monthly means.

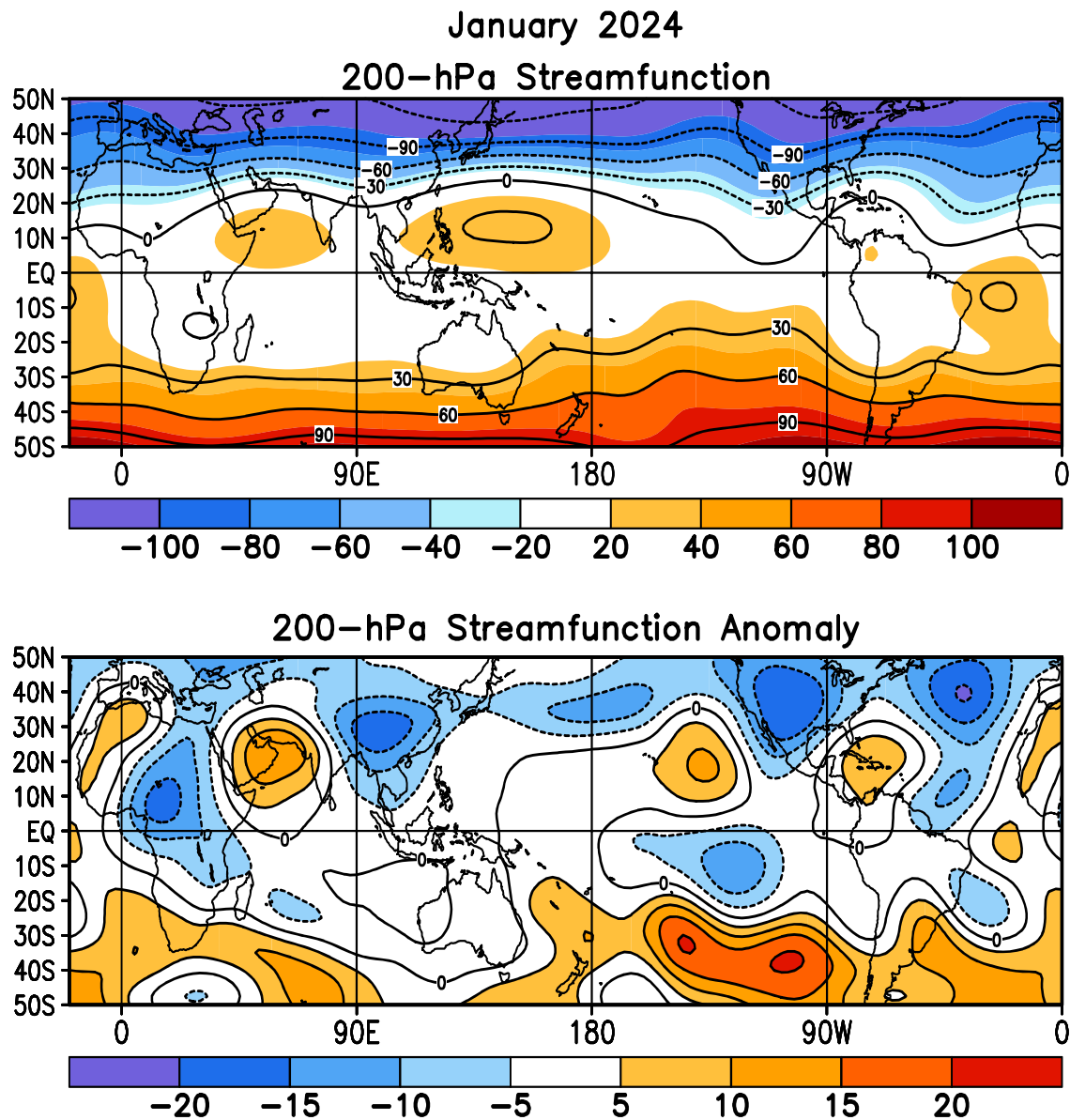


FIGURE T22. Mean (top) and anomalous (bottom) 200-hPa streamfunction (CDAS/Reanalysis). Contour interval is $20 \times 10^6 \text{ m}^2 \text{s}^{-1}$ (top) and $5 \times 10^6 \text{ m}^2 \text{s}^{-1}$ (bottom). Negative (positive) values are indicated by dashed (solid) lines. The non-divergent component of the flow is directed along the contours with speed proportional to the gradient. Thus, high (low) stream function corresponds to high (low) geopotential height in the Northern Hemisphere and to low (high) geopotential height in the Southern Hemisphere. Anomalies are departures from the 1991-2020 base period monthly means.

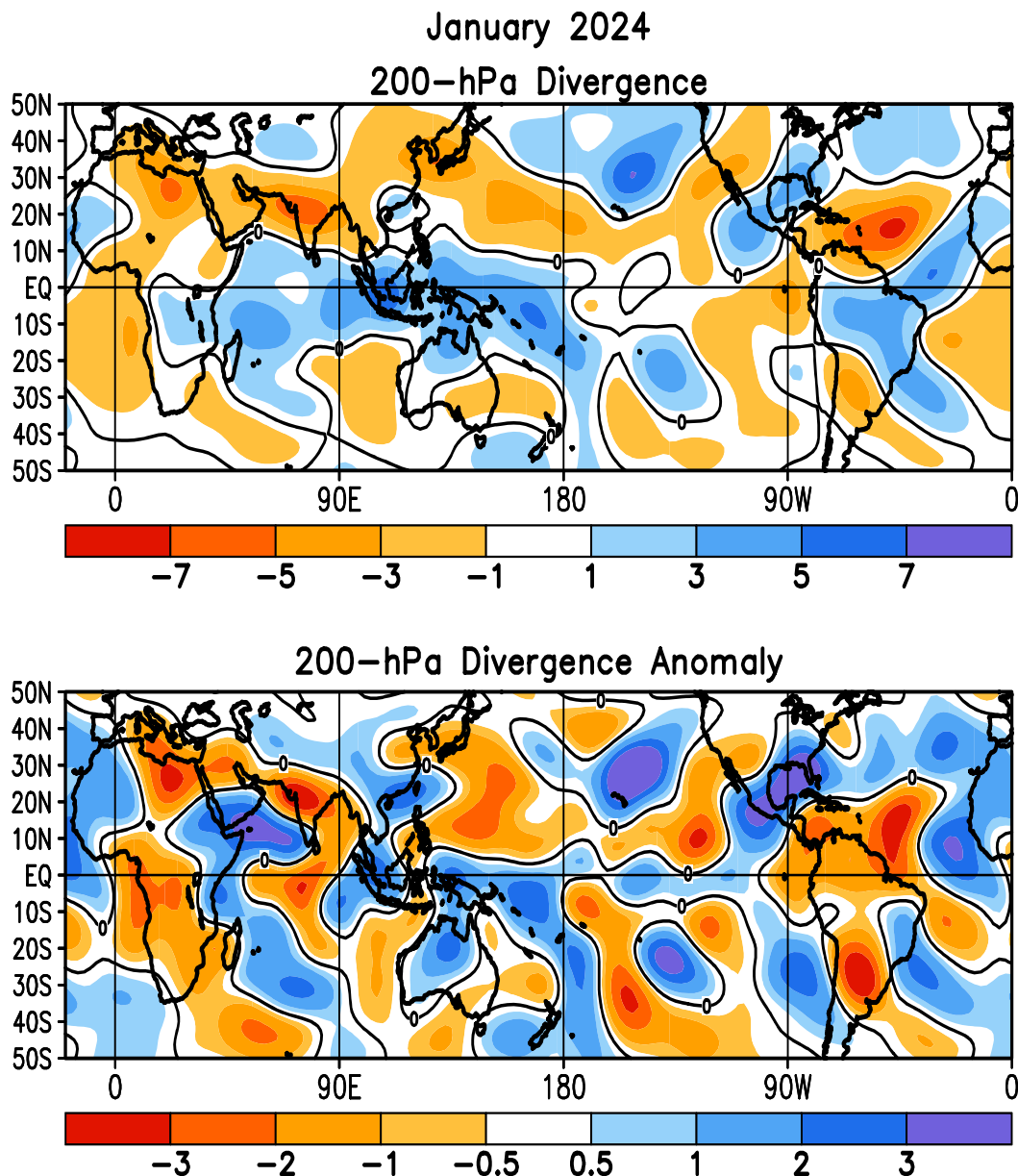


FIGURE T23. Mean (top) and anomalous (bottom) 200-hPa divergence (CDAS/Reanalysis). Divergence and anomalous divergence are shaded blue. Convergence and anomalous convergence are shaded orange. Anomalies are departures from the 1991-2020 base period monthly means.

January 2024

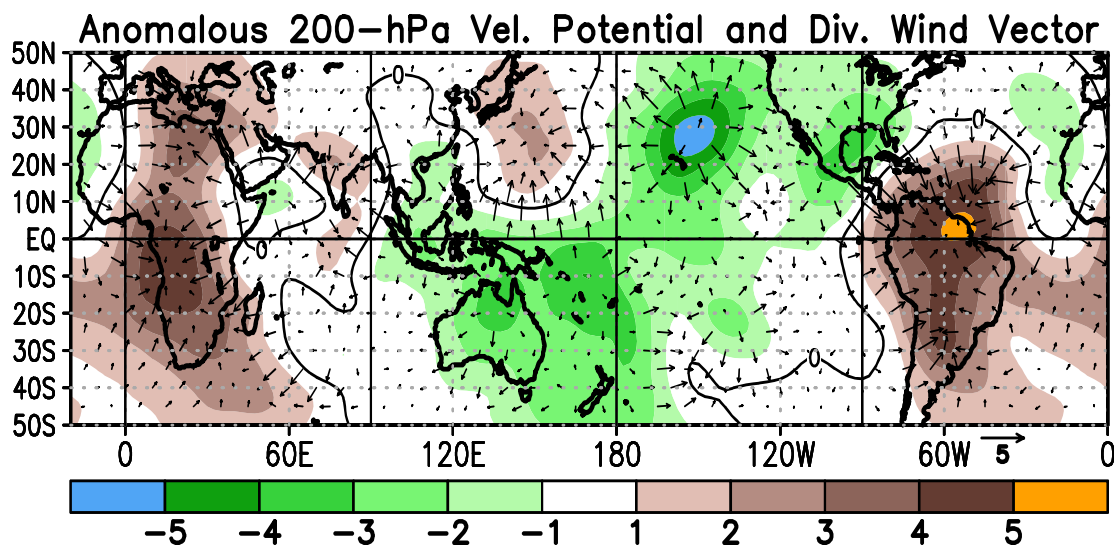
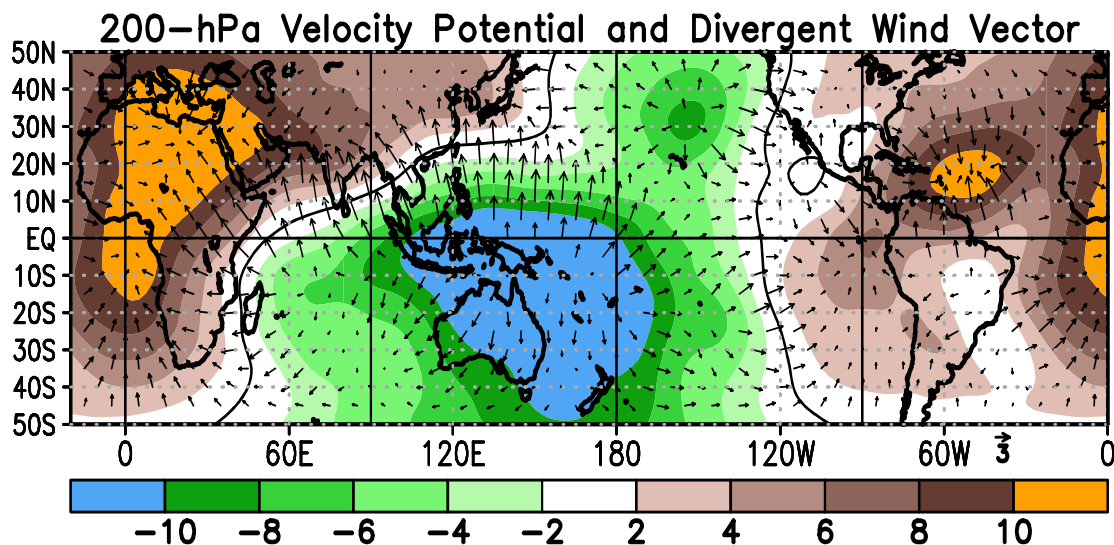


FIGURE T24. Mean (top) and anomalous (bottom) 200-hPa velocity potential ($10^6 \text{m}^2/\text{s}$) and divergent wind (CDAS/Reanalysis). Anomalies are departures from the 1991-2020 base period monthly means.

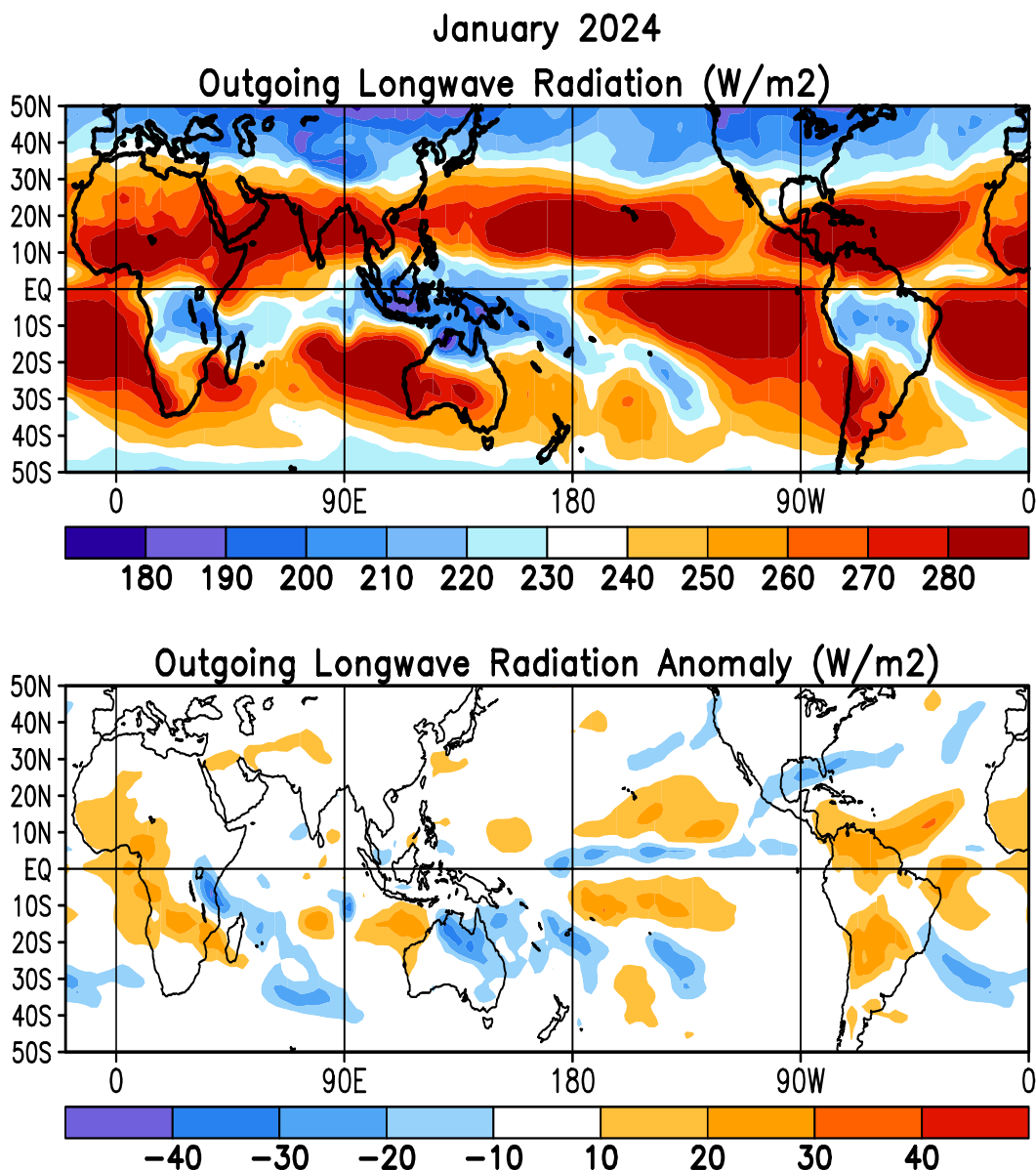


FIGURE T25. Mean (top) and anomalous (bottom) outgoing longwave radiation for JAN 2024 (NOAA 18 AVHRR IR window channel measurements by NESDIS/ORA). OLR contour interval is 20 W m^{-2} with values greater than 280 W m^{-2} indicated by dashed contours. Anomaly contour interval is 15 W m^{-2} with positive values indicated by dashed contours and light shading. Anomalies are departures from the 1991-2020 base period monthly means.

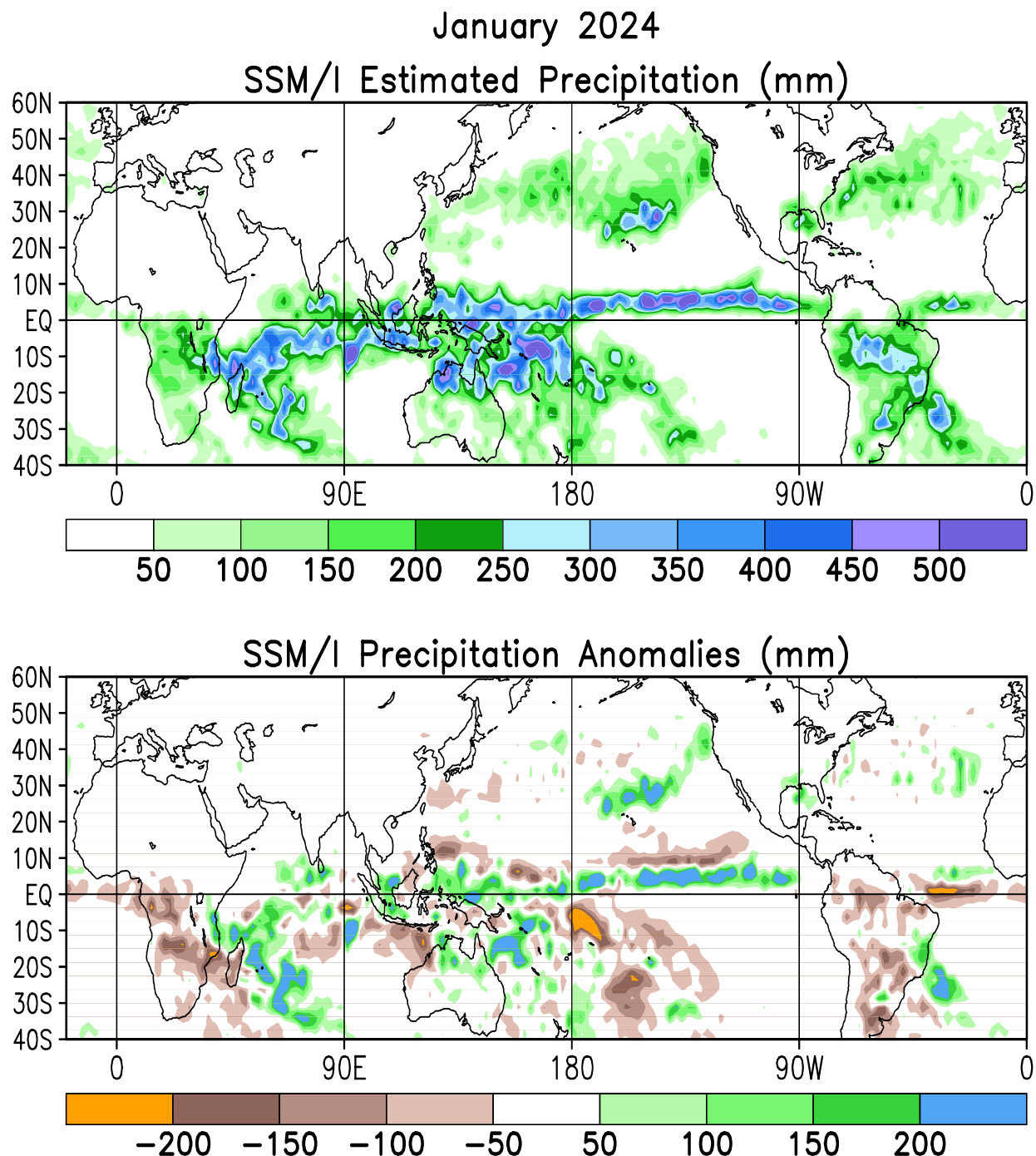
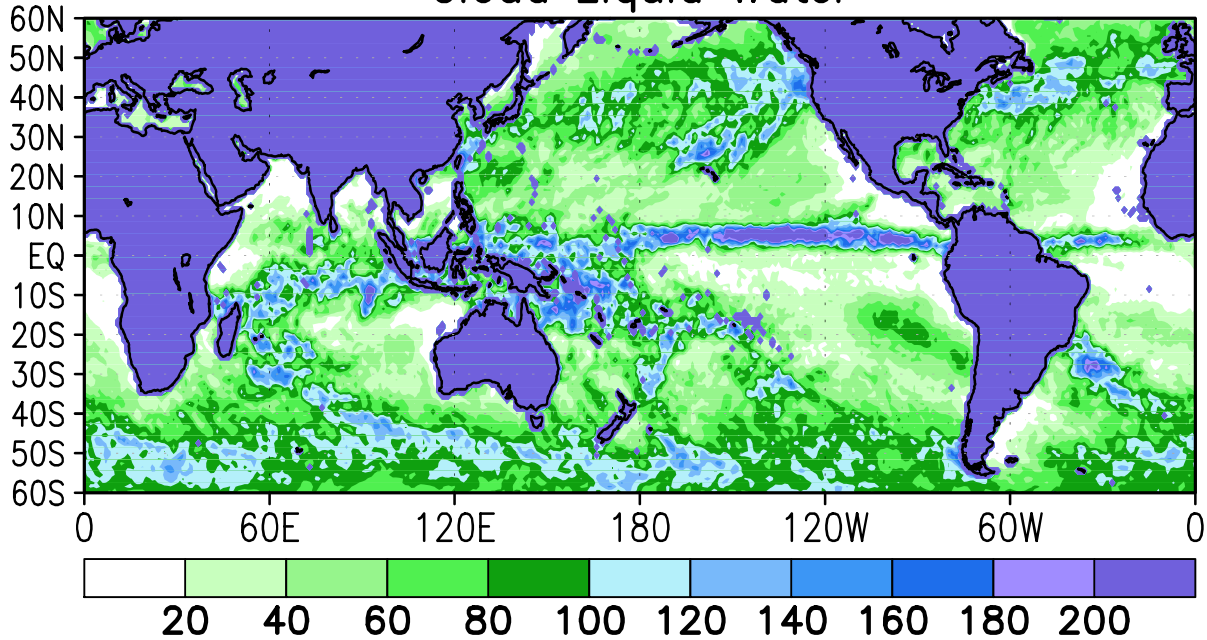


FIGURE T26. Estimated total (top) and anomalous (bottom) rainfall (mm) based on the Special Sensor Microwave/Imager (SSM/S) precipitation index (Ferraro 1997, *J. Geophys. Res.*, **102**, 16715–16735). Anomalies are computed from the SSM/I 1987–2010 base period monthly means. Anomalies have been smoothed for display purposes.

January 2024
Cloud Liquid Water



Cloud Liquid Water Anomaly

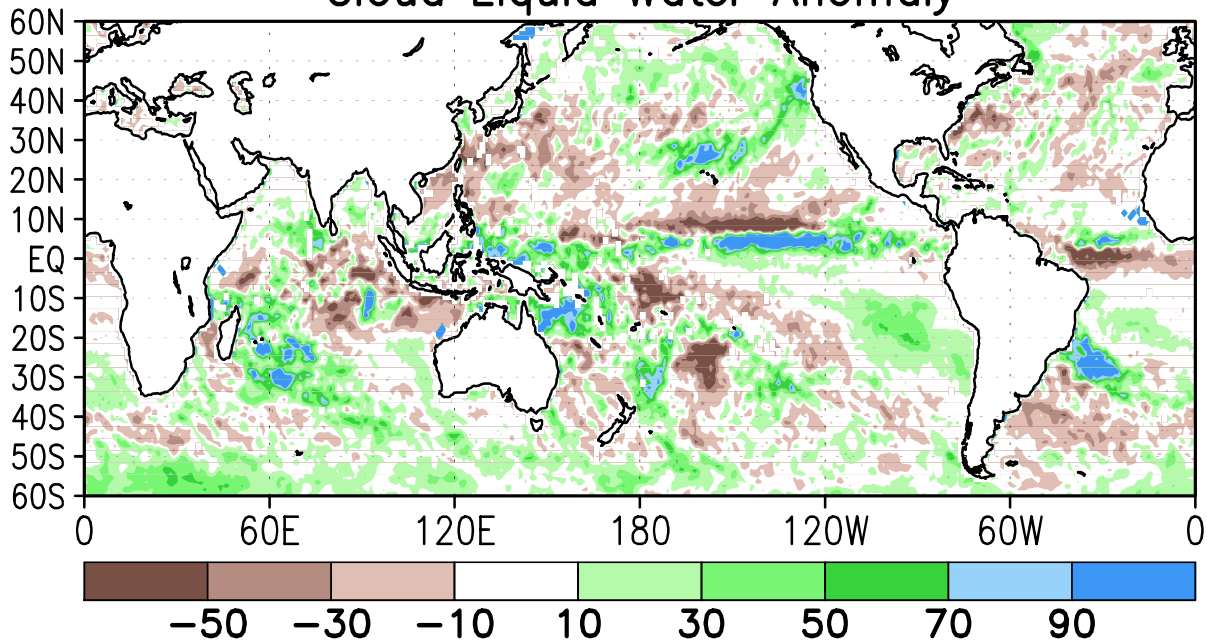


FIGURE T27. Mean (top) and anomalous (bottom) cloud liquid water (g m^{-2}) based on the Special Sensor Microwave/Imager (SSM/I) (Weng et al 1997: *J. Climate*, **10**, 1086-1098). Anomalies are calculated from the 1987-2010 base period means.

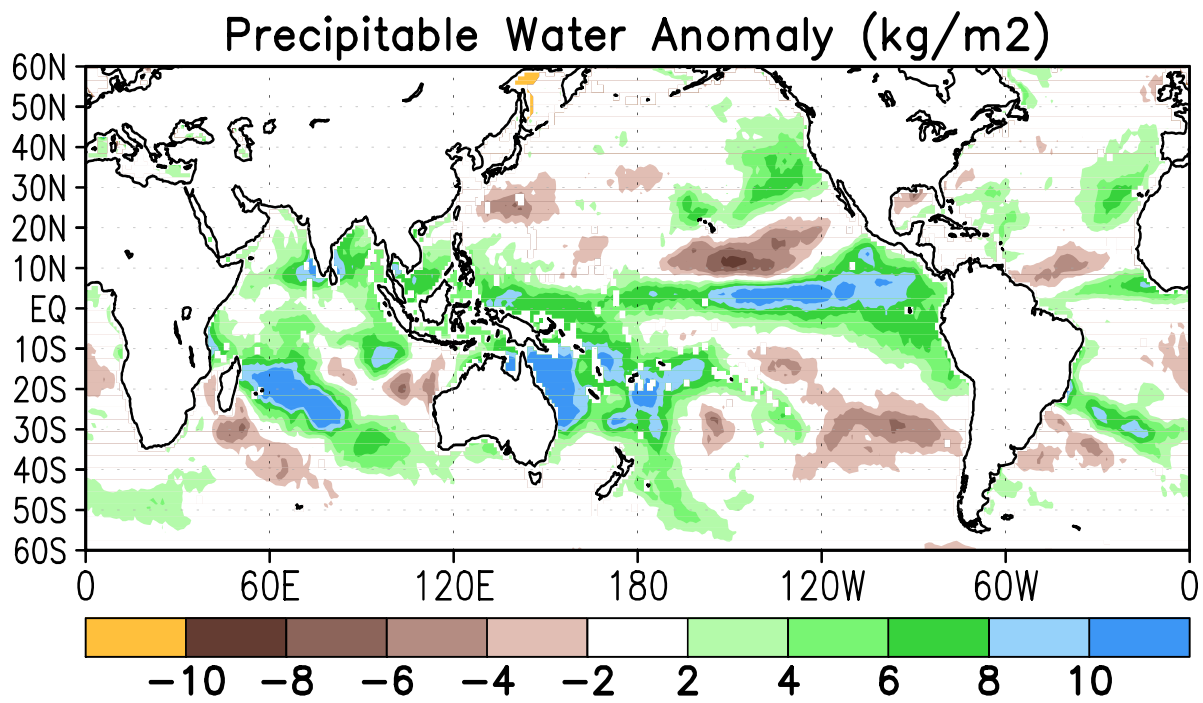
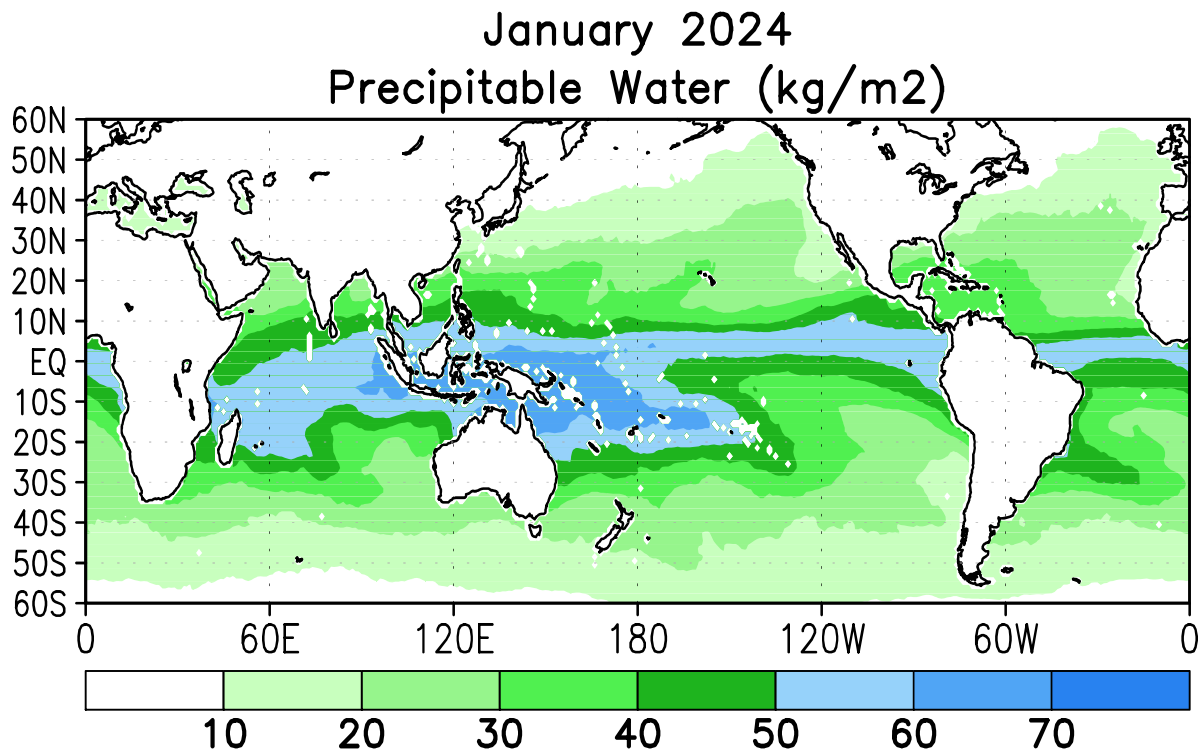


FIGURE T28. Mean (top) and anomalous (bottom) vertically integrated water vapor or precipitable water (kg m⁻²) based on the Special Sensor Microwave/Imager (SSM/I) (Ferraro et. al, 1996: *Bull. Amer. Meteor. Soc.*, 77, 891-905). Anomalies are calculated from the 1987-2010 base period means.

January 2024
Divergence and East–West Divergent Circulation

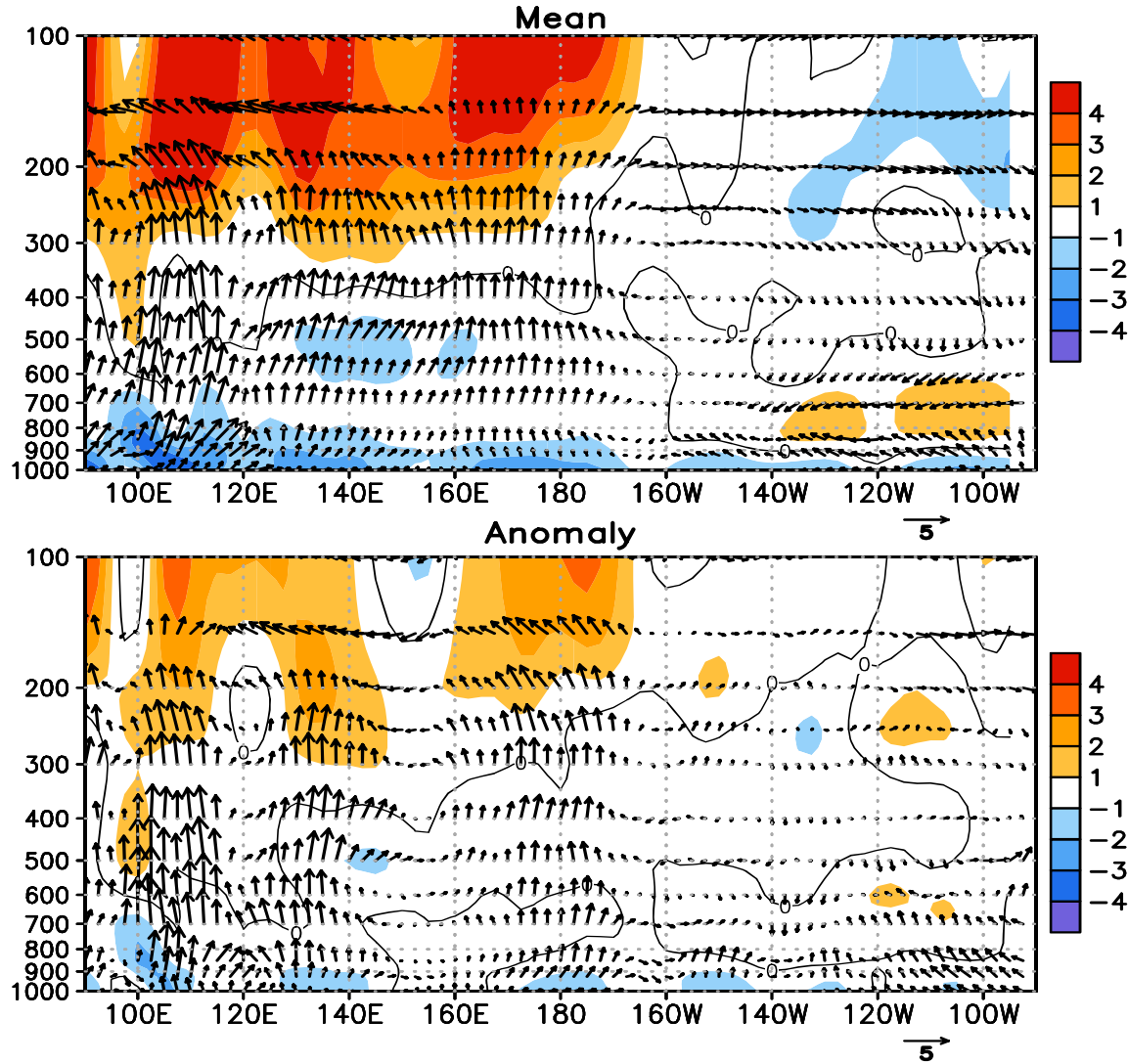


FIGURE T29. Pressure-longitude section (100E–80W) of the mean (top) and anomalous (bottom) divergence (contour interval is $1 \times 10^{-6} \text{ s}^{-1}$) and divergent circulation averaged between 5N–5S. The divergent circulation is represented by vectors of combined pressure vertical velocity and the divergent component of the zonal wind. Red shading and solid contours denote divergence (top) and anomalous divergence (bottom). Blue shading and dashed contours denote convergence (top) and anomalous convergence (bottom). Anomalies are departures from the 1991–2020 base period monthly means.

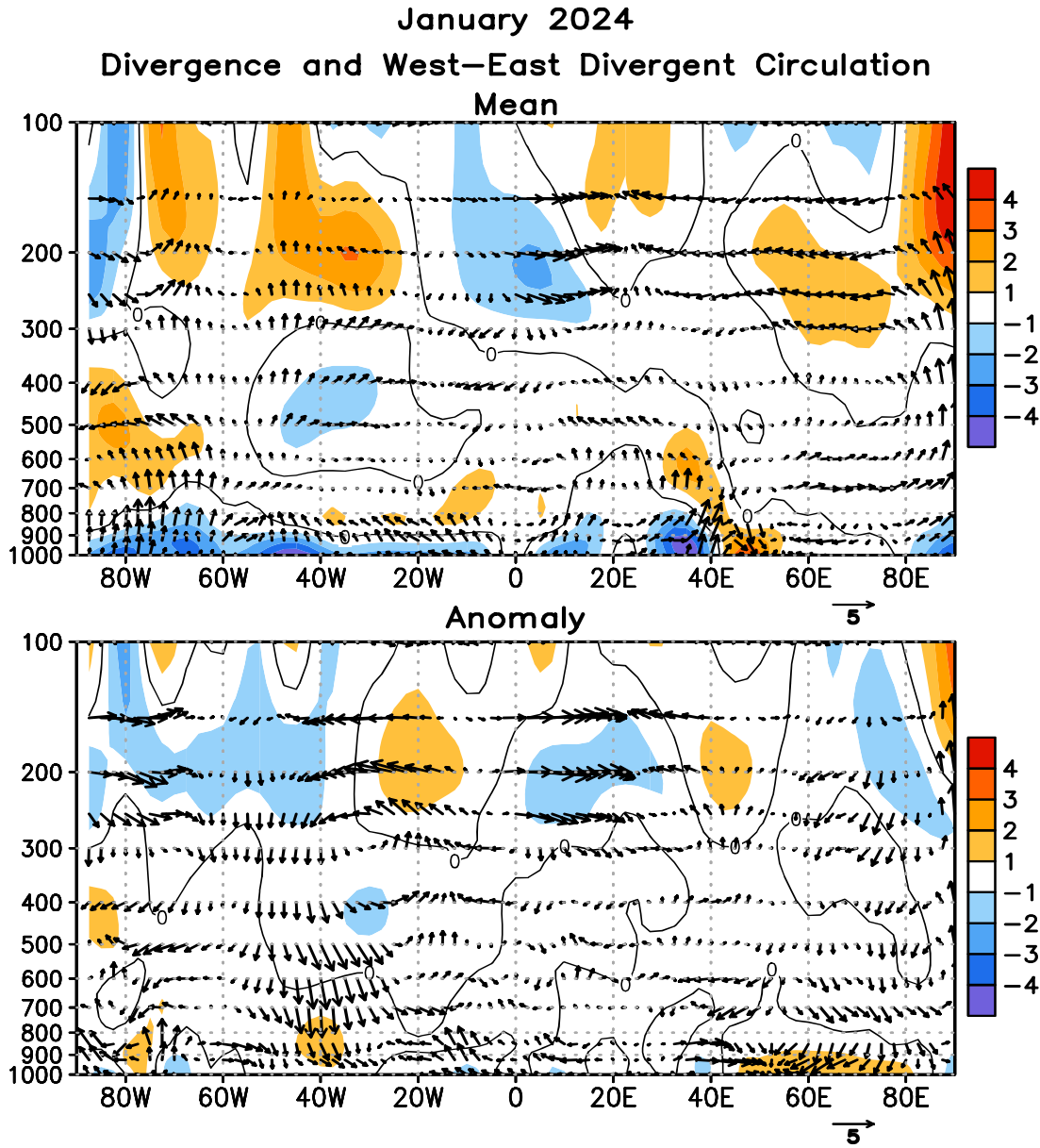


FIGURE T30. Pressure-longitude section (80W-100E) of the mean (top) and anomalous (bottom) divergence (contour interval is $1 \times 10^{-6} \text{ s}^{-1}$) and divergent circulation averaged between 5N-5S. The divergent circulation is represented by vectors of combined pressure vertical velocity and the divergent component of the zonal wind. Red shading and solid contours denote divergence (top) and anomalous divergence (bottom). Blue shading and dashed contours denote convergence (top) and anomalous convergence (bottom). Anomalies are departures from the 1991-2020 base period monthly means.

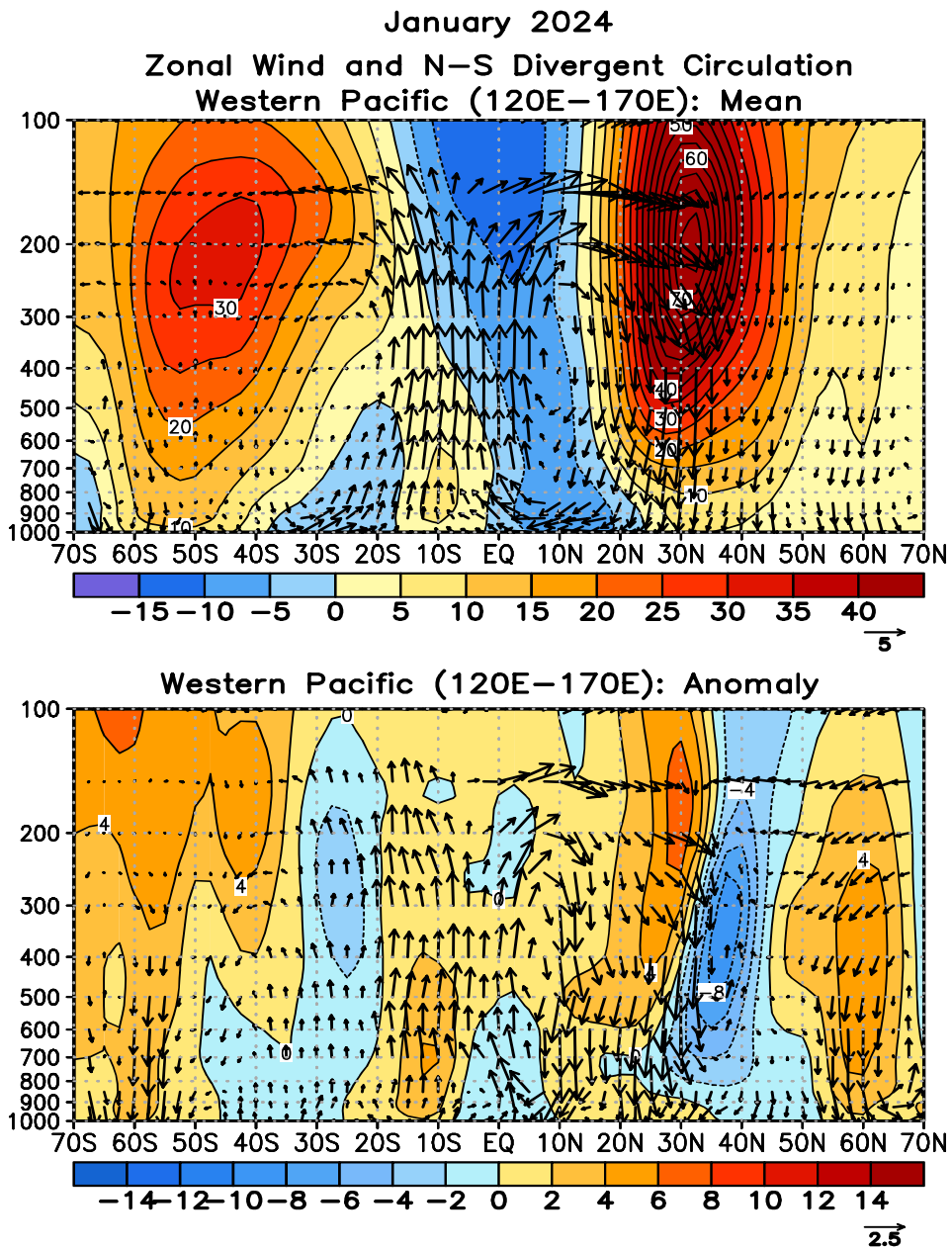


FIGURE T31. Pressure-latitude section of the mean (top) and anomalous (bottom) zonal wind (m s^{-1}) and divergent circulation averaged over the west Pacific sector (120E–170E). The divergent circulation is represented by vectors of combined pressure vertical velocity and the divergent component of the meridional wind. Red shading and solid contours denote a westerly (top) or anomalous westerly (bottom) zonal wind. Blue shading and dashed contours denote an easterly (top) or anomalous easterly (bottom) zonal wind. Anomalies are departures from the 1991–2020 base period monthly means.

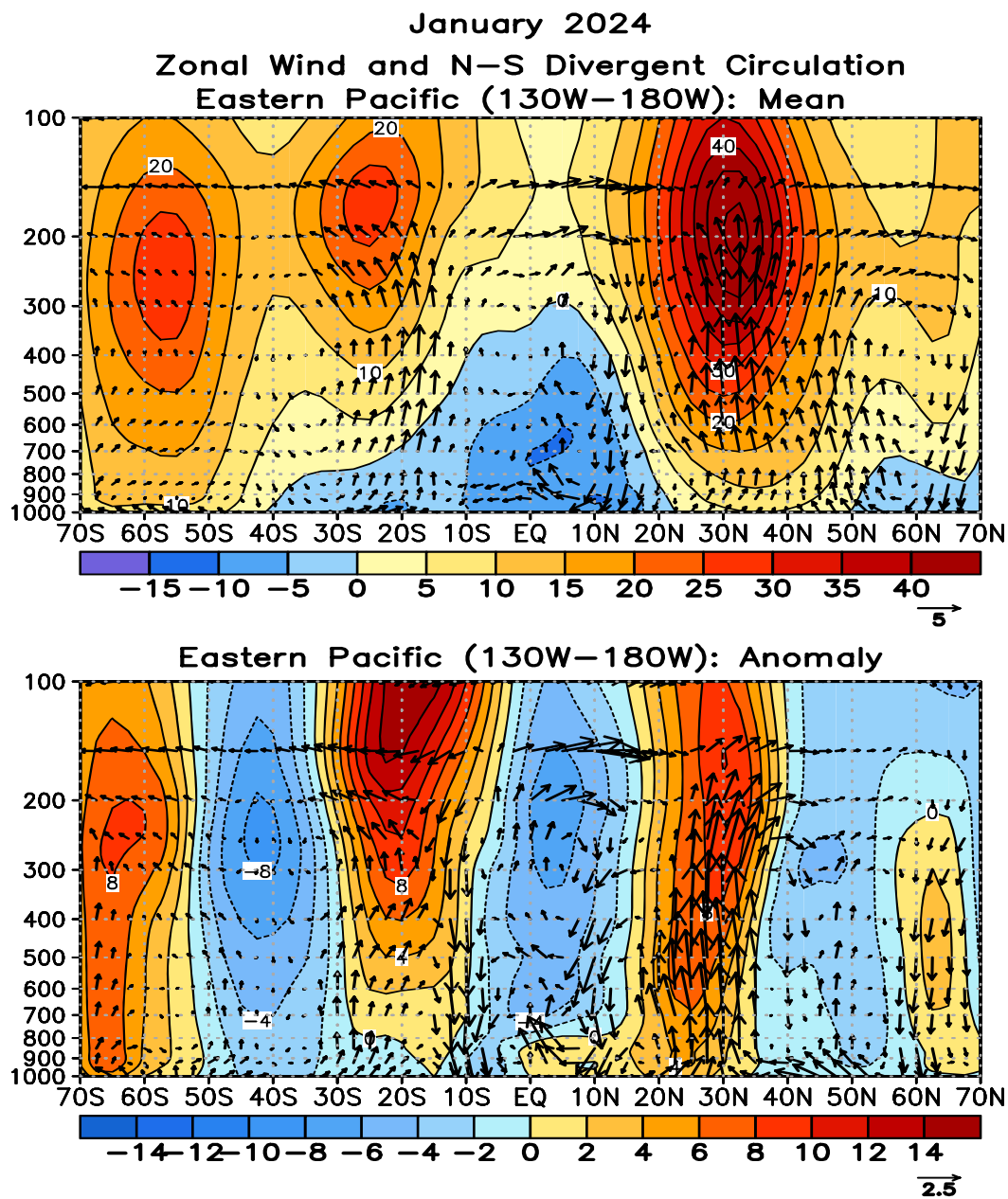


FIGURE T32. Pressure-latitude section of the mean (top) and anomalous (bottom) zonal wind (m s^{-1}) and divergent circulation averaged over the central Pacific sector (130W-180W). The divergent circulation is represented by vectors of combined pressure vertical velocity and the divergent component of the meridional wind. Red shading and solid contours denote a westerly (top) or anomalous westerly (bottom) zonal wind. Blue shading and dashed contours denote an easterly (top) or anomalous easterly (bottom) zonal wind. Anomalies are departures from the 1991-2020 base period monthly means.

During January 2024, 217 satellite-tracked surface drifting buoys were reporting from the tropical Pacific. Several drifters in the region 3-6N, 100-170W indicated eastward anomalies of 25-40 cm/s, indicating a strengthened and southward-shifted North Equatorial Countercurrent. This pattern has persisted since October 2023.

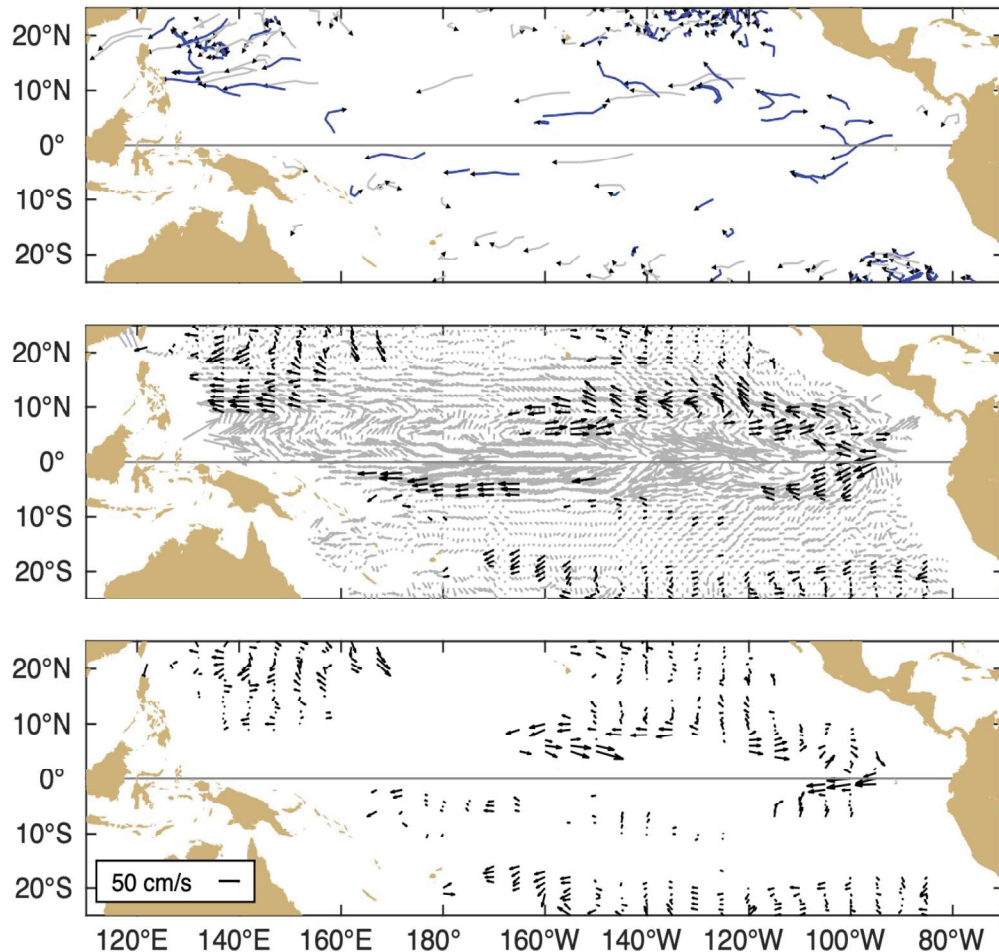


Figure A1.1 Top: Movements of drifting buoys in the tropical Pacific Ocean during January 2024. The linear segments of each trajectory represent a one week displacement. Trajectories of buoys which have lost their subsurface drogues are gray; those with drogues are black.

Middle: Monthly mean currents calculated from all buoys 1993-2002 (gray), and currents measured by the drogued buoys this month (black) smoothed by an optimal filter.

Bottom: Anomalies from the climatological monthly mean currents for this month.

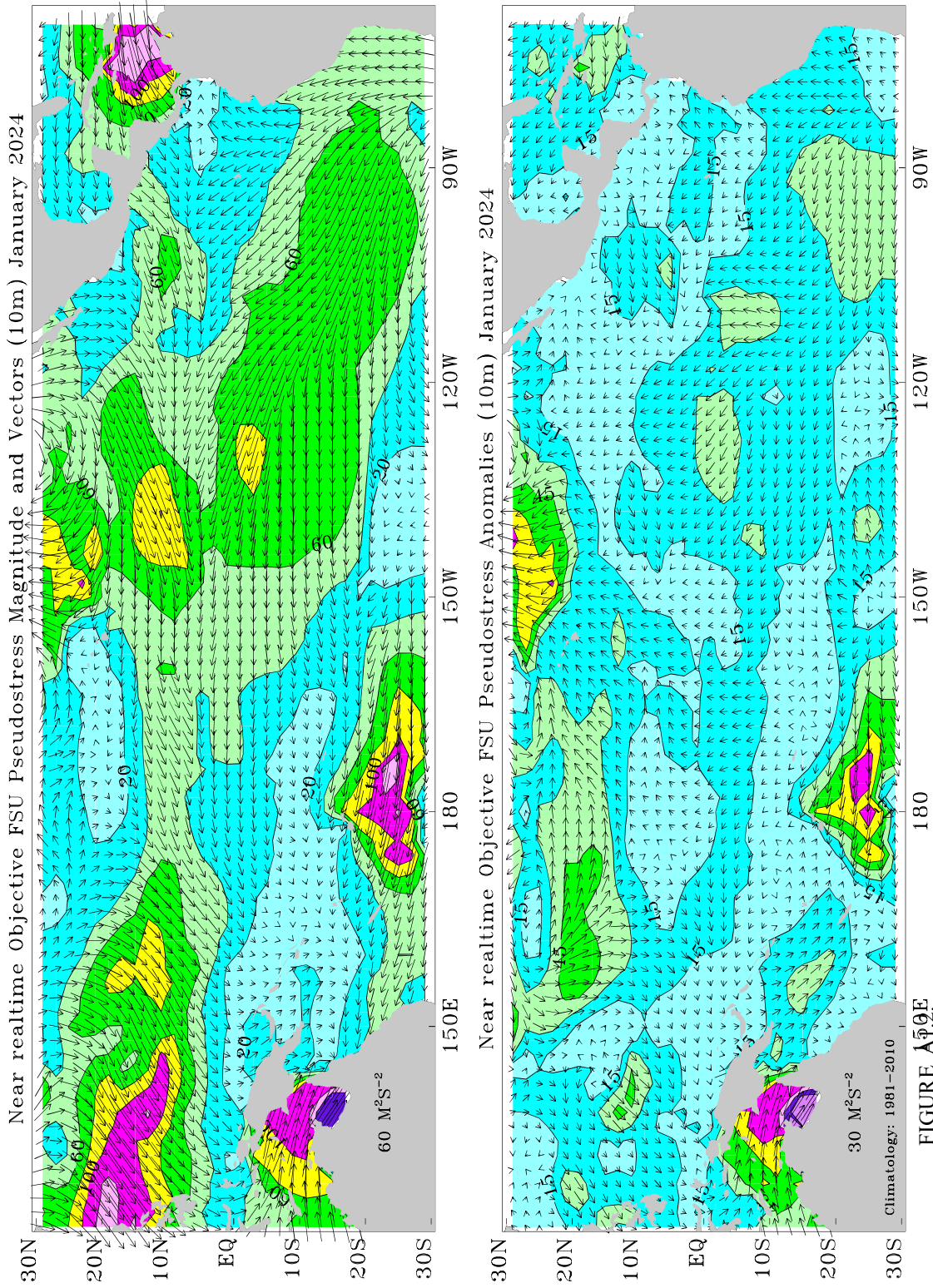


FIGURE A $\tilde{\Phi}$ 2E.

FSU SURFACE PSEUDO-STRESS VECTORS AND ANOMALIES: January 2024. Pseudo-stress vectors (top) are objectively analyzed from ship and buoy winds on a 2° grid. Ship and buoy data are independently weighted and the background field is created from the data. Contour interval of the vector magnitude is $20 M^2 S^{-2}$. Anomalies (bottom) are departures from $1981\text{--}2010$ mean. The contour interval is $15 M^2 S^{-2}$. For more information, please visit our web site at <http://www.coaps.fsu.edu/RVSMDC/html/winds.shtml>. Produced by Shawn R. Smith and Mark A. Bourassa, Center for Ocean-Atmospheric Prediction Studies, Florida State University, Tallahassee, FL 32306-2840, USA.

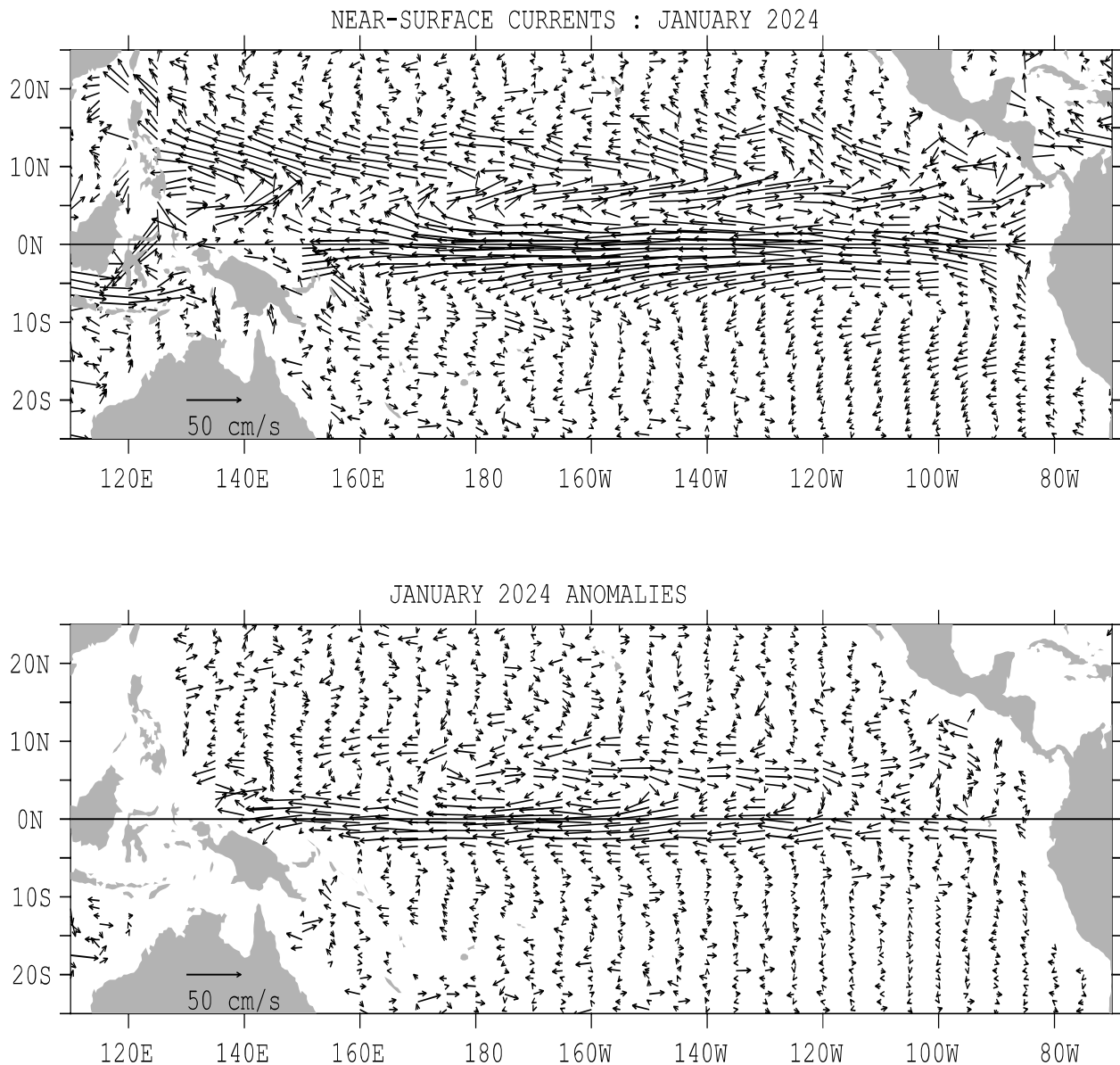


FIGURE A1.3. Ocean Surface Current Analysis-Real-time (OSCAR) for JAN 2024 (Bonjean and Lagerloef 2002, J. Phys. Oceanogr., Vol. 32, No. 10, 2938-2954; Lagerloef et al. 1999, JGR-Oceans, 104, 23313-23326). (top) Total velocity. Surface currents are calculated from satellite data including Jason sea level anomalies and NCEP winds. (bottom) Velocity anomalies. The subtracted climatology was based on SSM/I and QuickScat winds and Topex/Poseidon and Jason from 1993-2003. See also <http://www.oscar.noaa.gov>.

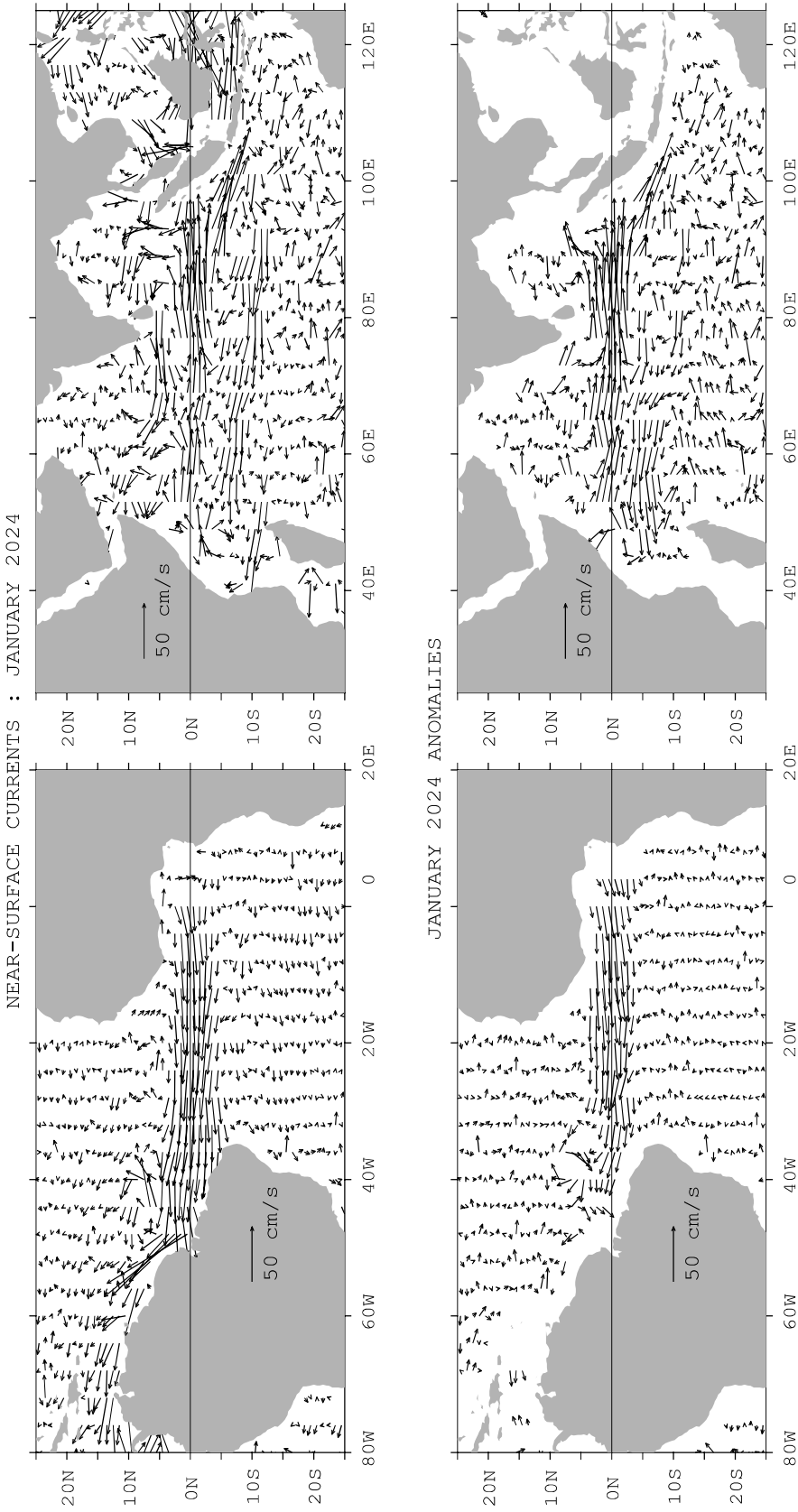


FIGURE A1.4. Ocean Surface Current Analysis-Real-time (OSCAR) for JAN 2024 (Bonjean and Lagerloef 2002, J. Phys. Oceanogr., Vol. 32, No. 10, 2938-2954; Lagerloef et al. 1999, JGR-Oceans, 104, 23313-23326). (top) Total velocity. Surface currents are calculated from satellite data including Jason sea level anomalies and NCEP winds. (bottom) Velocity anomalies. The subtracted climatology was based on SSM/I and QuickScat winds and Topex/Poseidon and Jason from 1993-2003. See also <http://www.oscar.noaa.gov>.

Forecast Forum

The canonical correlation analysis (CCA) forecast of SST in the central Pacific (Barnett et al. 1988, *Science*, **241**, 192196; Barnston and Ropelewski 1992, *J. Climate*, **5**, 13161345), is shown in **Figs. F1 and F2**. This forecast is produced routinely by the Prediction Branch of the Climate Prediction Center. The predictions from the National Centers for Environmental Prediction (NCEP) Coupled Forecast System Model (CFS03) are presented in **Figs. F3 and F4a, F4b**. Predictions from the Markov model (Xue, et al. 2000: *J. Climate*, **13**, 849871) are shown in **Figs. F5 and F6**. Predictions from the latest version of the LDEO model (Chen et al. 2000: *Geophys. Res. Lett.*, **27**, 25852587) are shown in **Figs. F7 and F8**. Predictions from the ENSO CLIPER statistical model (Knaff and Landsea 1997, *Wea. Forecasting*, **12**, 633 652) are shown in **Fig. F9**. Niño 3.4 predictions are summarized in **Fig. F10**, provided by the Forecasting and Prediction Research Group of the IRI.

The CPC and the contributors to the **Forecast Forum** caution potential users of this predictive information that they can expect only modest skill.

ENSO Alert System Status: El Niño Advisory

Outlook

A transition from El Niño to ENSO-neutral is likely by April-June 2024 (79% chance), with increasing odds of La Niña developing in June-August 2024 (55% chance).

Discussion

During January 2024, above-average sea surface temperatures (SST) continued across most of the equatorial Pacific Ocean (Fig. T18). SST anomalies weakened slightly in the eastern and east-central Pacific, as indicated by the monthly Niño index values (Table T2). However, changes were more pronounced below the surface of the equatorial Pacific Ocean, with area-averaged subsurface temperature anomalies returning to near zero. Although above-average temperatures persisted in the upper 100 meters of the equatorial Pacific, below-average temperatures were widespread at greater depths (Fig. T17). Atmospheric anomalies across the tropical Pacific also weakened during January. Low-level winds were near average over the equatorial Pacific, while upper-level wind anomalies were easterly over the east-central Pacific (Figs. T20 & T21). Convection remained slightly enhanced near the Date Line and was close to average around Indonesia (Fig. T25). Collectively, the coupled ocean-atmosphere system reflected a weakening El Niño.

The most recent IRI plume indicates a transition to ENSO-neutral during spring 2024, with La Niña potentially developing during summer 2024 (Figs. F1-F12). Even though forecasts made through the spring season tend to be less reliable, there is a historical tendency for La Niña to follow strong El Niño events. The forecast team is in agreement with the latest model guidance, with some

uncertainty around the timing of transitions to ENSO-neutral and, following that, La Niña. Even as the current El Niño weakens, impacts on the United States could persist through April 2024 (see CPC seasonal outlooks for probabilities of temperature and precipitation). In summary, a transition from El Niño to ENSO-neutral is likely by April-June 2024 (79% chance), with increasing odds of La Niña developing in June-August 2024 (55% chance).

Weekly updates of oceanic and atmospheric conditions are available on the Climate Prediction Center homepage ([El Niño/La Niña Current Conditions and Expert Discussions](#)).

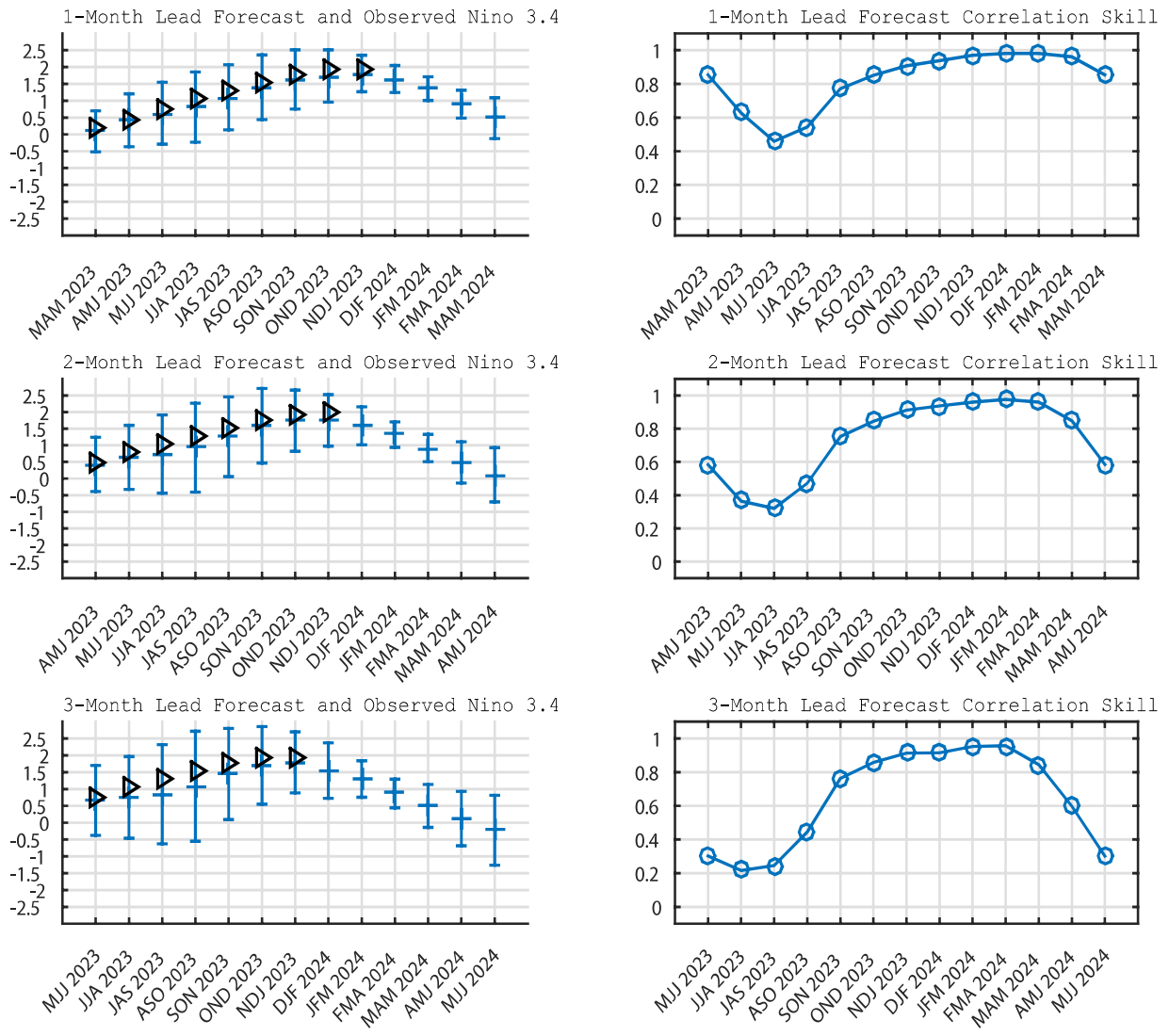


FIGURE F1. Canonical correlation analysis (CCA) sea surface temperature (SST) anomaly prediction for the central Pacific (5N to 5S, 120W to 170W (Barnston and Ropelewski, 1992, *i* J. Climate, 5, 1316-1345)). The three plots on the left are, from top to bottom, the 1-month, 2-month, and 3-month lead seasonal forecasts from the past 12 months plus the current month. The triangles in each plot are the observed SST anomaly through the latest available season. The lines at the mid-points of the forecast error bars represent the real-time CCA predictions based on the anomalies of quasi-global sea level pressure, the anomalies of tropical Pacific SST, and heat content of the upper 300 meters of the near-equator tropical Pacific (10S to 10N). The vertical lines represent the two standard deviation error bars for the predictions based on past performance. The three plots on the right are skill values for the corresponding seasons, from the correlations of the predicted and observed SST in the prior 10 years of simulated real-time forecasts. Skill values show a clear annual cycle and are inversely proportional to the length of the error bars depicted in the forecast time series.

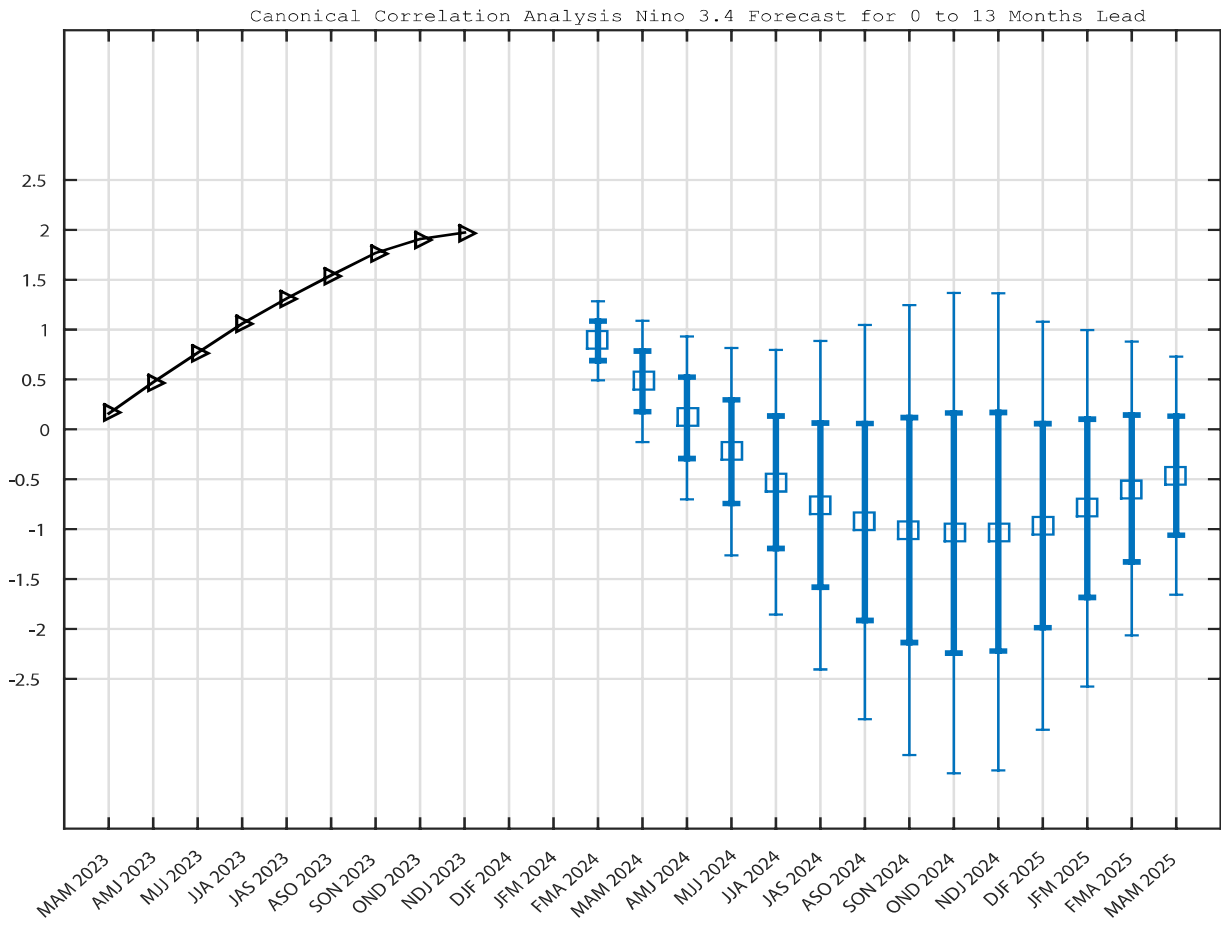


FIGURE F2. Canonical Correlation Analysis (CCA) forecast of sea-surface temperature anomalies for the Nino 3.4 region (5°N - 5°S , 120°W - 170°W) for the upcoming year of three-month overlapping periods. The CCA predictions are based on anomaly patterns of sea level pressure, tropical Pacific SST, and heat content of the upper 300 meters of the near-equator tropical Pacific (10°S to 10°N). Small squares at the midpoints of the vertical forecast bars represent the CCA predictions, and the bars show the one (thick) and two (thin) standard deviation errors. The triangles and line represent the observed three-month mean SST anomaly in the Nino 3.4 region up to the most recently available data.

Last update: Fri Feb 2 2024
Initial condition: 23Jan2024–01Feb2024

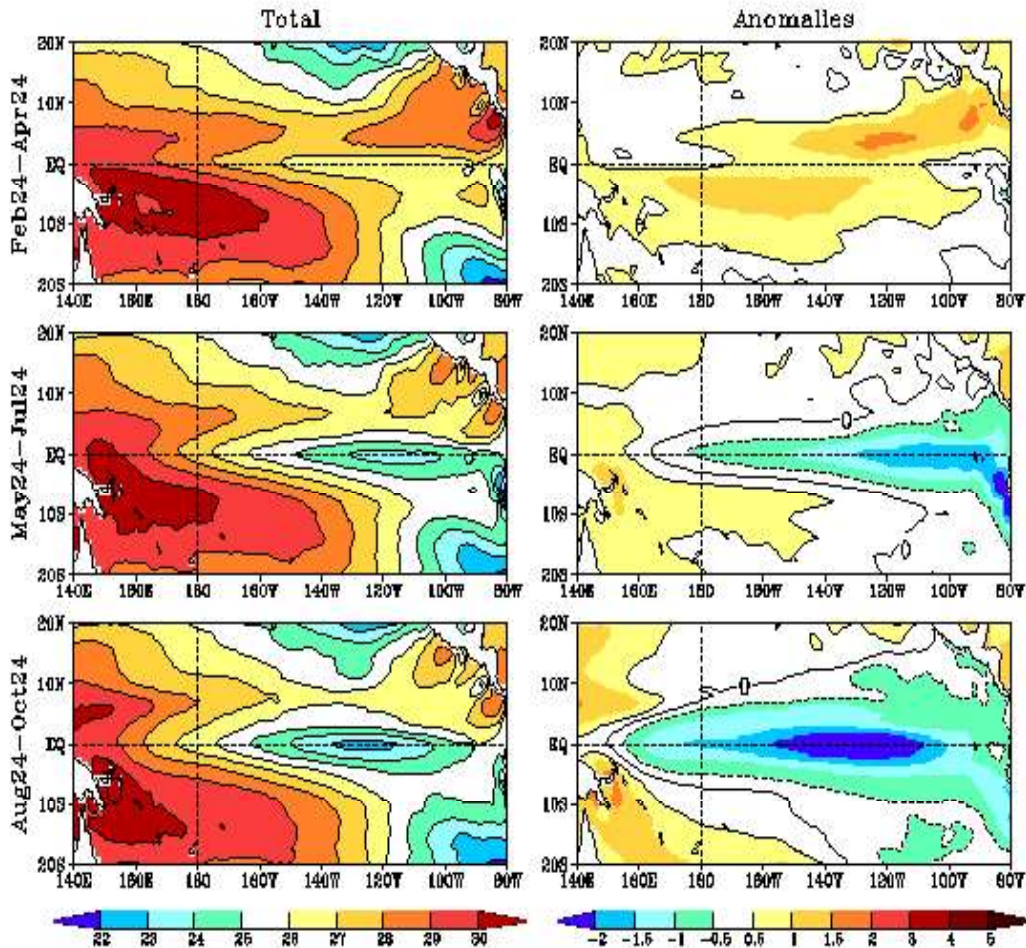


FIGURE F3. Predicted 3-month average sea surface temperature (left) and anomalies (right) from the NCEP Coupled Forecast System Model (CFS03). The forecasts consist of 40 forecast members. Contour interval is 1°C, with additional contours for 0.5°C and -0.5°C. Negative anomalies are indicated by dashed contours.

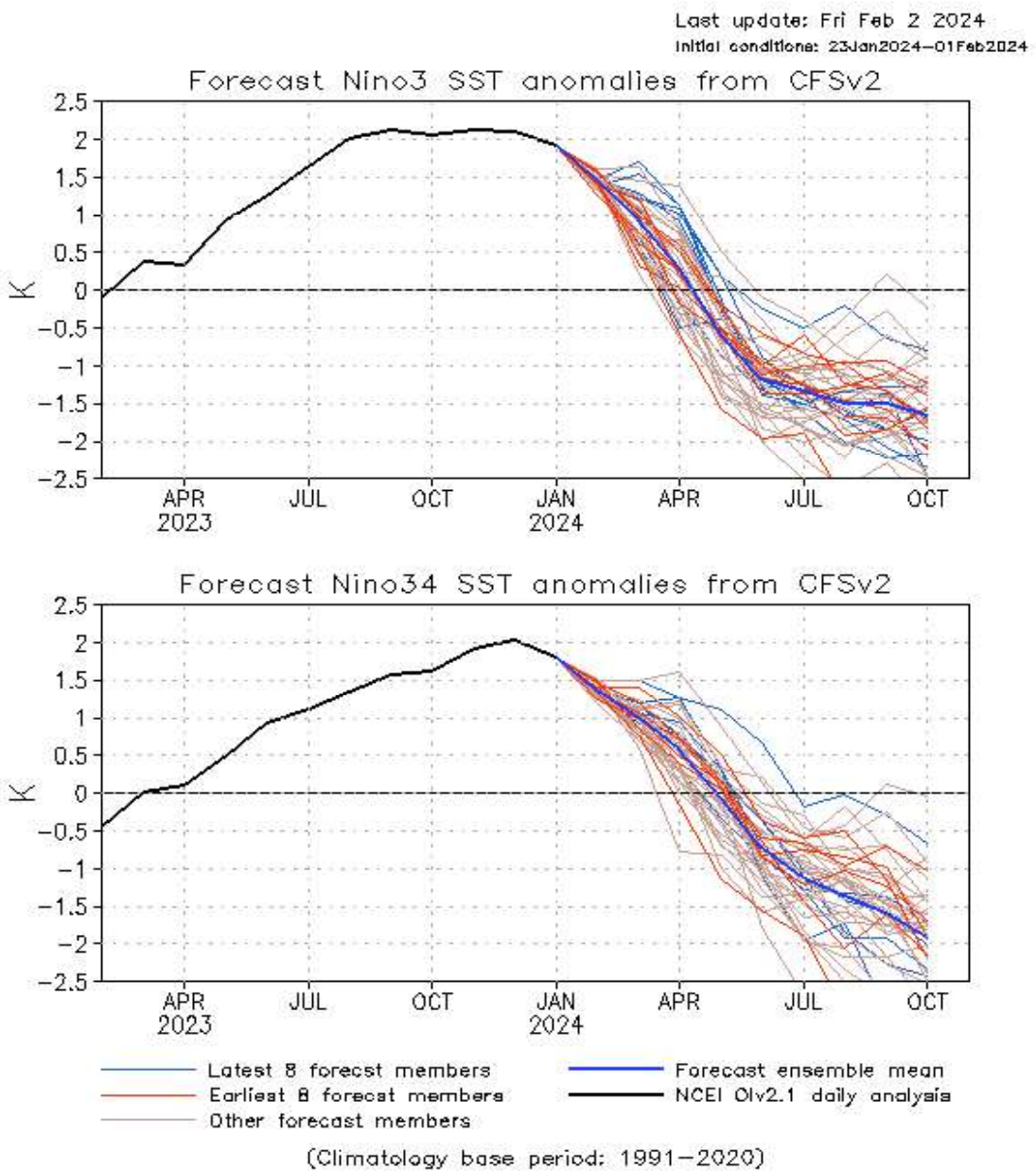


FIGURE F4. Predicted and observed sea surface temperature (SST) anomalies for the Nino 3 (top) and Nino 3.4 (bottom) regions from the NCEP Coupled Forecast System Model (CFS03). The forecasts consist of 40 forecast members. The ensemble mean of all 40 forecast members is shown by the blue line, individual members are shown by thin lines, and the observation is indicated by the black line. The Nino-3 region spans the eastern equatorial Pacific between 5N-5S, 150W-90W. The Nno 3.4 region spans the east-central equatorial Pacific between 5N-5S, 170W-120W.

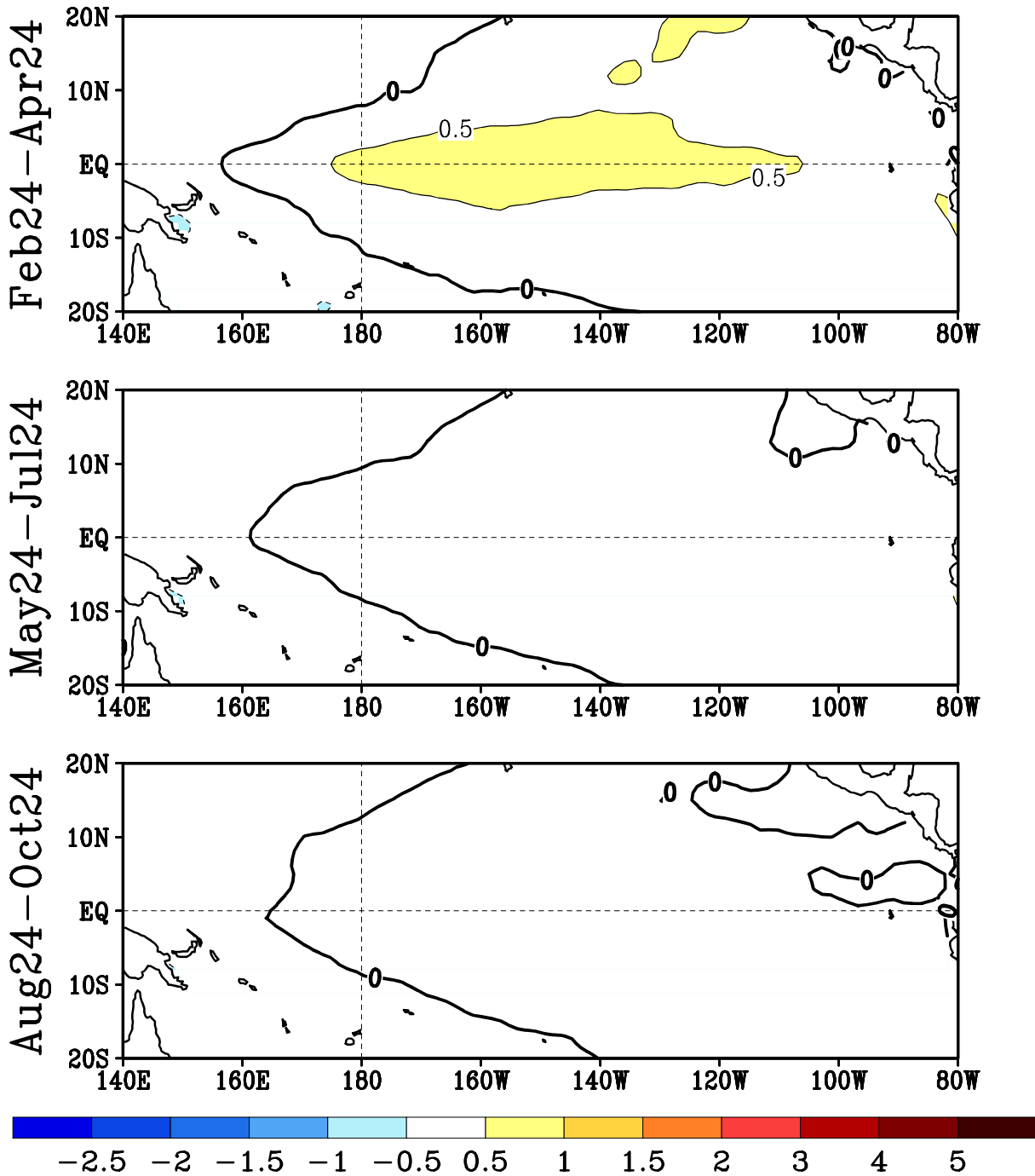


FIGURE F5. Predicted 3-month average sea surface temperature anomalies from the NCEP/CPC Markov model (Xue et al. 2000, *J. Climate*, **13**, 849–871). The forecast is initiated in JAN 2024 . Contour interval is 0.3C and negative anomalies are indicated by dashed contours. Anomalies are calculated relative to the 1971–2000 climatology.

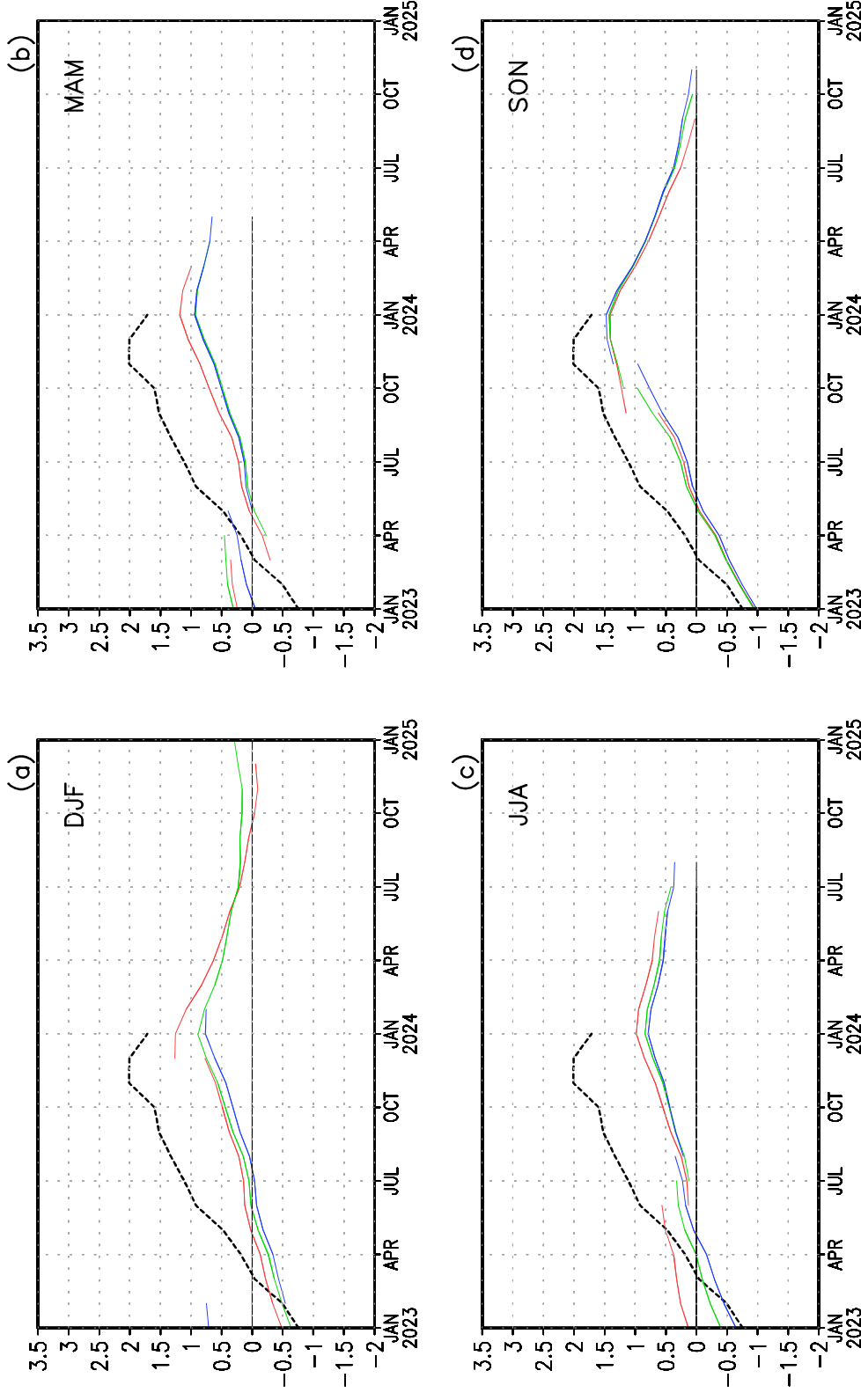


FIGURE F6. Time evolution of observed and predicted SST anomalies in the Niño 3.4 region (up to 12 lead months) by the NCEP/CPC Markov model (Xue et al. 2000, *J. Climate*, **13**, 849–871). Anomalies are calculated relative to the 1971–2000 climatology. Shown in each panel are the forecasts grouped by three consecutive starting months: (a) is for December, January, and February, (b) is for March, April, and May, (c) is for June, July, and August, and (d) is for September, October, and November. The observed Niño 3.4 SST anomalies are indicated by the black dashed lines. The Niño 3.4 region spans the east-central equatorial Pacific between 5N–5S, 170W–120W.

LDEO FORECASTS OF SST AND WIND STRESS ANOMALIES

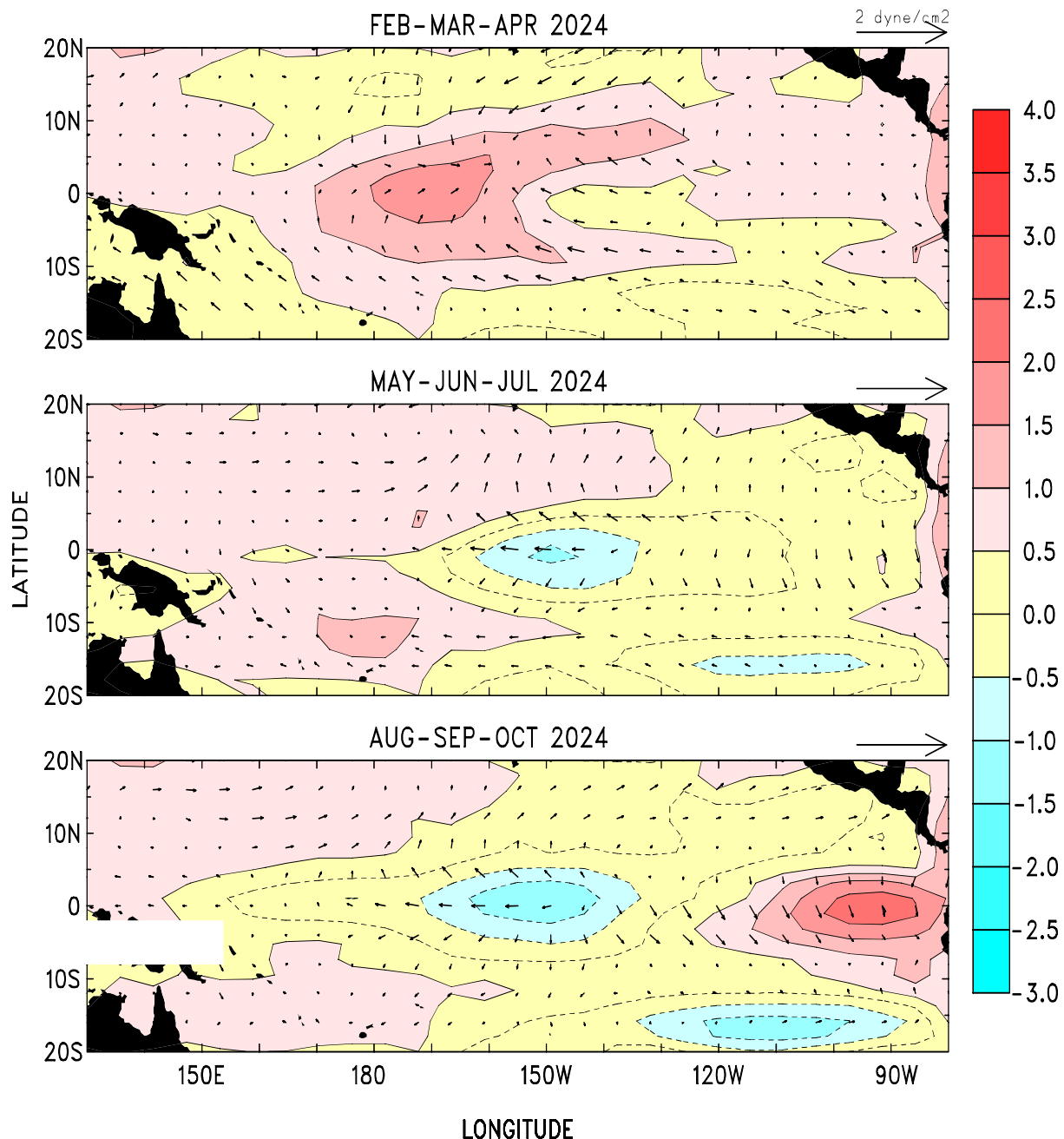


FIGURE F7. Forecasts of the tropical Pacific Predicted SST (shading) and vector wind anomalies for the next 3 seasons based on the LDEO model. Each forecast represents an ensemble average of 3 sets of predictions initialized during the last three consecutive months (see Figure F8).

LDEO FORECASTS OF NIN03

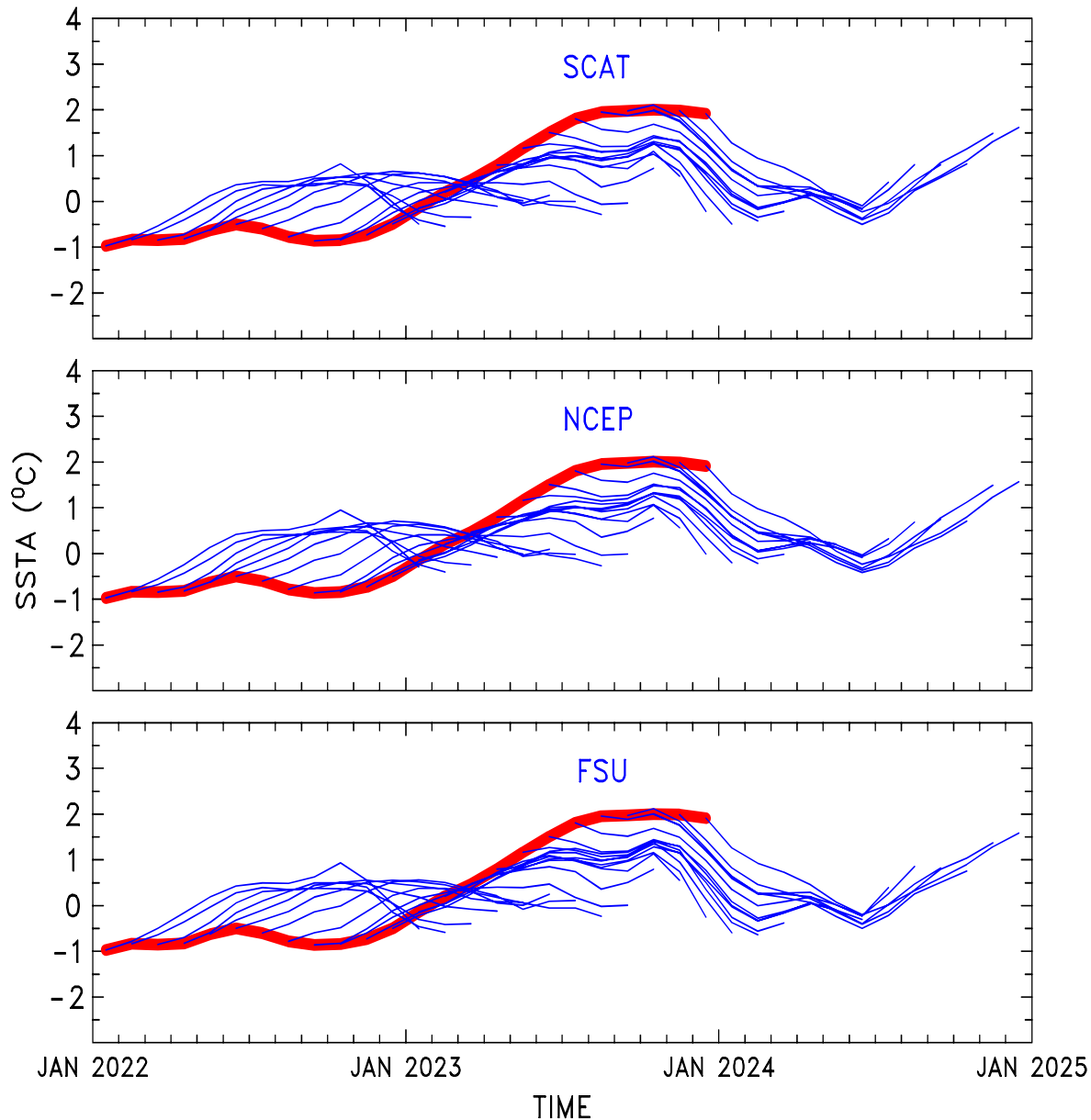


FIGURE F8. LDEO forecasts of SST anomalies for the Nino 3 region using wind stresses obtained from (top) Qui-kSCAT, (middle) NCEP, and (bottom) Florida State Univ. (FSU), along with SSTs (obtained from NCEP), and sea surface height data (obtained from TOPEX/POSEIDON) data. Each thin blue line represents a 12-month forecast, initialized one month apart for the past 24 months. Observed SST anomalies are indicated by the thick red line. The Nino-3 region spans the eastern equatorial Pacific between 5N-5S, 150W-90W.

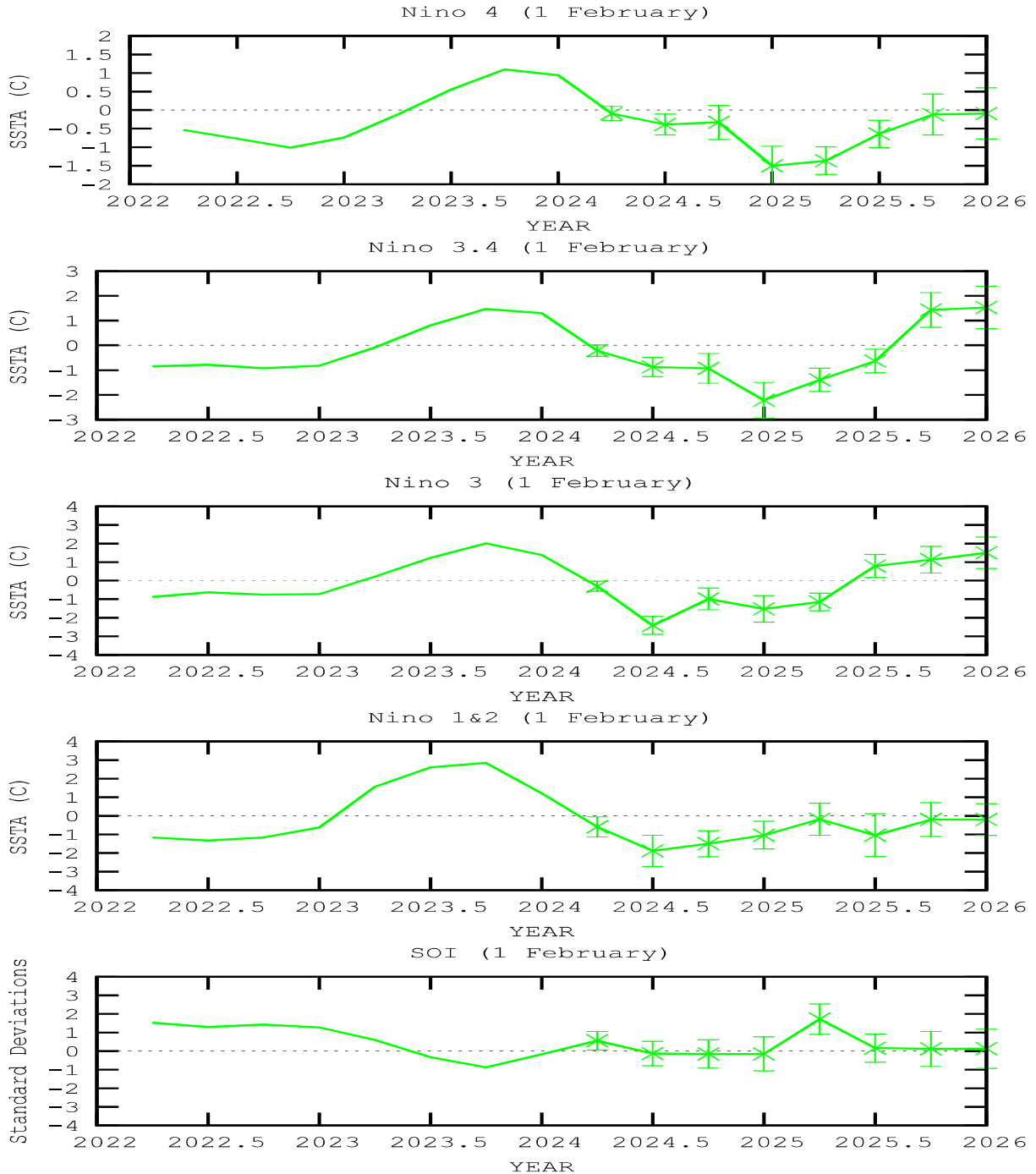


FIGURE F9. ENSO-CLIPER statistical model forecasts of three-month average sea surface temperature anomalies (green lines, deg. C) in (top panel) the Nino 4 region (5°N - 5°S , 160°E - 150°W), (second panel) the Nino 3.4 region (5°N - 5°S , 170°W - 120°W), (third panel) the Nino 3 region (5°N - 5°S , 150°W - 90°W), and (fourth panel) the Nino 1+2 region (0° - 10°S , 90°W - 80°W) (Knaff and Landsea 1997, *Wea. Forecasting*, **12**, 633-652). Bottom panel shows predictions of the three-month standardized Southern Oscillation Index (SOI, green line). Horizontal bars on green line indicate the adjusted root mean square error (RMSE). The Observed three-month average values are indicated by the thick blue line. SST anomalies are departures from the 1991-2020 base period means, and the SOI is calculated from the 1951-1980 base period means.

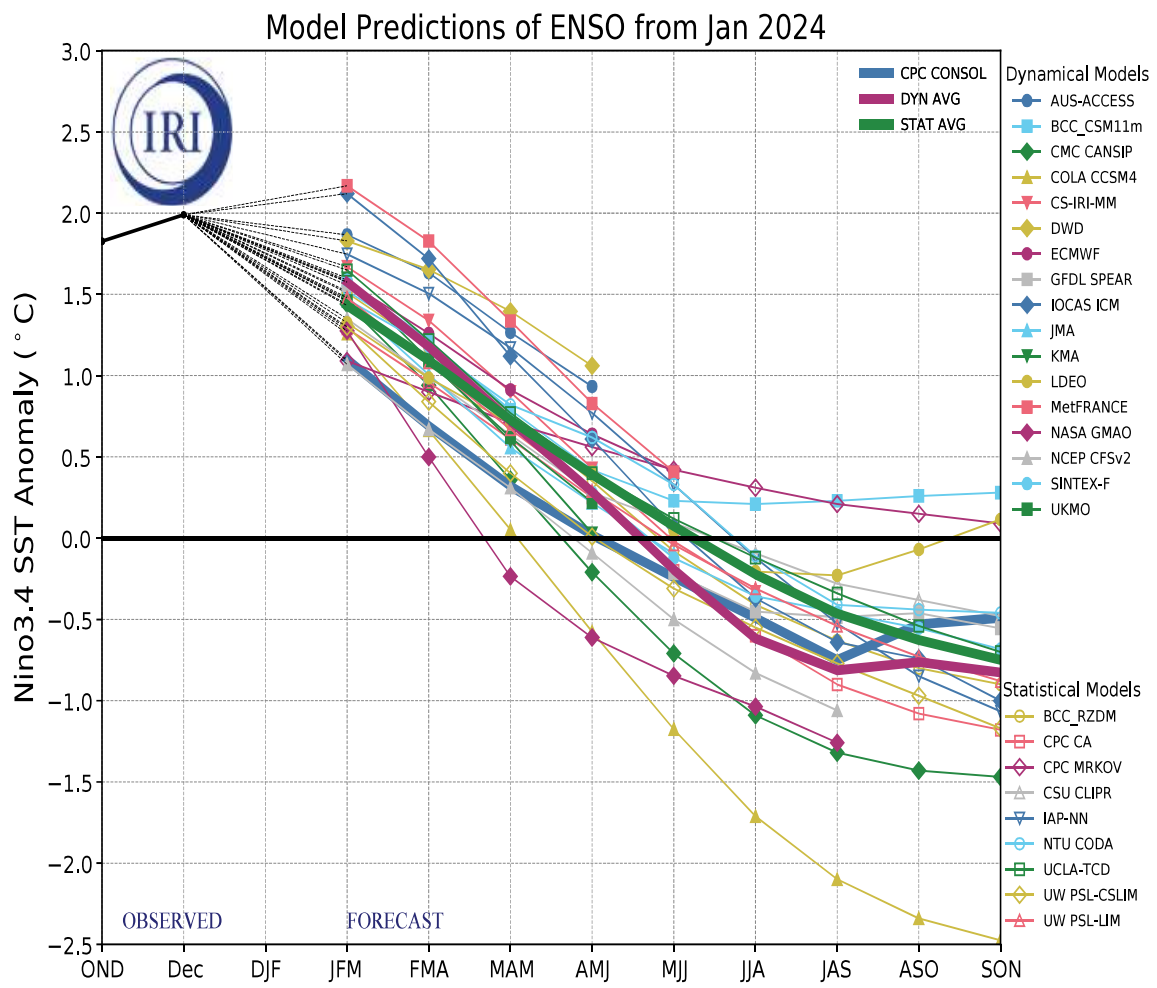


FIGURE F10. Time series of predicted sea surface temperature anomalies for the Nino 3.4 region (deg. C) from various dynamical and statistical models for nine overlapping 3-month periods. The Nino 3.4 region spans the east-central equatorial Pacific between 5N-5S, 170W-120W. Figure provided by the International Research Institute (IRI).

Extratropical Highlights – January 2024

1. Northern Hemisphere

The 500-hPa circulation during January resembled a weak negative Arctic Oscillation (AO) teleconnection pattern with above-average heights over the Polar region and below-average heights in the middle latitudes (Fig. E9). The main land-surface temperature signals include above-average temperatures across most of Europe, Asia, eastern Canada, and the western U.S. (Fig. E1). The main precipitation signals include above-average rainfall in the eastern U.S. and eastern Europe (Fig. E3).

a. North America

The 500-hPa circulation over North America in January was characterized by above-average heights over the eastern half of Canada and Alaska, and slightly below-average heights over the central U.S. (Fig. E9). For much of the U.S., temperature anomalies were largely near normal with the exception of the Pacific Northwest where temperatures were above normal with some areas recording anomalies in the highest 90th percentile of occurrences. In eastern Canada, temperature anomalies were above normal with a large area recording values in the highest 70th percentile of occurrences (Fig. 1). The eastern half of the U.S. recorded above-average rainfall with a large area reaching the highest 90th percentile of occurrences and many areas seeing a Class 1 Improvement in drought conditions, according to the U.S. Drought Monitor. The Great Lakes and Midwest recorded rainfall in the 90th percentile or greater during January, after a previous 4 months of below-average rainfall (Figs. E3, E5 E6). The Pacific Northwest also recorded wetter than average conditions with some areas reaching 175% of normal (Figs. E3, E5, E6).

b. Europe and Asia

The 500-hPa height anomalies featured below-average heights over central Russia and above-average heights over eastern Russia and southern Europe (Fig. E9). Temperatures were above normal across southern Eurasia and central Russia with many areas recording values in the upper 70th and 90th percentile of occurrences (Fig. E1). The strongest anomalies were in a widespread area located in central Russia (Fig. E1). Central and southern parts of Scandinavia recorded below-average temperatures (Fig. E1). The majority of Eurasia recorded near normal precipitation anomalies. Eastern Europe recorded precipitation in the upper 70th and 90th percentile of occurrences (Fig. E3).

2. Southern Hemisphere

The 500-hPa height pattern during January featured below-average heights over the Polar region and above-average heights in the middle latitudes. Temperatures across South America were above-average with many areas recording values in the highest 90th percentile of occurrences. Near the coasts in Africa, temperatures were above-average, and along the eastern region of Australia, temperatures were also recorded at above-average values (Fig. E3). Most of South America experienced drier than average conditions during January (Figs. E3, E4). Drier than average conditions were recorded for western portions of central Africa with the Democratic Republic of Congo and Gabon recording values in the lowest 10th percentile of occurrences (Fig. E3). The eastern portion of Africa recorded above-average rainfall in areas such as Tanzania, Kenya, and Uganda where values reached the highest 90th percentile of occurrences (Fig. E3). Precipitation anomalies were also elevated in the eastern half of Australia where areas recorded precipitation in the highest 70th percentile of occurrences (Fig. E3). The South African monsoon season runs from October to April. This area received below-average rainfall for January with values recorded in the lowest 20th percentile of occurrences (Fig. E4).

TELECONNECTION INDICES

| Month | North Atlantic | | | | North Pacific | | | | EURASIA | | |
|--------|----------------|------|------|-------|---------------|------|-----------|-------|---------|------|--|
| | NAO | EA | WP | EP-NP | PNA | TNH | EATL/WRUS | SCAND | POLEUR | | |
| JAN 24 | -0.3 | 2.6 | 0.7 | 0.1 | -0.1 | -0.3 | 0.5 | -1.2 | | -0.9 | |
| DEC 23 | 1.7 | 1.5 | 1.2 | --- | 0.9 | -1.1 | 0.1 | 0.7 | | -0.5 | |
| NOV 23 | -0.5 | 1.2 | 0.6 | 0.4 | 0.5 | --- | 0.1 | -0.1 | 0.3 | | |
| OCT 23 | -1.7 | 1.2 | -0.8 | 0.3 | 1.5 | --- | 0.6 | -0.6 | | -0.1 | |
| SEP 23 | -0.3 | 2.7 | 1.3 | -2.6 | 0.8 | --- | -2.1 | -0.3 | 0.8 | | |
| AUG 23 | -1.6 | 2.1 | -0.4 | -1.2 | 0.4 | --- | -2.4 | -1.1 | | -1.1 | |
| JUL 23 | -2.1 | 1.8 | 1.3 | 0.8 | 0.7 | --- | -1.8 | -0.6 | 0.0 | | |
| JUN 23 | -0.3 | -1.1 | 0.3 | -1.9 | 0.8 | --- | 0.4 | 0.8 | 0.2 | | |
| MAY 23 | 0.4 | -0.1 | 1.0 | -0.8 | -0.7 | --- | -2.2 | -1.1 | 1.9 | | |
| APR 23 | -0.8 | -0.2 | -0.2 | -0.7 | -0.7 | --- | -0.2 | 1.3 | | -0.7 | |
| MAR 23 | -1.6 | 0.5 | 0.6 | 0.4 | -1.9 | --- | 2.0 | -2.1 | 0.9 | | |
| FEB 23 | 0.6 | -0.8 | 2.5 | -0.5 | -1.2 | 1.7 | 1.5 | -0.7 | | -0.9 | |
| JAN 23 | 0.9 | -1.0 | 2.0 | 1.4 | -0.4 | -0.4 | -0.6 | 0.7 | | -1.1 | |

TABLE E1-Standardized amplitudes of selected Northern Hemisphere teleconnection patterns for the most recent thirteen months (computational procedures are described in Fig. E7). Pattern names and abbreviations are North Atlantic Oscillation (NAO); East Atlantic pattern (EA); West Pacific pattern (WP); East Pacific - North Pacific pattern (EP-NP); Pacific/North American pattern (PNA); Tropical/Northern Hemisphere pattern (TNH);East Atlantic/Western Russia pattern (EATL/WRUS-called Eurasia-2 pattern by Barnston and Livezey, 1987, *Mon Wea. Rev.*, **115**, 1083-1126); Scandanavia pattern (SCAND-called Eurasia-1 pattern by Barnston and Livezey 1987); and Polar Eurasia pattern (POLEUR). No value is plotted for calendar months in which the pattern does not appear as a leading mode.

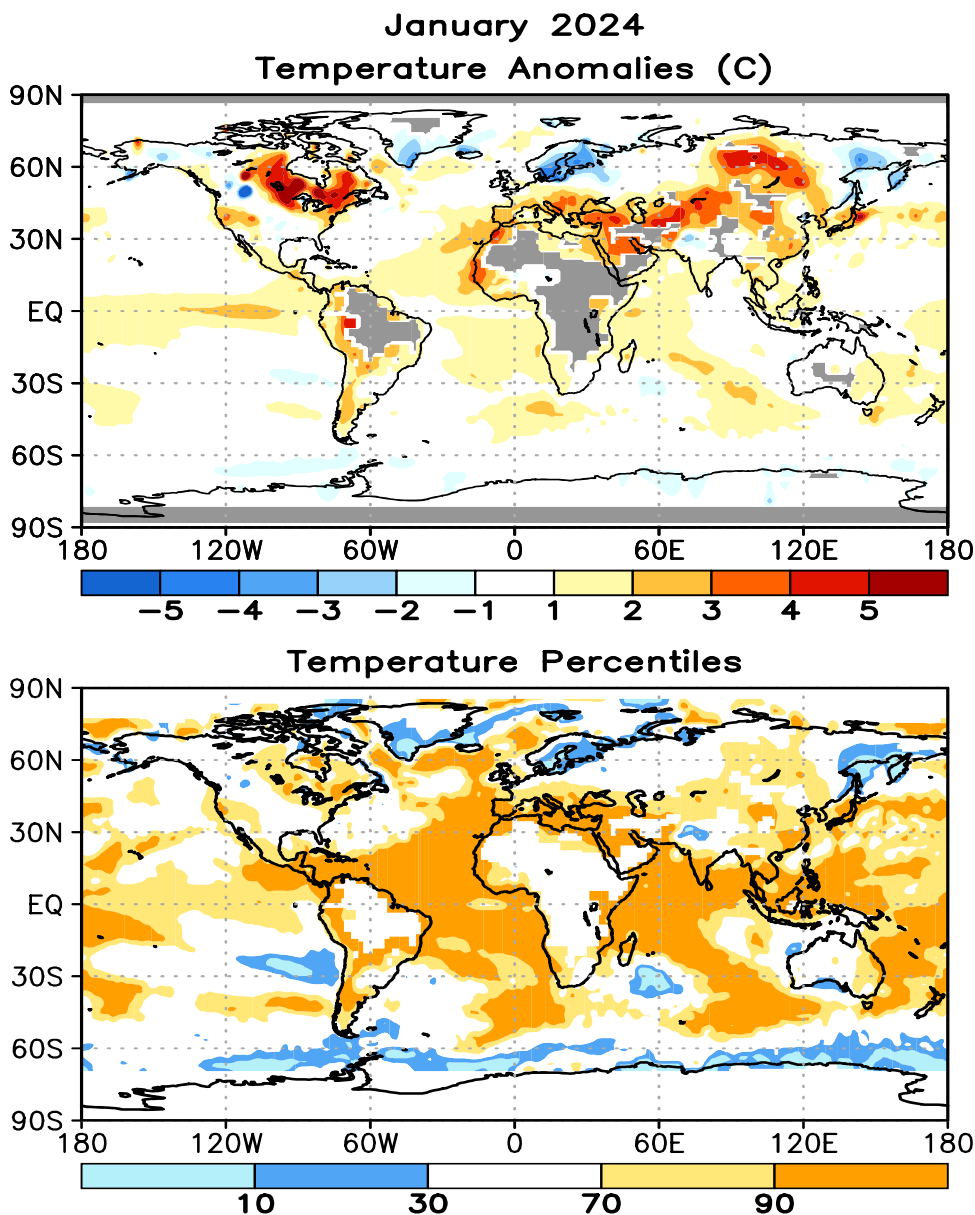


FIGURE E1. Surface temperature anomalies ($^{\circ}\text{C}$, top) and surface temperature expressed as percentiles of the normal (Gaussian) distribution fit to the 1991-2020 base period data (bottom) for JAN 2024. Analysis is based on station data over land and on SST data over the oceans (top). Anomalies for station data are departures from the 1991-2020 base period means, while SST anomalies are departures from the 1991-2020 adjusted OI climatology. (Smith and Reynolds 1998, *J. Climate*, **11**, 3320-3323). Regions with insufficient data for analysis in both figures are indicated by shading in the top figure only.

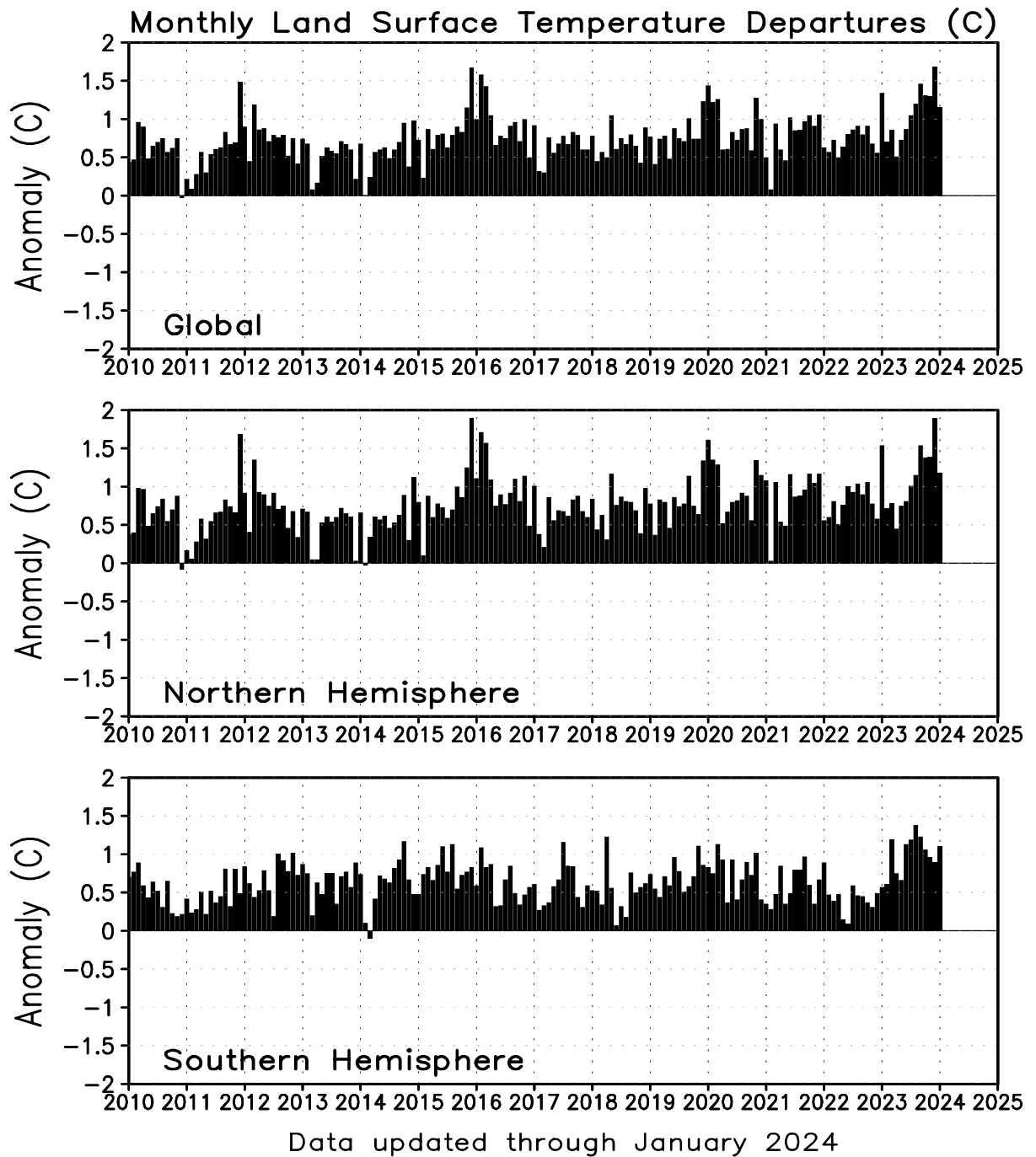


FIGURE E2. Monthly global (top), Northern Hemisphere (middle), and Southern Hemisphere (bottom) surface temperature anomalies (land only, °C) from January 1990 - present, computed as departures from the 1991-2020 base period means.

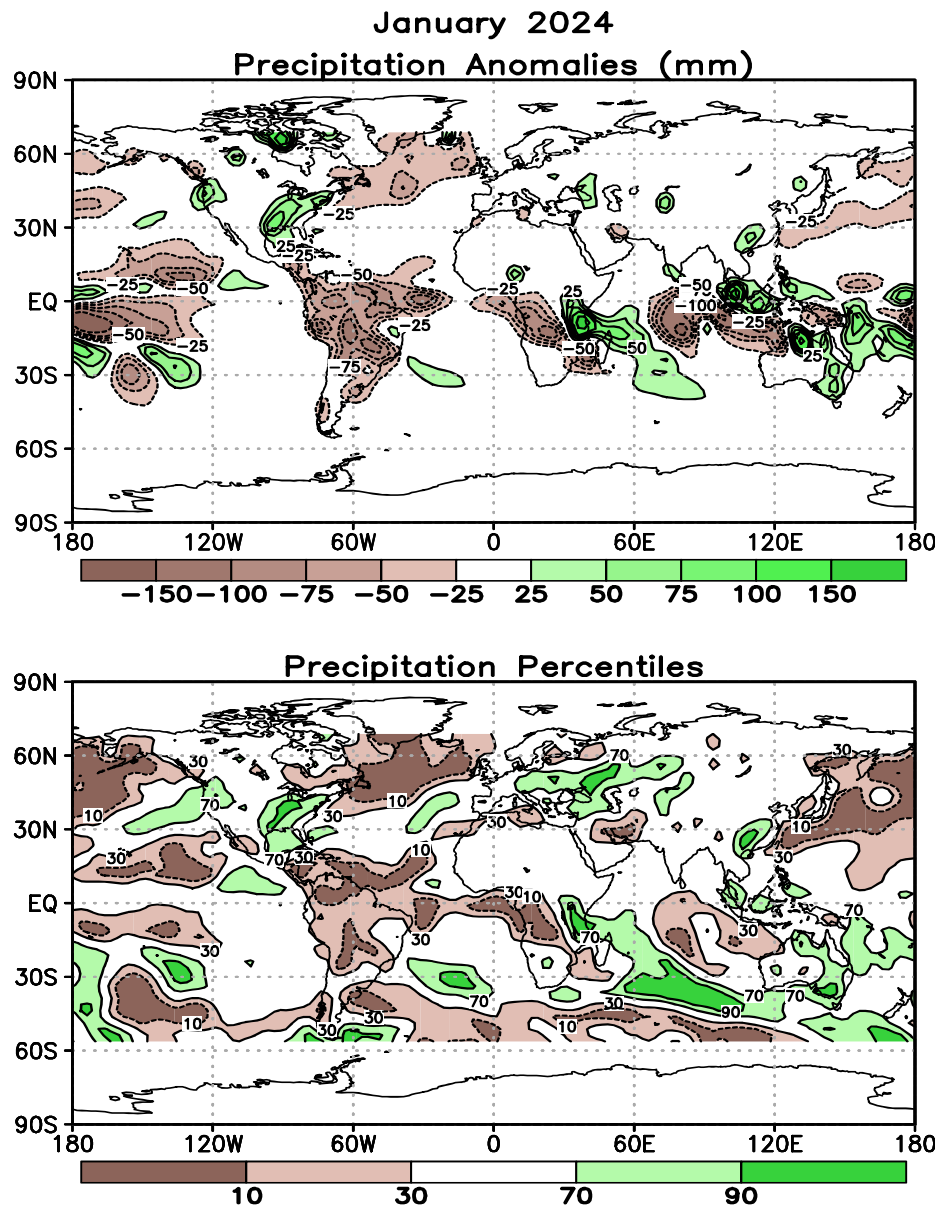
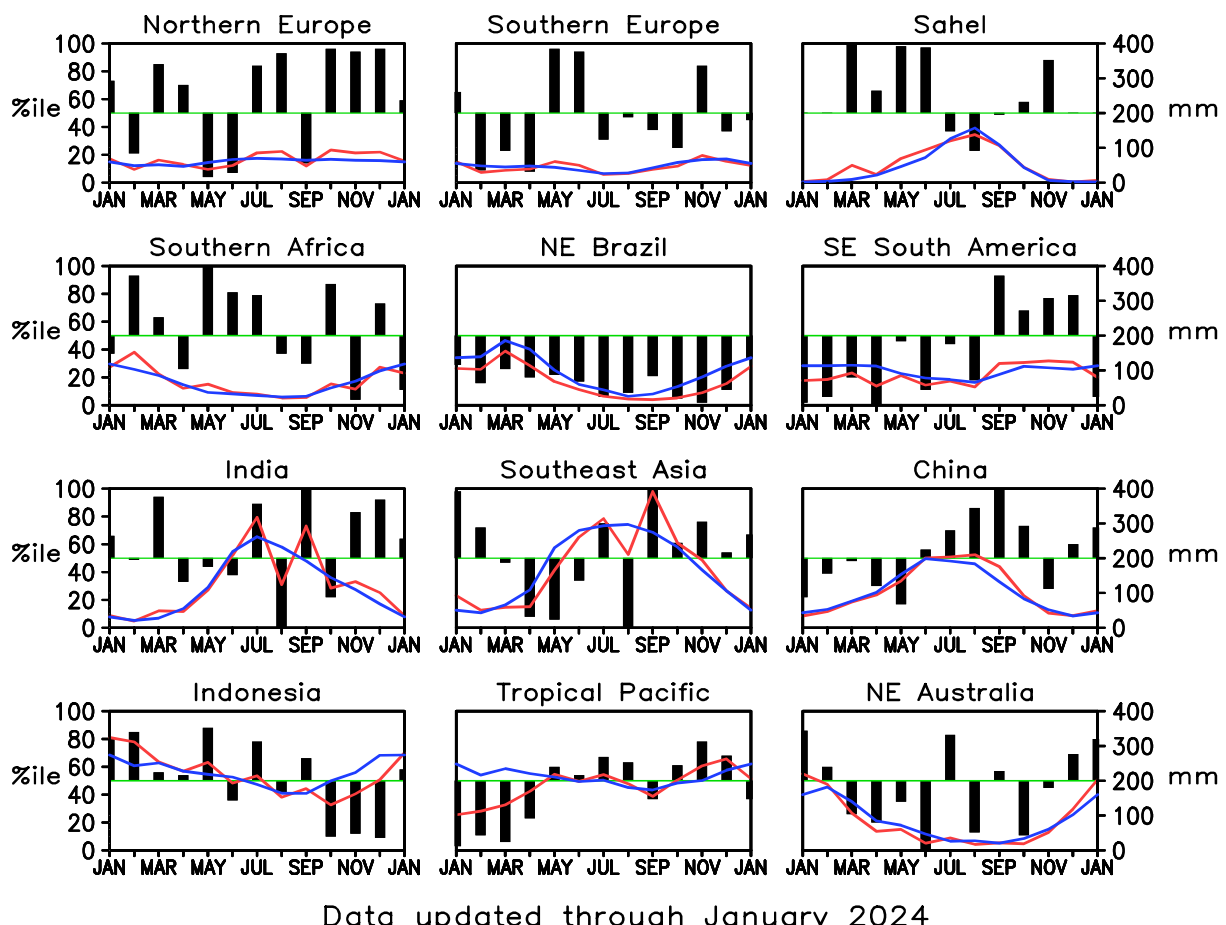
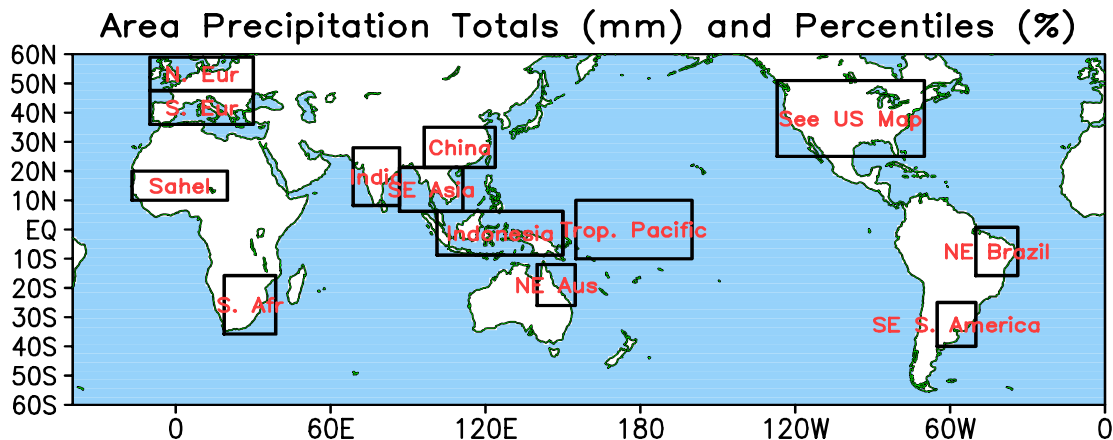


FIGURE E3. Anomalous precipitation (mm, top) and precipitation percentiles based on a Gamma distribution fit to the 1981-2010 base period data (bottom) for JAN 2024. Data are obtained from a merge of rain gauge observations and satellite-derived precipitation estimates (Janowiak and Xie 1999, *J. Climate*, **12**, 3335–3342). Contours are drawn at 200, 100, 50, 25, -25, -50, -100, and -200 mm in top panel. Percentiles are not plotted in regions where mean monthly precipitation is <5mm/month.



Data updated through January 2024

FIGURE E4. Areal estimates of monthly mean precipitation amounts (mm, solid lines) and precipitation percentiles (%) (bars) for the most recent 13 months obtained from a merge of raingauge observations and satellite-derived precipitation estimates (Janowiak and Xie 1999, *J. Climate*, **12**, 3335–3342). The monthly precipitation climatology (mm, dashed lines) is from the 1981–2010 base period monthly means. Monthly percentiles are not shown if the monthly mean is less than 5 mm.

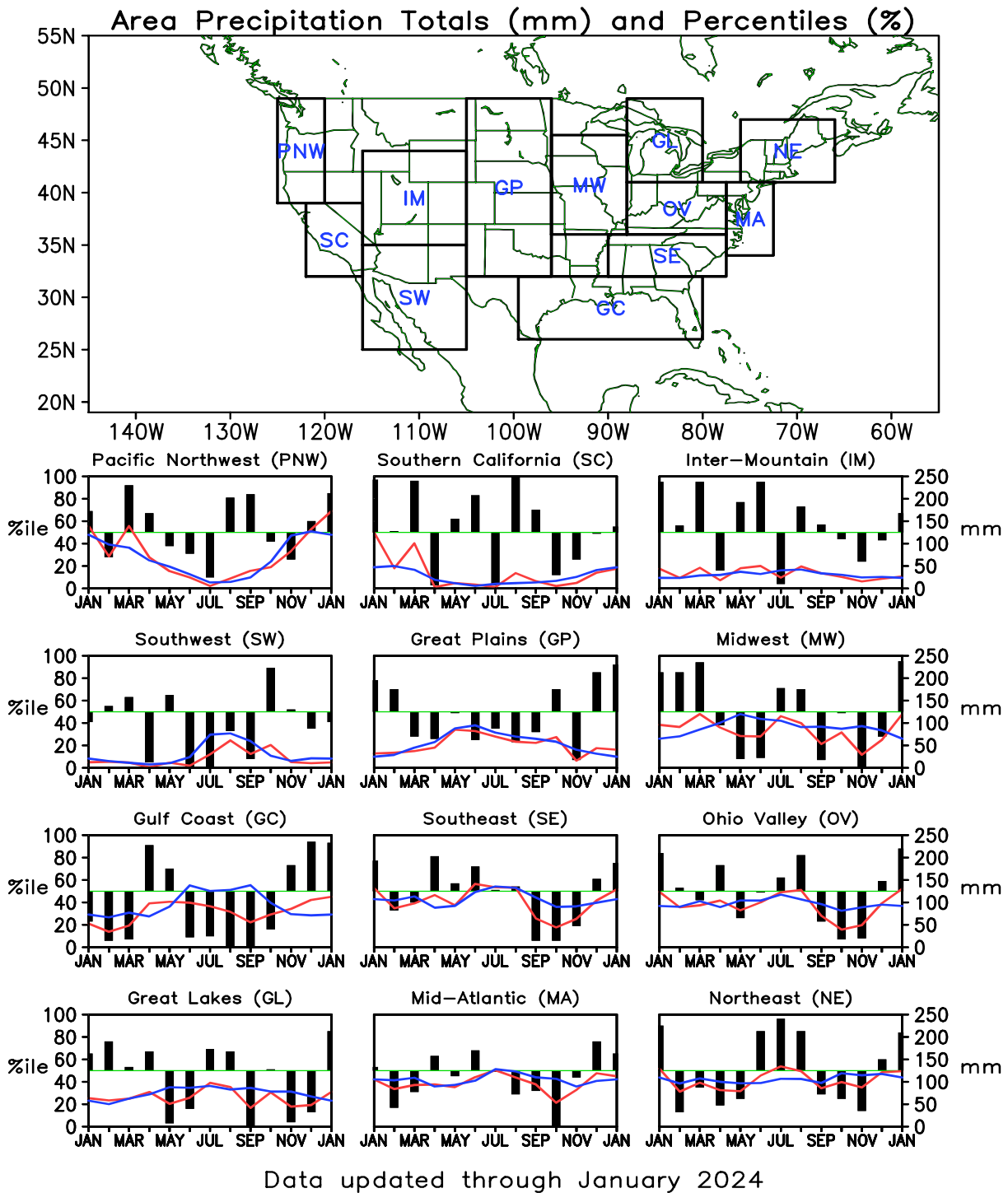


FIGURE E5. Areal estimates of monthly mean precipitation amounts (mm, solid lines) and precipitation percentiles (%) bars for the most recent 13 months obtained from a merge of raingauge observations and satellite-derived precipitation estimates (Janowiak and Xie 1999, *J. Climate*, **12**, 3335–3342). The monthly precipitation climatology (mm, dashed lines) is from the 1981–2010 base period monthly means. Monthly percentiles are not shown if the monthly mean is less than 5 mm.

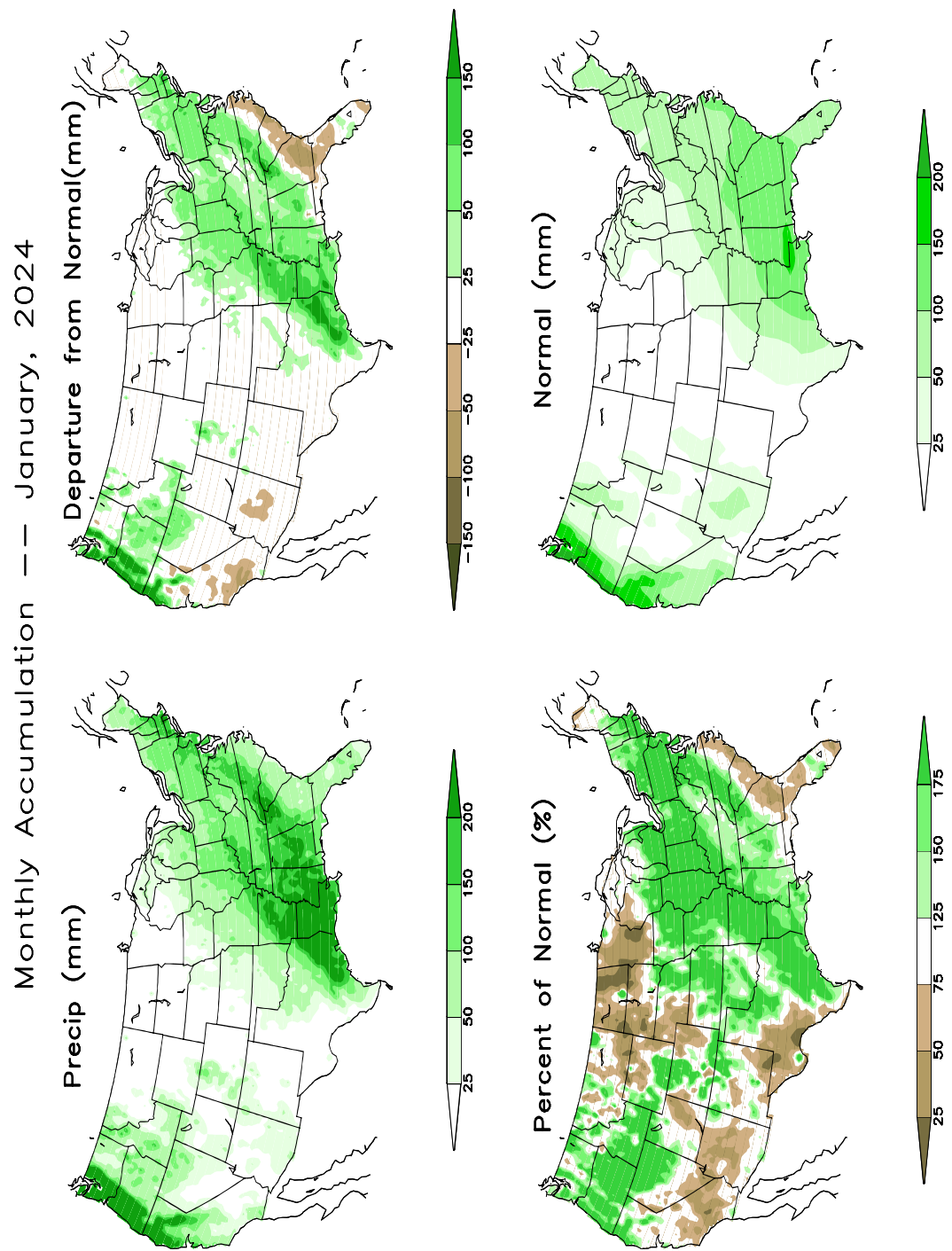


FIGURE E6. Observed precipitation (upper left), departure from average (upper right), percent of average (lower left), and average precipitation (lower right) for JAN 2024. The units are given on each panel. Base period for averages is 1991-2020. Results are based on CPC's U. S. daily precipitation analysis, which is available at <http://www.cpc.ncep.noaa.gov/products/precip/realtime>.

Monthly Teleconnection Indices Through January 2024

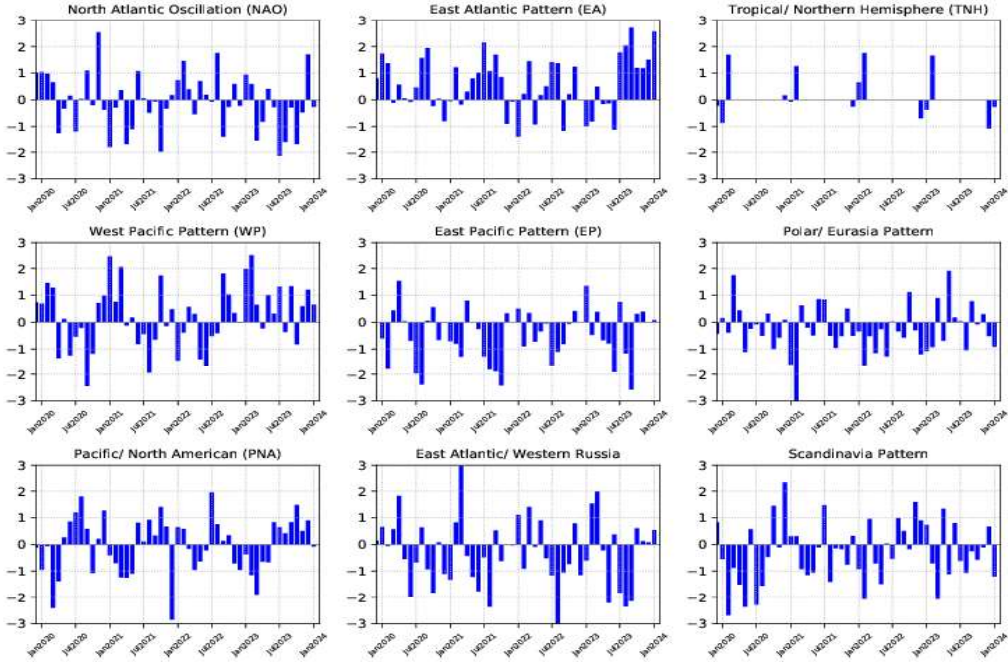


FIGURE E7. Standardized monthly Northern Hemisphere teleconnection indices. The teleconnection patterns are calculated from a Rotated Principal Component Analysis (RPCA) applied to monthly standardized 500-hPa height anomalies during the 1991–2020 base period. To obtain these patterns, ten leading un-rotated modes are first calculated for each calendar month by using the monthly height anomaly fields for the three-month period centered on that month: [i.e., The July modes are calculated from the June, July, and August standardized monthly anomalies]. A Varimax spatial rotation of the ten leading un-rotated modes for each calendar month results in 120 rotated modes (12 months \times 10 modes per month) that yield ten primary teleconnection patterns. The teleconnection indices are calculated by first projecting the standardized monthly anomalies onto the teleconnection patterns corresponding to that month (eight or nine teleconnection patterns are seen in each calendar month). The indices are then solved for simultaneously using a Least-Squares approach. In this approach, the indices are the solution to the Least-Squares system of equations which explains the maximum spatial structure of the observed height anomaly field during the month. The indices are then standardized for each pattern and calendar month independently. No index value exists when the teleconnection pattern does not appear as one of the ten leading rotated EOF's valid for that month.

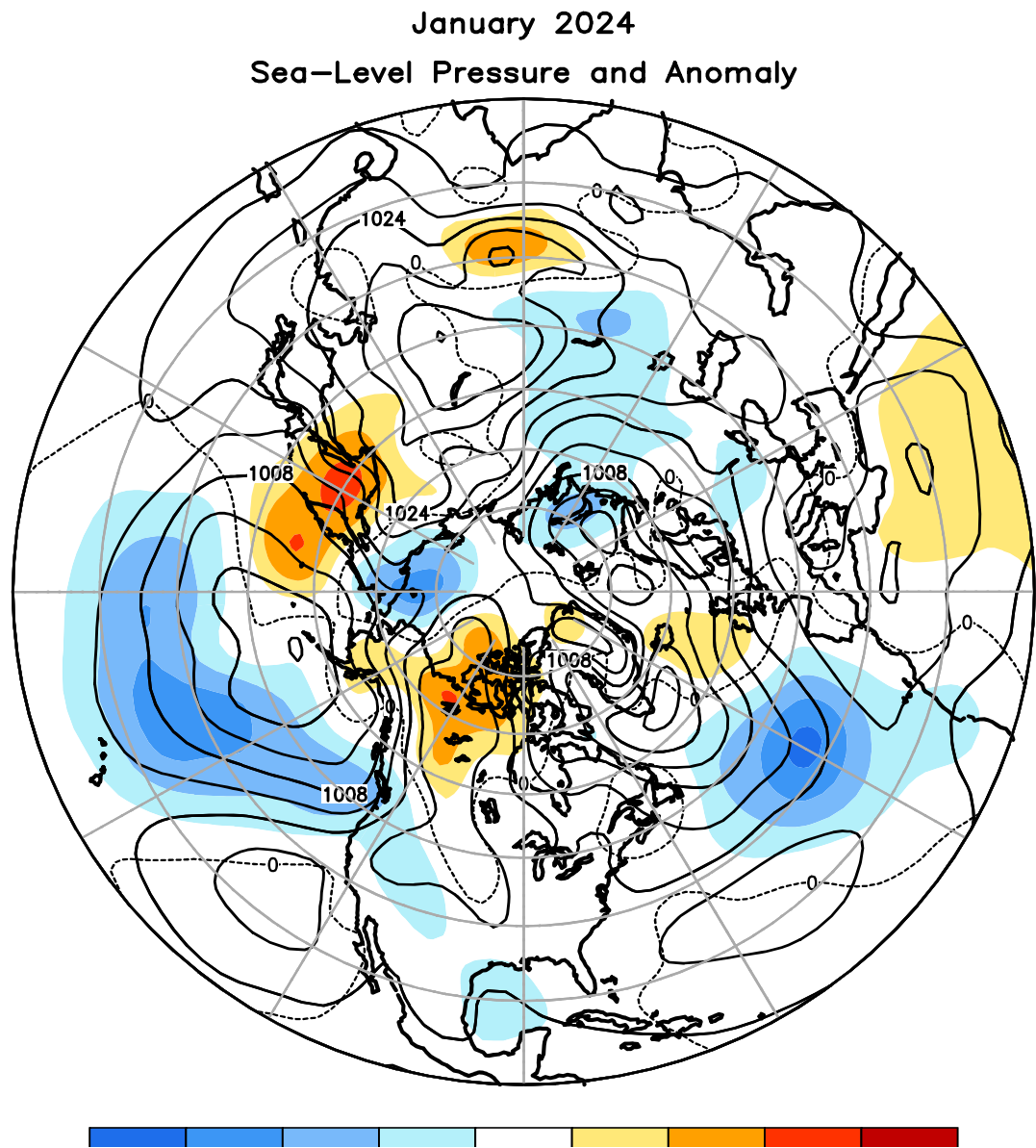


FIGURE E8. Northern Hemisphere mean and anomalous sea level pressure (CDAS/Reanalysis) for JAN 2024. Mean values are denoted by solid contours drawn at an interval of 4 hPa. Anomaly contour interval is 2 hPa with values less (greater) than -2 hPa (2 hPa) indicated by dark (light) shading. Anomalies are calculated as departures from the 1991-2020 base period monthly means.

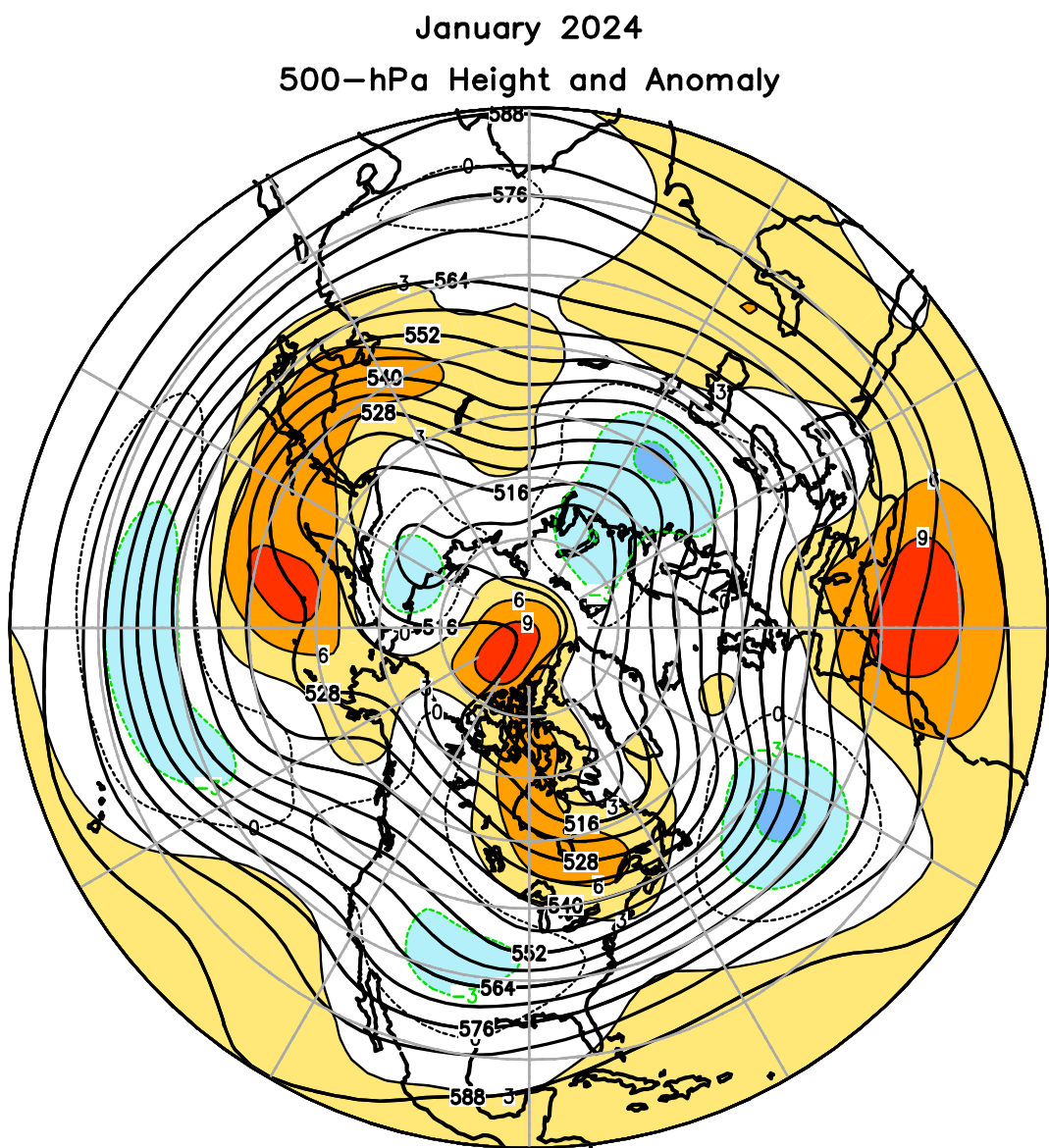


FIGURE E9. Northern Hemisphere mean and anomalous 500-hPa geopotential height (CDAS/Reanalysis) for JAN 2024. Mean heights are denoted by solid contours drawn at an interval of 6 dam. Anomaly contour interval is 3 dam with values less (greater) than -3 dam (3 dam) indicated by dark (light) shading. Anomalies are calculated as departures from the 1991-2020 base period monthly means.

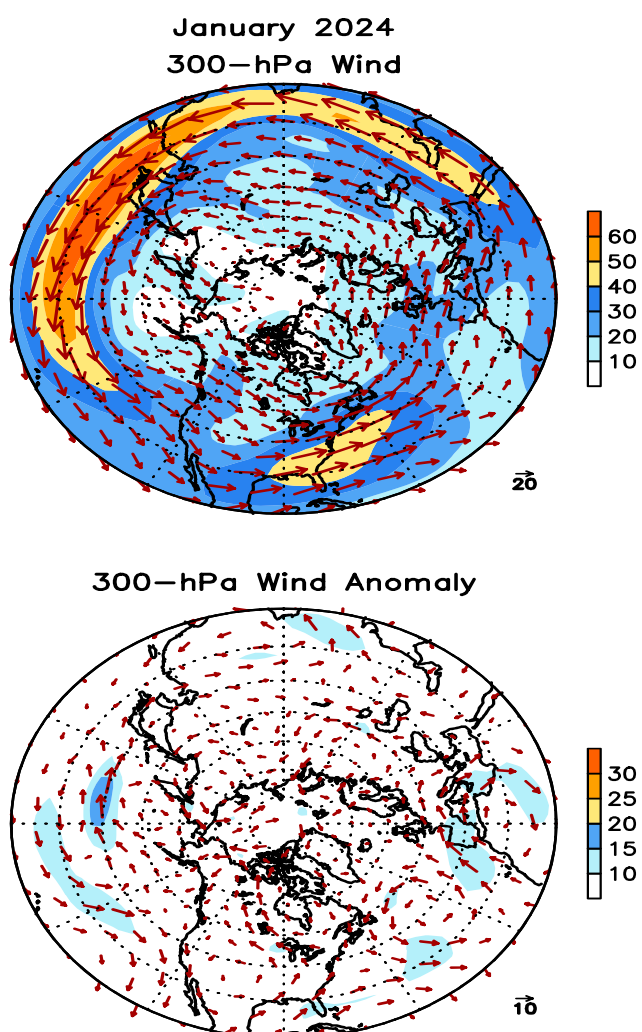


FIGURE E10. Northern Hemisphere mean (left) and anomalous (right) 300-hPa vector wind (CDAS/Reanalysis) for JAN 2024. Mean (anomaly) isotach contour interval is $10\ (5)\ \text{ms}^{-1}$. Values greater than $30\ \text{ms}^{-1}$ (left) and $10\ \text{ms}^{-1}$ (rights) are shaded. Anomalies are departures from the 1991-2020 base period monthly means.

January 2024
500-hPa: Percentage of Anomaly Days

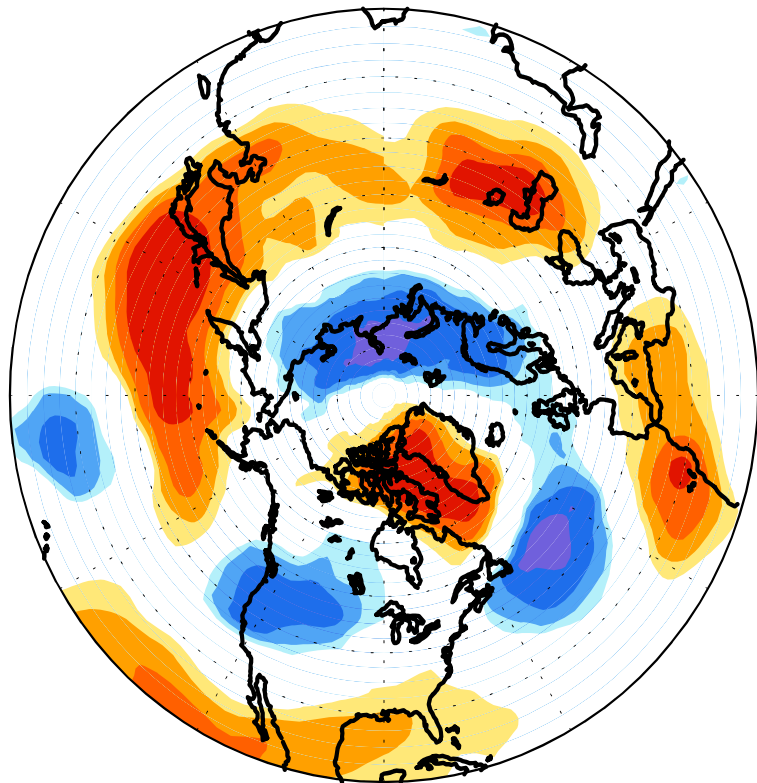


FIGURE E11. Northern Hemisphere percentage of days during JAN 2024 in which 500-hPa height anomalies greater than 15 m (red) and less than -15 m (blue) were observed. Values greater than 70% are shaded and contour in-

January 2024
500-hPa Height Anomalies: 40°N

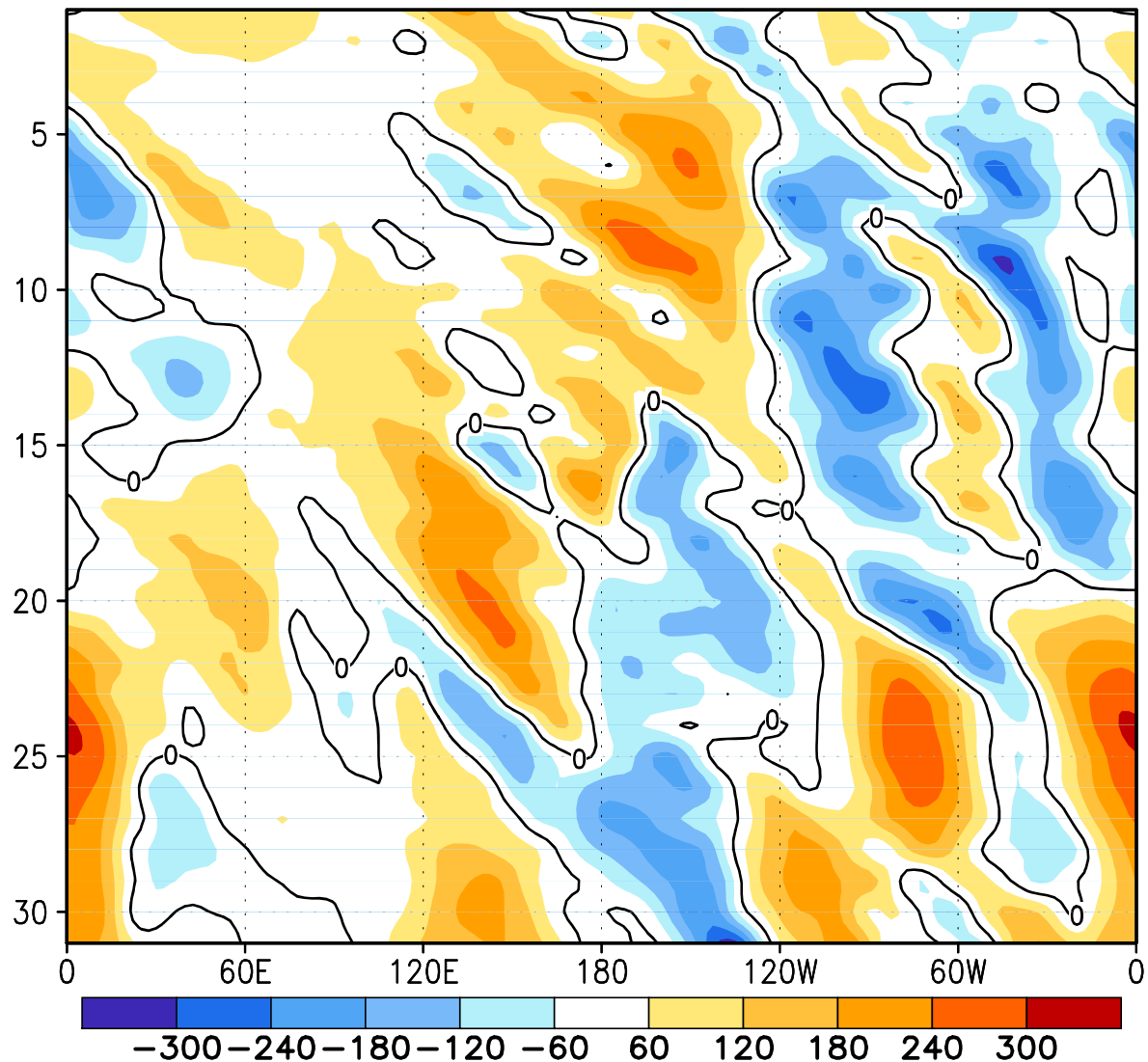
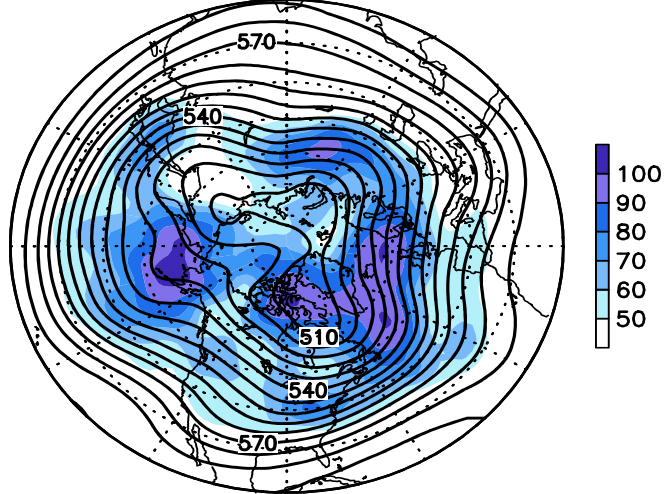


FIGURE E12. Northern Hemisphere: Daily 500-hPa height anomalies for JAN 2024 averaged over the 5° latitude band centered on 40°N. Positive values are indicated by solid contours and dark shading. Negative values are indicated by dashed contours and light shading. Contour interval is 60 m. Anomalies are departures from the 1991-2020 base period daily means.

January 2024
500-hPa Heights (Contours)
High Frequency Std. Dev. (Shading)



500-hPa Heights (Contours)
Normalized High Frequency Variance (Shading)

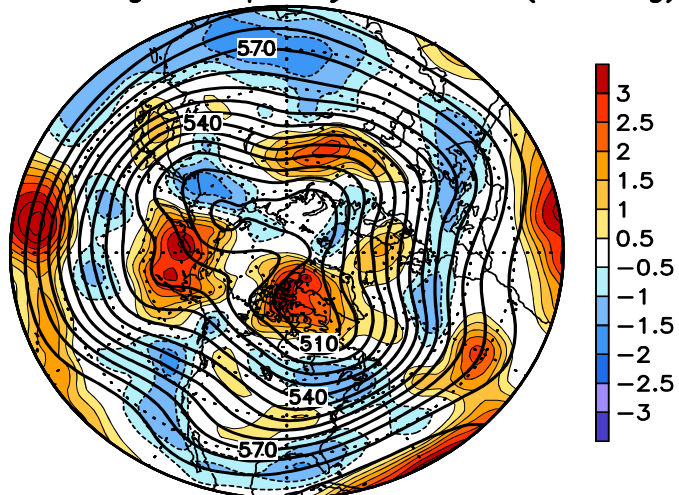


FIGURE E13. Northern Hemisphere 500-hPa heights (thick contours, interval is 6 dam) overlaid with (Top) Standard deviation of 10-day high-pass (HP) filtered height anomalies and (Bottom) Normalized anomalous variance of 10-day HP filtered height anomalies. A Lanczos filter is used to calculate the HP filtered anomalies. Anomalies are departures from the 1991-2020 daily means.

January 2024
Sea-Level Pressure and Anomaly

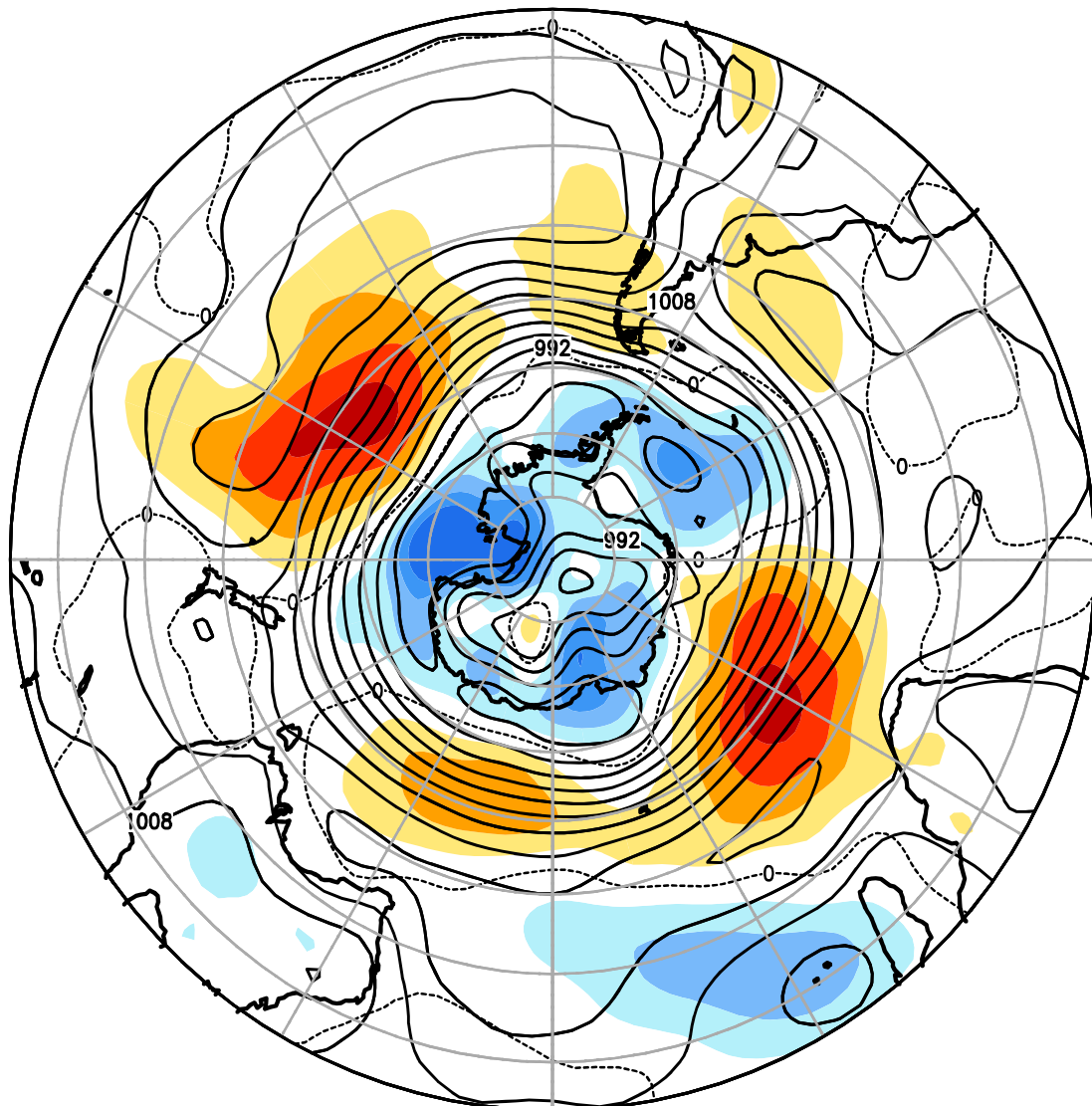


FIGURE E14. Southern Hemisphere mean and anomalous sea level pressure(CDAS/Reanalysis) for JAN 2024. Mean values are denoted by solid contours drawn at an interval of 4 hPa. Anomaly contour interval is 2 hPa with values less (greater) than -2 hPa (2 hPa) indicated by dark (light) shading. Anomalies are calculated as departures from the 1991-2020 base period monthly means.

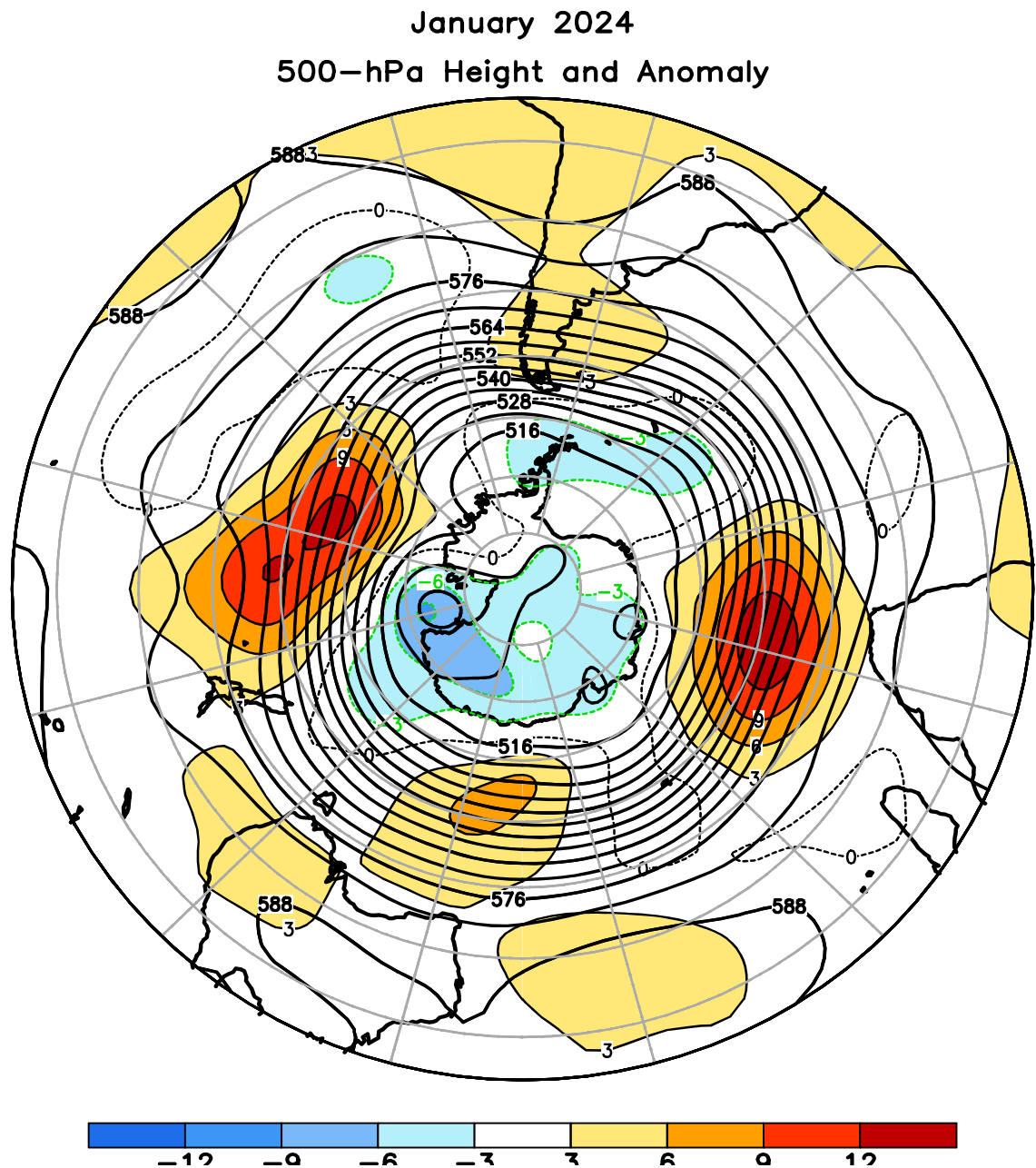


FIGURE E15. Southern Hemisphere mean and anomalous 500-hPa geopotential height (CDAS/Reanalysis) for JAN 2024. Mean heights are denoted by solid contours drawn at an interval of 6 dam. Anomaly contour interval is 3 dam with values less (greater) than -3 dam (3 dam) indicated by dark (light) shading. Anomalies are calculated as departures from the 1991-2020 base period monthly means.

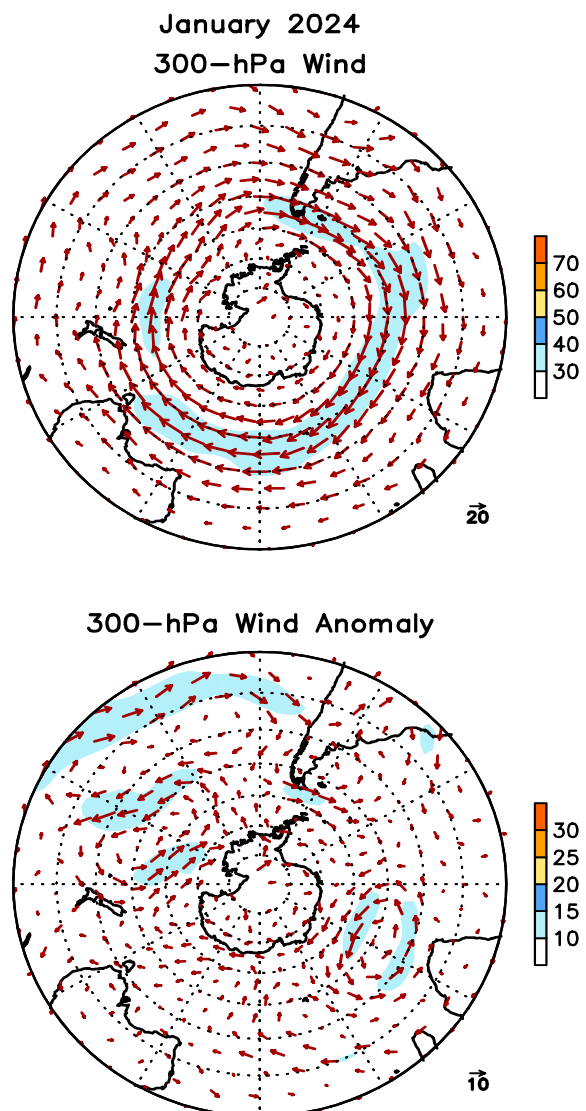


FIGURE E16. Southern Hemisphere mean (left) and anomalous (right) 300-hPa vector wind (CDAS/Reanalysis) for JAN 2024. Mean (anomaly) isotach contour interval is 10 (5) ms^{-1} . Values greater than 30 ms^{-1} (left) and 10 ms^{-1} (rights) are shaded. Anomalies are departures from the 1991-2020 base period monthly means.

January 2024
500-hPa: Percentage of Anomaly Days

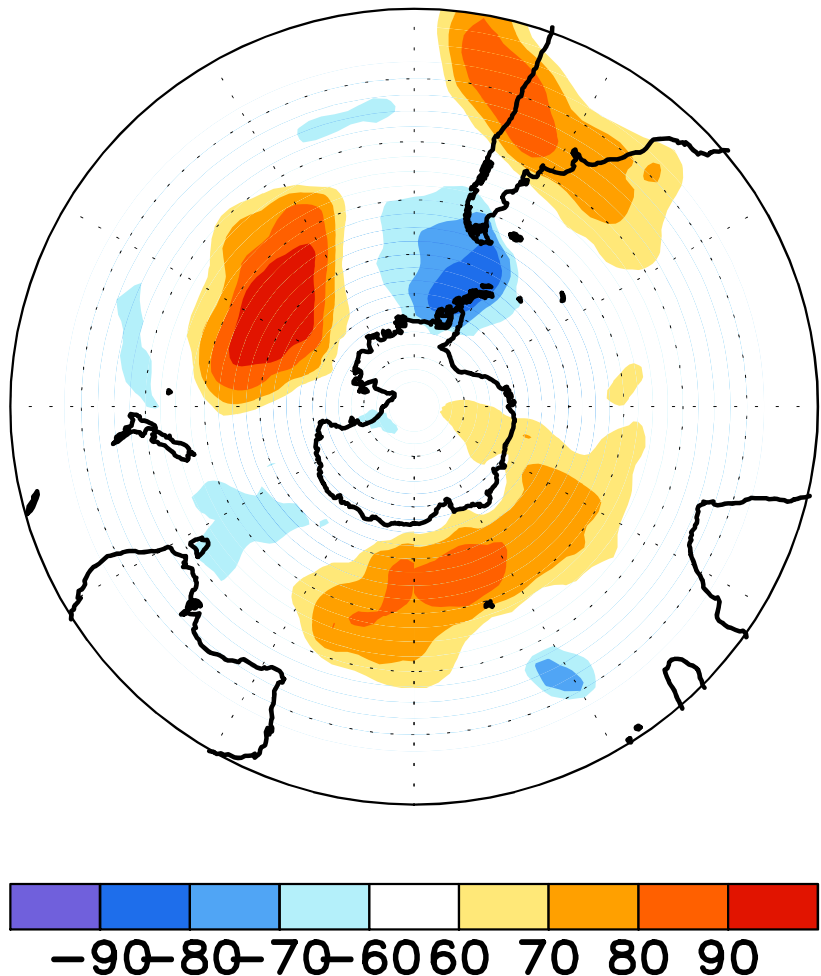


FIGURE E17. Southern Hemisphere percentage of days during JAN 2024 in which 500-hPa height anomalies greater than 15 m (red) and less than -15 m (blue) were observed. Values greater than 70% are shaded and contour in-

January 2024
500-hPa Height Anomalies: 40°S

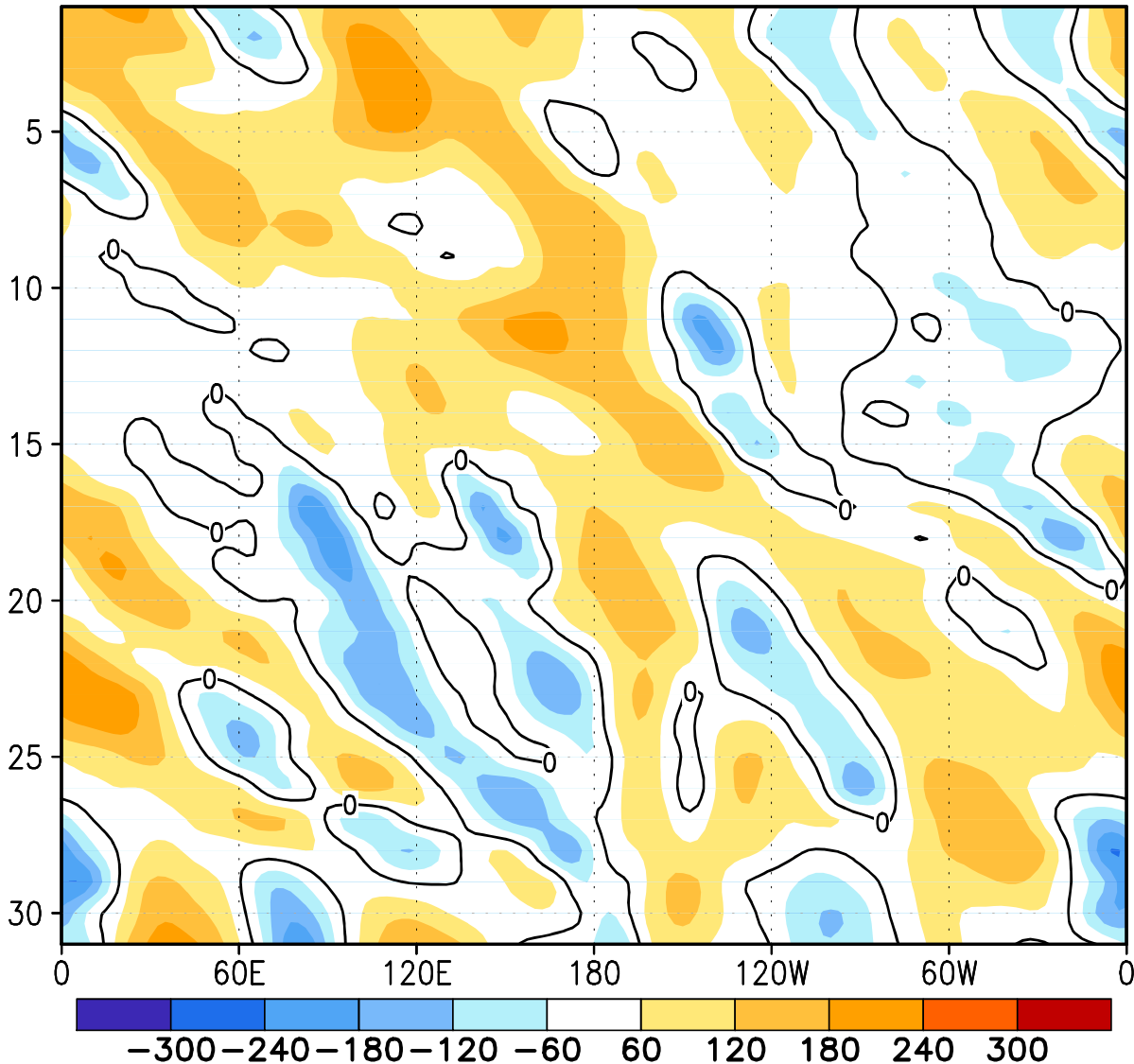


FIGURE E18. Southern Hemisphere: Daily 500-hPa height anomalies for JAN 2024 averaged over the 5° latitude band centered on 40°S. Positive values are indicated by solid contours and dark shading. Negative values are indicated by dashed contours and light shading. Contour interval is 60 m. Anomalies are departures from the 1991-2020 base period daily means.

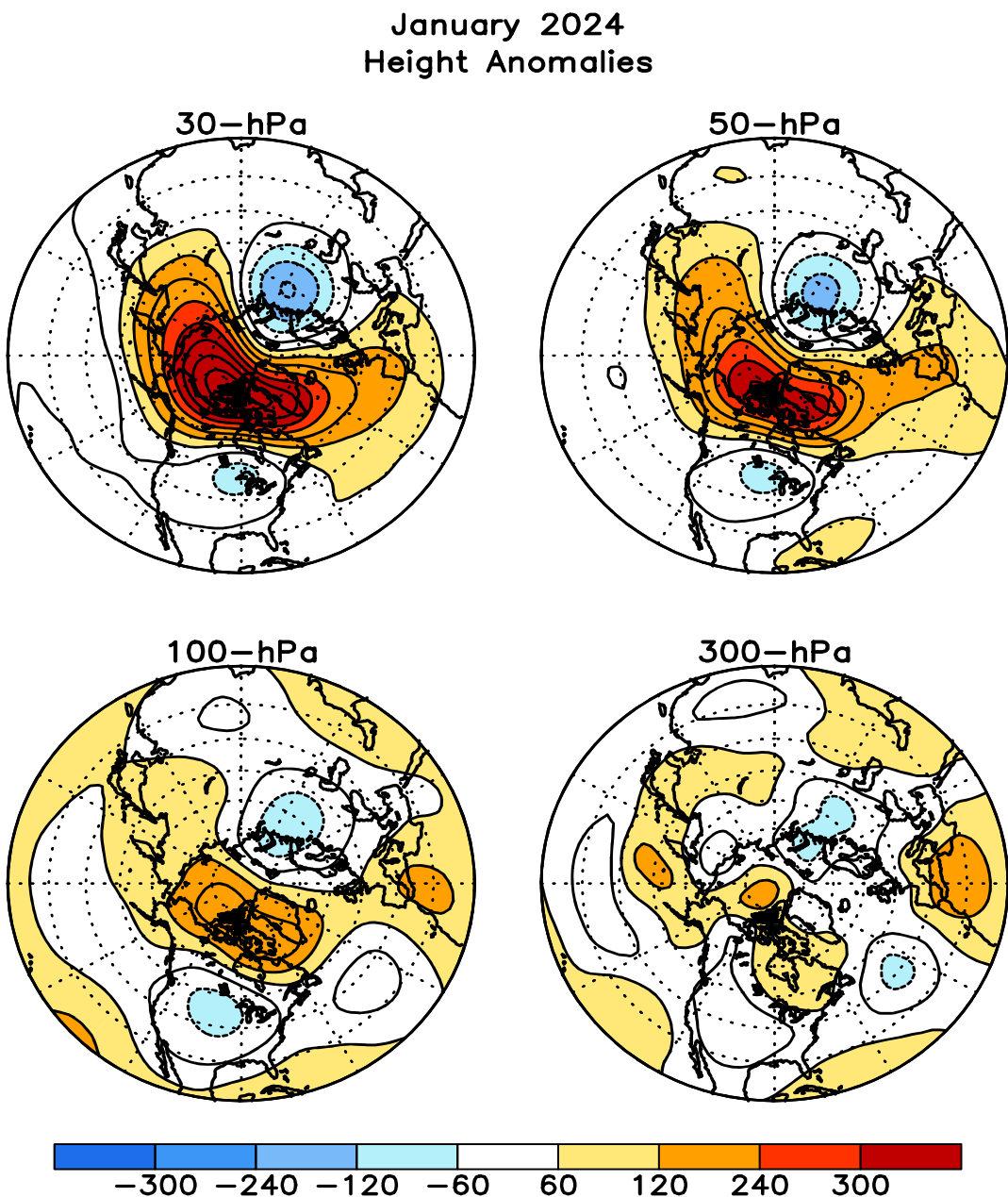


FIGURE S1. Stratospheric height anomalies (m) at selected levels for JAN 2024. Positive values are indicated by solid contours and dark shading. Negative values are indicated by dashed contours and light shading. Contour interval is 60 m. Anomalies are calculated from the 1991-2020 base period means. Winter Hemisphere is shown.

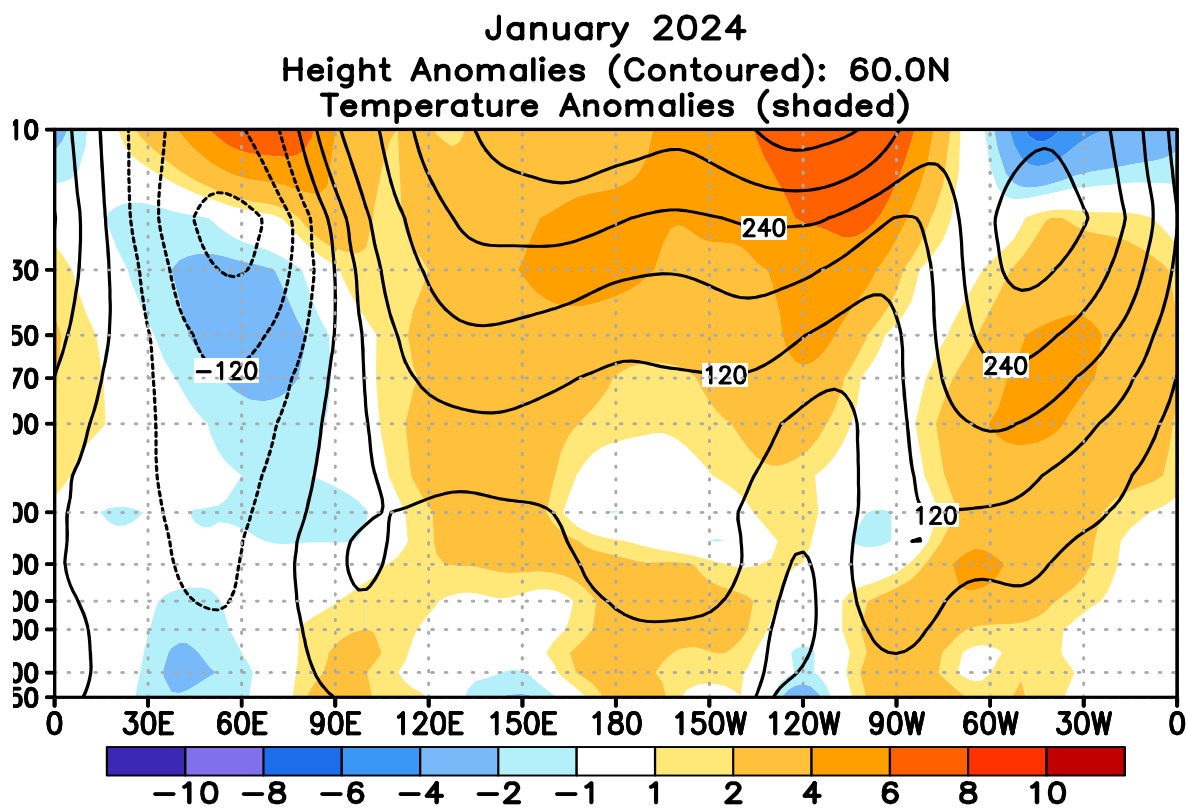


FIGURE S2. Height-longitude sections during JAN 2024 for height anomalies (contour) and temperature anomalies (shaded). In both panels, positive values are indicated by solid contours and dark shading, while negative anomalies are indicated by dashed contours and light shading. Contour interval for height anomalies is 60 m and for temperature anomalies is 2°C. Anomalies are calculated from the 1991-2020 base period monthly means. Winter Hemisphere is shown.

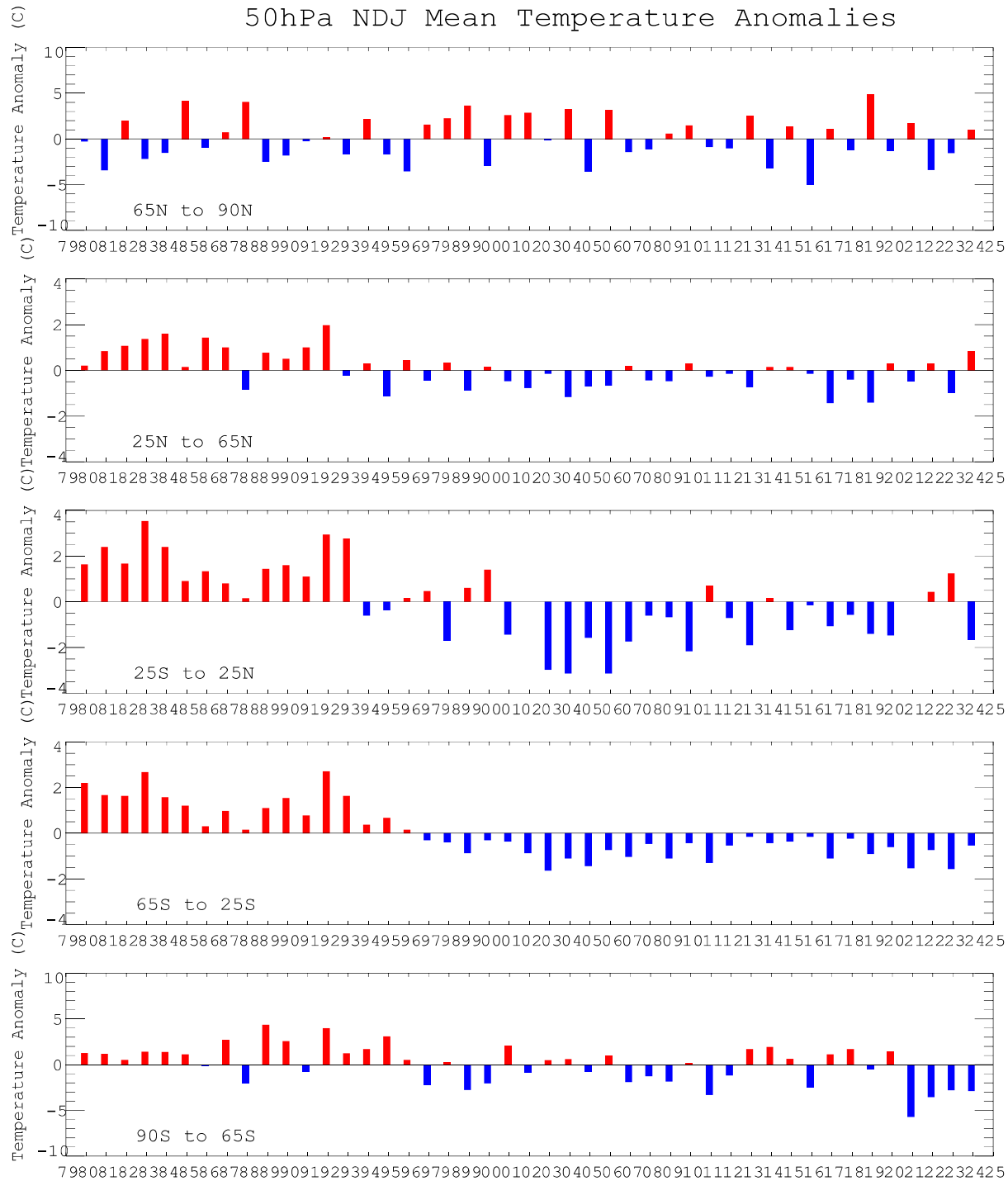


FIGURE S3. Seasonal mean temperature anomalies at 50-hPa for the latitude bands 65° - 90° N, 25° - 65° N, 25° N- 25° S, 25° - 65° S, 65° - 90° S. The seasonal mean is comprised of the most recent three months. Zonal anomalies are taken from the mean of the entire data set.

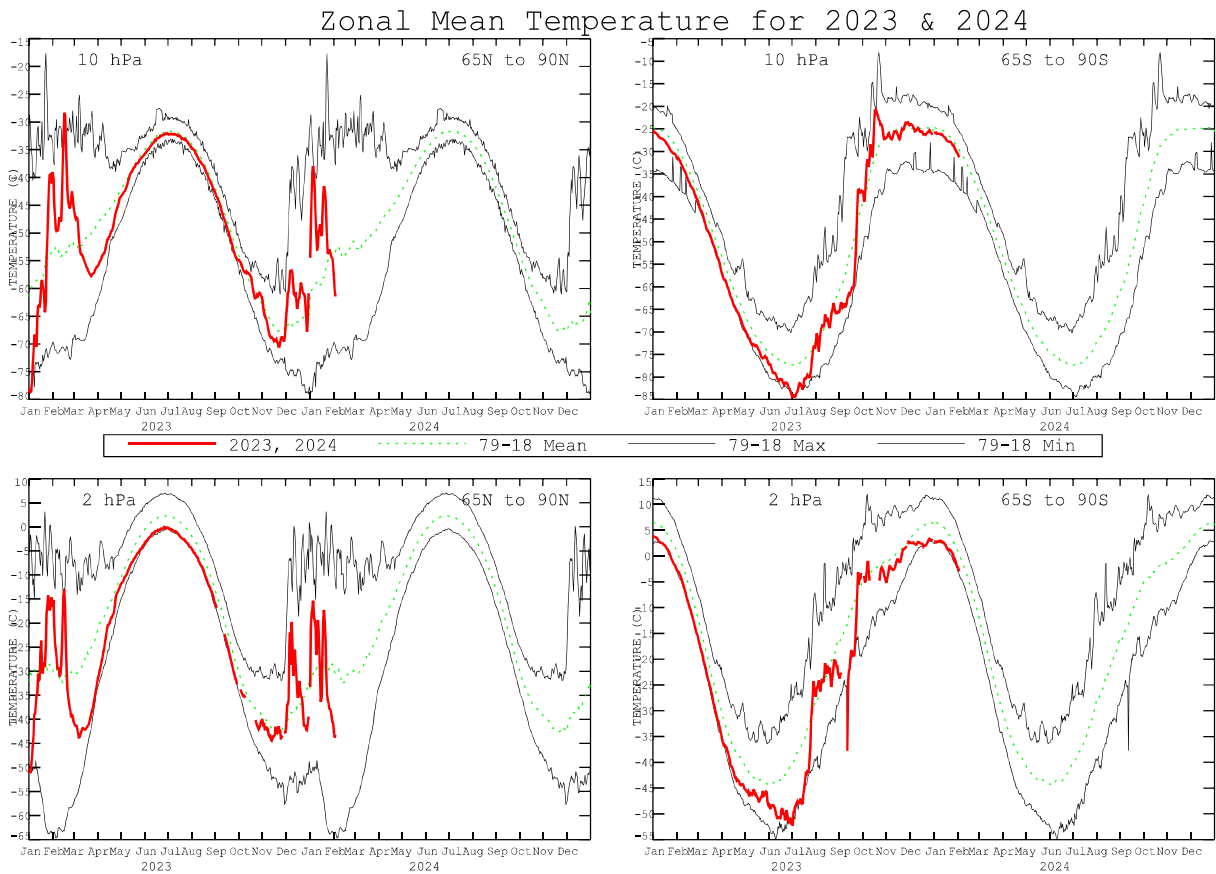


FIGURE S4. Daily mean temperatures at 10-hPa and 2-hPa (thick line) in the region 65° – 90° N and 65° – 90° S for the past two years. Dashed line depicts the 1991–2020 base period daily mean. Thin solid lines depict the daily extreme maximum and minimum temperatures.

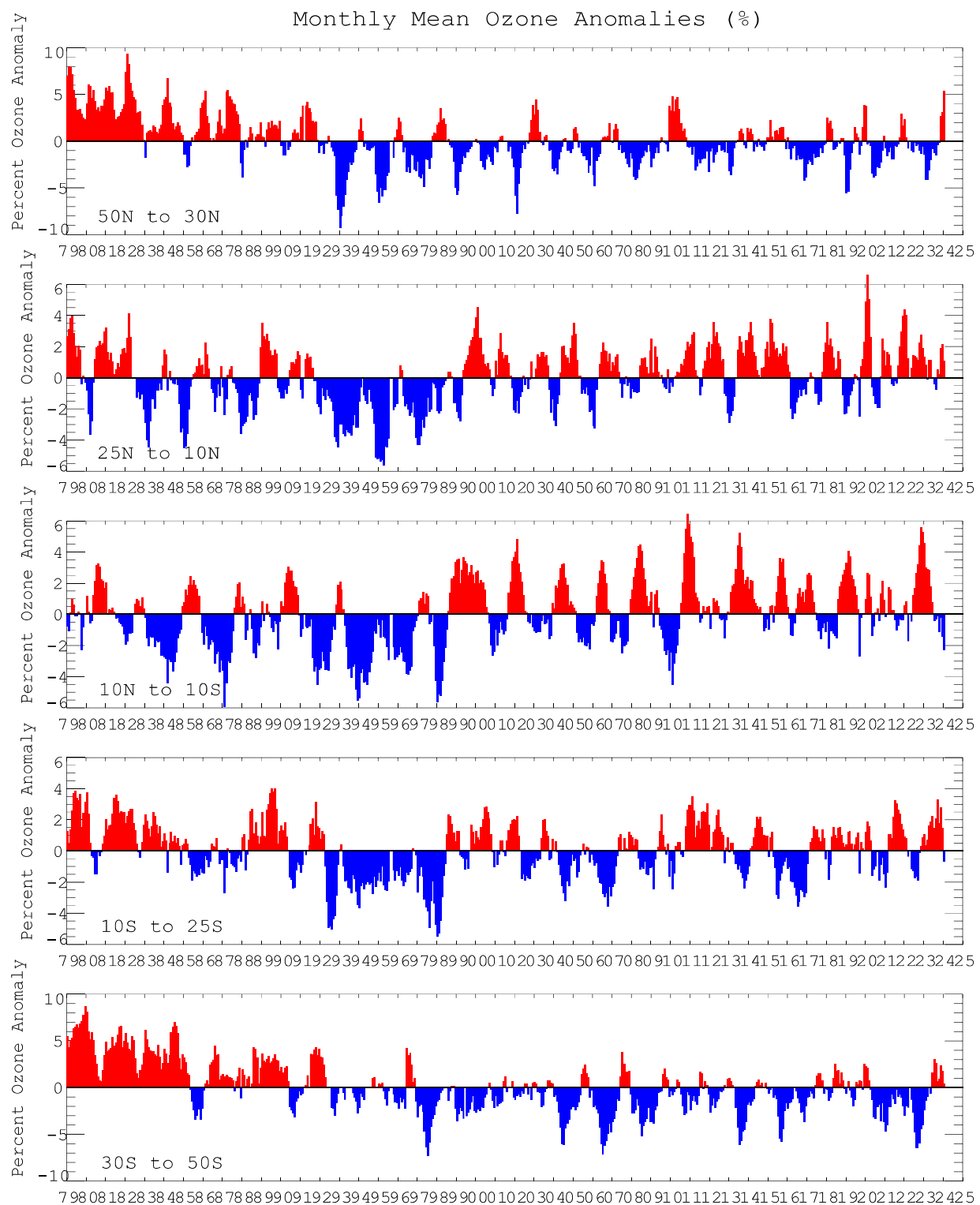


FIGURE S5. Monthly ozone anomalies (percent) from the long term monthly means for five zones: 50N-30N (NH mid-latitudes), 25N-10N (NH tropical surf zone), 10N-10S (Equatorial-QBO zone), 10S-25S (SH tropical surf zone), and 30S-50S (SH mid-latitudes). The long term monthly means are determined from the entire data set

JANUARY PERCENT DIFF (2024 - AVG[79-86])

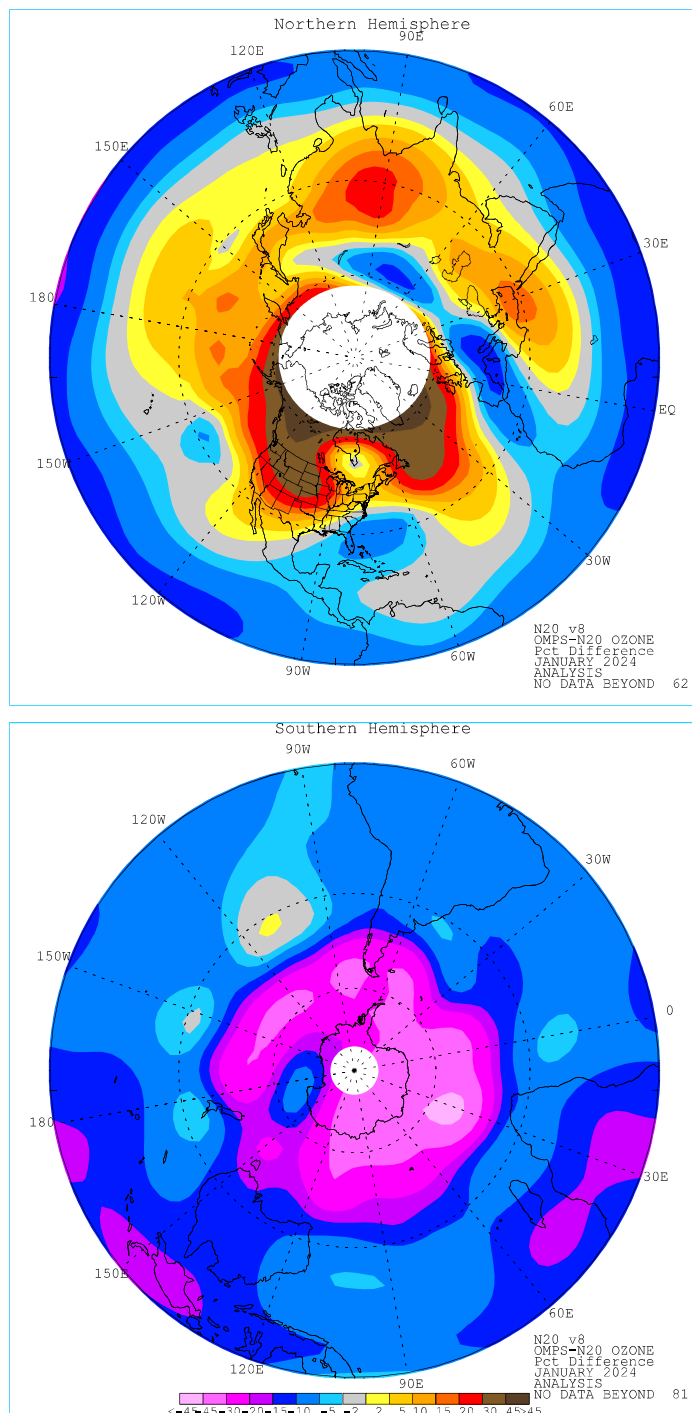


FIGURE S6. Northern (top) and Southern (bottom) Hemisphere total ozone anomaly (percent difference from monthly mean for the period 1979-1986). The region near the winter pole has no SBUV/2 data.

Fz at 100 hPa (Jan. 2024)

30N–90N

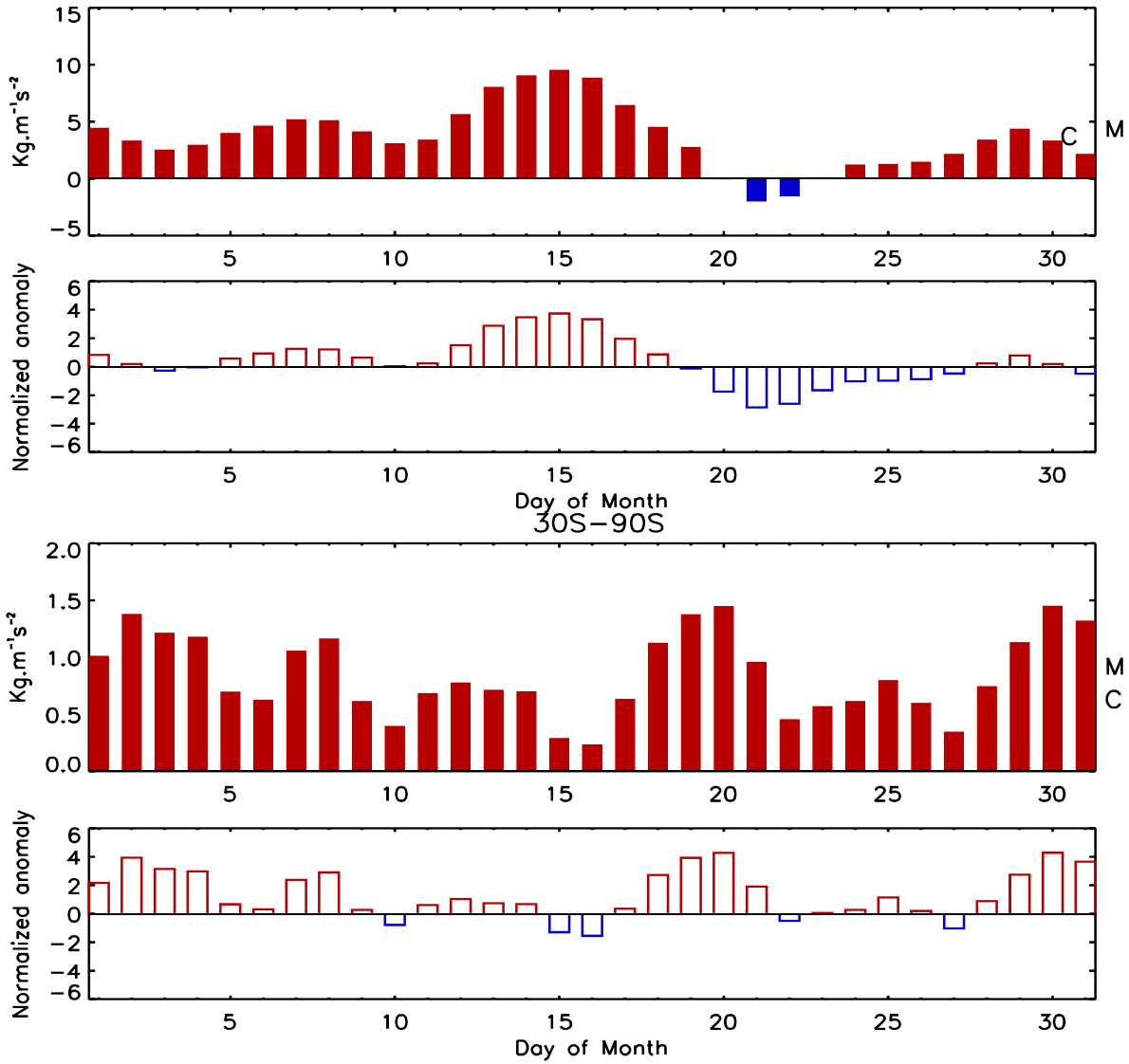


FIGURE S7. Daily vertical component of EP flux (which is proportional to the poleward transport of heat or upward transport of potential energy by planetary wave) at 100 hPa averaged over (top) 30°N–90°N and (bottom) 30°S–90°S for JAN 2024. The EP flux unit ($\text{kg m}^{-1} \text{s}^{-2}$) has been scaled by multiplying a factor of the Brunt Vaisala frequency divided by the Coriolis parameter and the radius of the earth. The letter ‘M’ indicates the current monthly mean value and the letter ‘C’ indicates the climatological mean value. Additionally, the normalized departures from the monthly climatological EP flux values are shown.

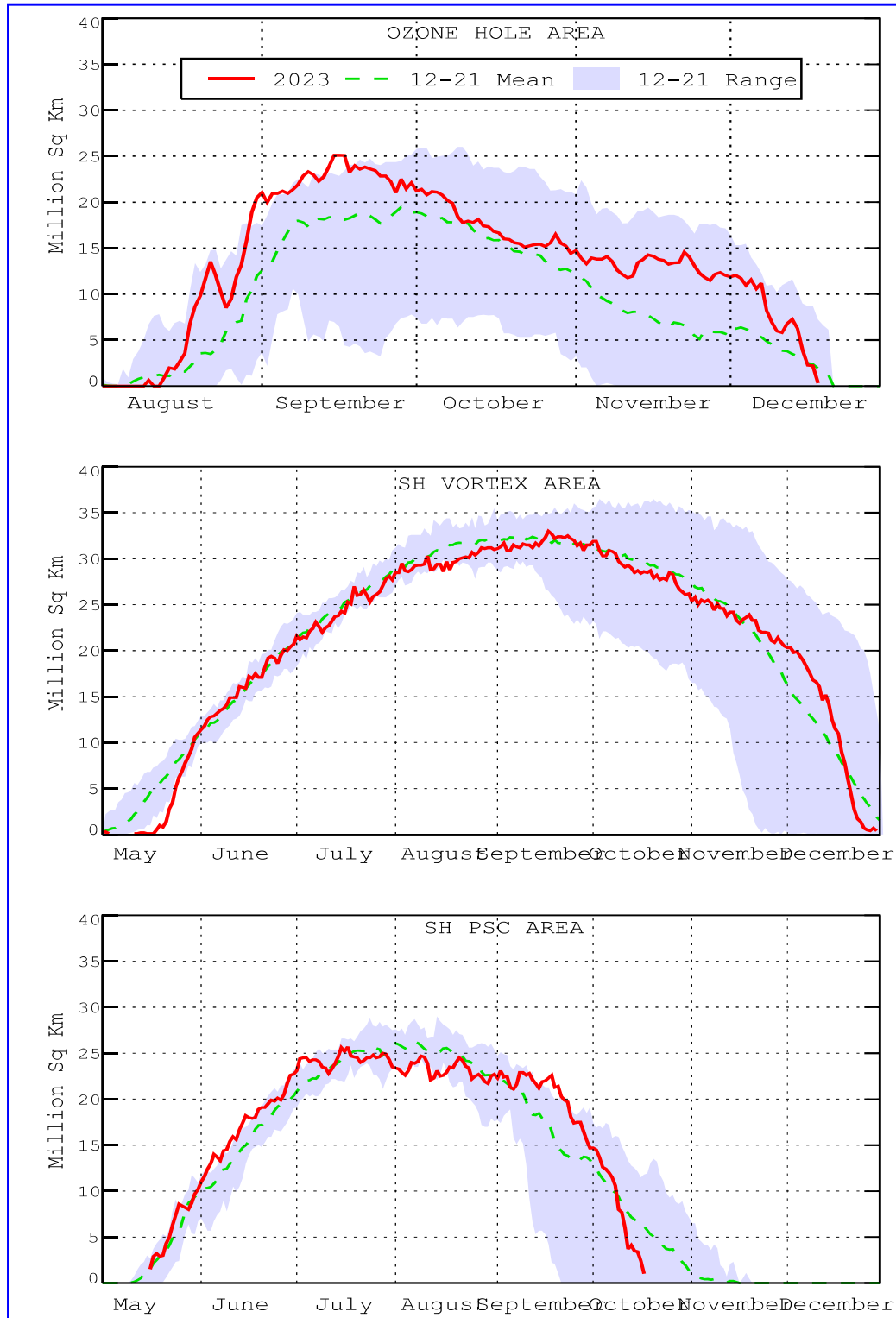


FIGURE S8. Daily time series showing the size of the SH polar vortex (representing the area enclosed by the 32 PVU contour on the 450K isentropic surface), and the areal coverage of temperatures $< -78^{\circ}\text{C}$ on the 450K isentropic surface.

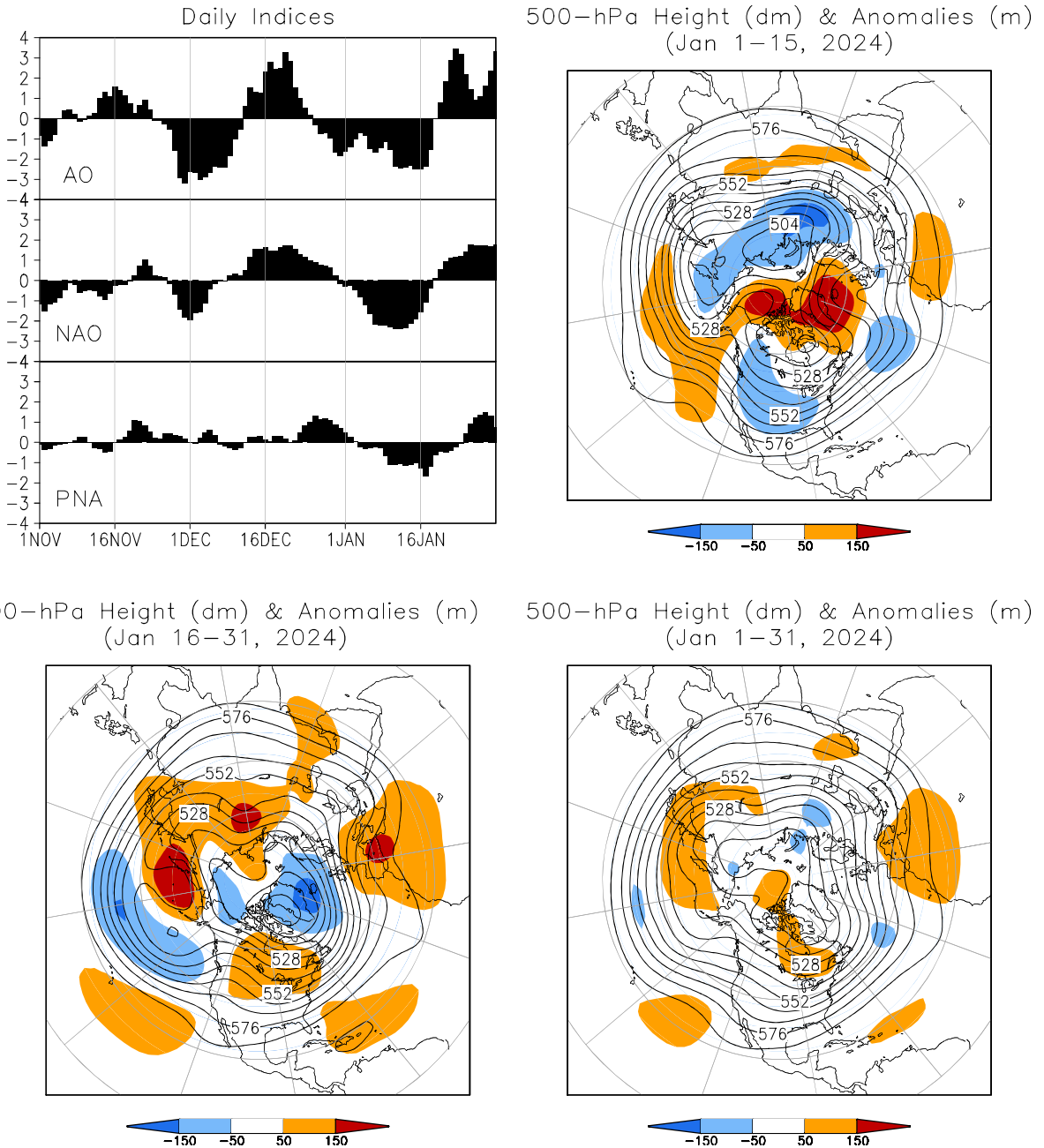


FIGURE A2.1. (a) Daily amplitudes of the Arctic Oscillation (AO) the North Atlantic Oscillation (NAO), and the Pacific-North American (PNA) pattern. The pattern amplitudes for the AO, (NAO, PNA) are calculated by projecting the daily 1000-hPa (500-hPa) height anomaly field onto the leading EOF obtained from standardized time-series of daily 1000-hPa (500-hPa) height for all months of the year. The base period is 1991-2020.

(b-d) Northern Hemisphere mean and anomalous 500-hPa geopotential height (CDAS/Reanalysis) for selected periods during JAN 2024 are shown in the remaining 3 panels. Mean heights are denoted by solid contours drawn at an interval of 8 dam. Dark (light) shading corresponds to anomalies greater than 50 m (less than -50 m). Anomalies are calculated as departures from the 1991-2020 base period daily means.

SSM/I Snow Cover for Jan 2024
anomaly based on departure from 1987–2010 baseline

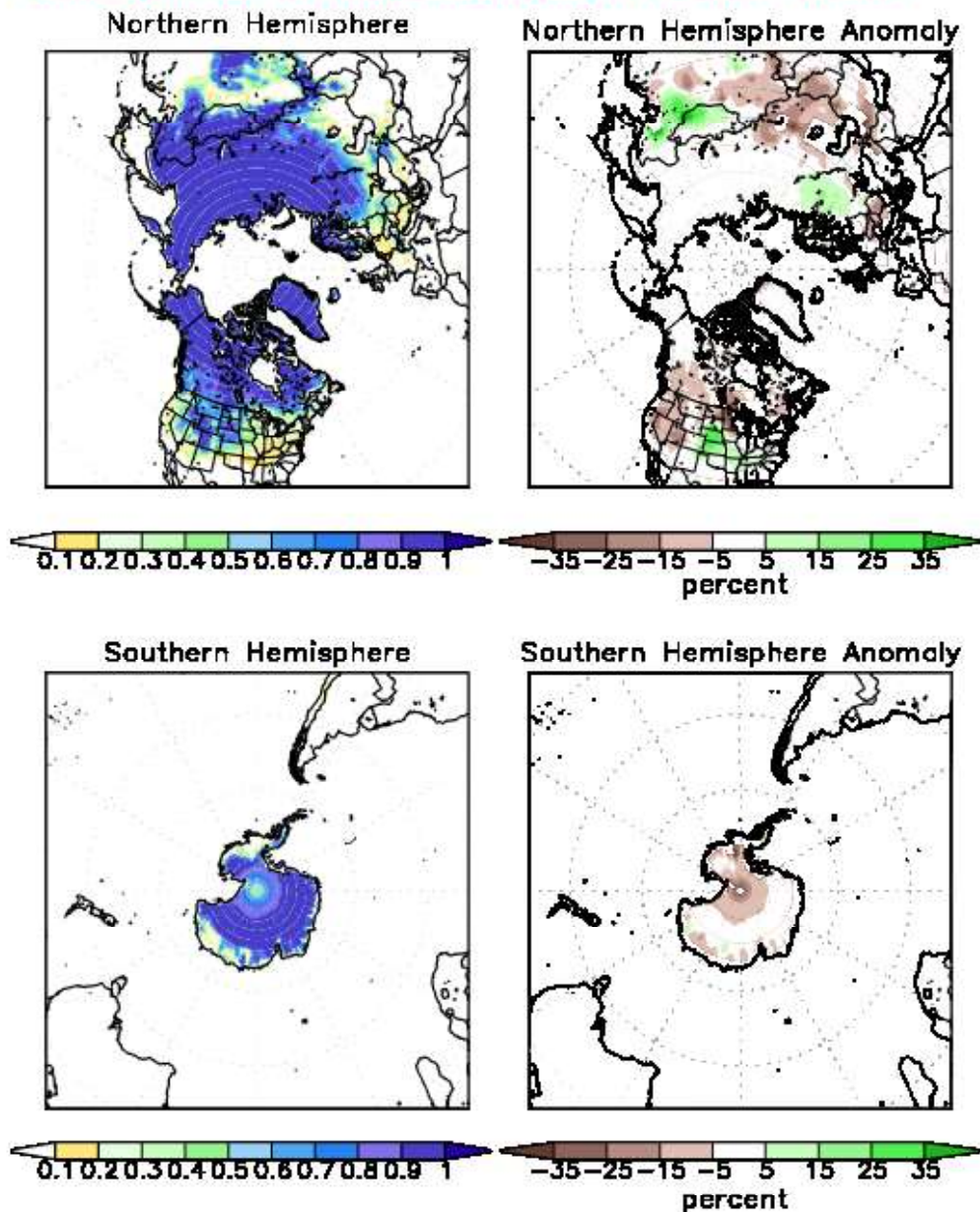


FIGURE A2.2. SSM/I derived snow cover frequency (%) (left) and snow cover anomaly (%) (right) for the month of JAN 2024 based on 1987 - 2010 base period for the Northern Hemisphere (top) and Southern Hemisphere (bottom). It is generated using the algorithm described by Ferraro et. al, 1996, Bull. Amer. Meteor. Soc., vol 77, 891-905.